
PSEUDOALTEROMONAS
HALOPLANKTIS TAC125 AS A CELL
FACTORY FOR THE PRODUCTION OF
RECOMBINANT PROTEINS: STRAIN
IMPROVEMENT AND NOVEL
ENGINEERING TECHNOLOGIES

Concetta Lauro

Dottorato in Biotecnologie – XXXIII ciclo

Università di Napoli Federico II



Dottorato in Biotecnologie – XXXIII ciclo

Università di Napoli Federico II



PSEUDOALTEROMONAS HALOPLANKTIS
TAC125 AS A CELL FACTORY FOR THE
PRODUCTION OF RECOMBINANT PROTEINS:
STRAIN IMPROVEMENT AND NOVEL
ENGINEERING TECHNOLOGIES

Concetta Lauro

Dottorando: Concetta Lauro
Relatore: Prof.ssa Maria Luisa Tutino
Coordinatore: Prof. Marco Moracci

Settore Scientifico Disciplinare:
Chimica e Biotecnologia delle Fermentazioni

*Da qua giù mi hai vista nascere
da lassù mi guardi crescere*

INDEX

	Riassunto	pag.	1
	Summary	pag.	5
	Introduction	pag.	6
1.	Strain engineering as a tool for enhancing recombinant protein productivity	pag.	6
2.	<i>Pseudoalteromonas haloplanktis</i> TAC125 as unconventional host for the recombinant protein production	pag.	7
	Chapter 1: Optimization of <i>PhTAC125</i> as a cell-factory	pag.	11
	Chapter 2: Exploitation of the engineered strain <i>PhTAC125 lacY⁺</i> for the production of the recombinant human protein CDKL5_1	pag.	43
	Chapter 3: Development of a novel genetic down-regulation system in <i>PhTAC125</i> based on antisense RNAs	pag.	80
	Appendix	pag.	101

Riassunto

Introduzione

L'ingegnerizzazione di molti ceppi batterici utilizzati come ospiti per la produzione di proteine ricombinanti ha rappresentato una notevole svolta nel contesto dell'ottimizzazione dei processi biotecnologici. La disponibilità di dati omici, modelli matematici e svariate tecnologie di ingegnerizzazione genetica ha consentito l'applicazione di diverse strategie di ottimizzazione del ceppo, anche in organismi non-modello. Il batterio antartico *Pseudoalteromonas haloplanktis* TAC125 (*PhTAC125*) si inserisce nel contesto dei processi di produzione di proteine ricombinanti grazie alle sue spiccate capacità di sintesi proteica. Nonostante numerose proteine siano state prodotte con successo, le potenzialità di tale piattaforma possono essere ulteriormente sfruttate attraverso lo sviluppo di ceppi ottimizzati, in grado di aumentare la produttività, e di nuove tecnologie geniche, utili per lo studio e caratterizzazione dei meccanismi molecolari ancora inesplorati coinvolti nel processo di espressione eterologa.

Capito 1: Ottimizzazione di *PhTAC125* come piattaforma per la produzione di proteine ricombinanti.

Le promettenti prestazioni di *PhTAC125* come piattaforma non convenzionale per la produzione di proteine ricombinanti "difficili" ha diretto i successivi studi verso il miglioramento del ceppo. Nel primo capitolo del presente lavoro di tesi, lo sviluppo di un nuovo sistema di espressione ricombinante inducibile da IPTG è stato accoppiato alla costruzione di un ceppo mutante, progettato per potenziare l'internalizzazione dell'induttore e controllare la degradazione dei prodotti ricombinanti. In particolare, il ceppo di *PhTAC125* privo del plasmide endogeno pMtBI e noto come KrPI è stato sottoposto ad una strategia di mutagenesi di integrazione e delezione di un vettore suicida. Il nuovo ceppo, denominato KrPI *lacY*⁺, si è dimostrato capace di produrre la permeasi LacY derivante da *E. coli* e una forma tronca della proteasi Lon priva del suo dominio catalitico. Dopo aver osservato nessun effetto deleterio sul fenotipo del batterio psicofilo, abbiamo impiegato il mutante KrPI *lacY*⁺ come ospite per la produzione ricombinante di proteine *reporter*. I risultati ottenuti hanno evidenziato il prezioso contributo della permeasi nell'ottimizzazione della concentrazione di IPTG usata come induttore, consentendo l'utilizzo del nuovo sistema anche a temperature estremamente basse. Inoltre, la capacità del batterio ingegnerizzato di utilizzare il lattosio come induttore gratuito apre nuovi orizzonti verso lo sviluppo di processi di produzione sostenibili su scala industriale.

Capito 2: Impiego del ceppo ingegnerizzato *PhTAC125* KrPI *lacY*⁺ per la produzione della proteina ricombinante umana CDKL5 1

La proteina umana *Cyclin-Dependent Kinase-Like 5* (CDKL5) è una serin/treonina chinasi abbondantemente espressa nel cervello e coinvolta in numerosi processi dello sviluppo neuronale. Mutazioni a carico del gene *X-linked* hCDKL5 sono stati associati a un disordine del neurosviluppo noto come Disordine da Deficienza di CDKL5 (CDD). Tale malattia ultra rara è caratterizzata da deficit motori e cognitivi ed epilessia ad esordio precoce, spesso farmaco-resistente. Nonostante la comunità scientifica si sia fortemente concentrata sullo studio del ruolo fisiologico e patologico di CDKL5, numerosi sono ancora i meccanismi molecolari da chiarire e ad oggi non esiste ancora una specifica terapia per la cura di tale condizione. Diverse sono le strategie terapeutiche attualmente oggetto di sviluppo e studi preclinici. Grandi aspettative sono rivolte verso la terapia proteica sostitutiva che si è dimostrata capace di ripristinare un fenotipo sano in modelli murini. Tuttavia, la difficoltà di produrre per via ricombinante la proteina CDKL5 limita sensibilmente la progressione della ricerca scientifica finalizzata sia a studi molecolari che terapeutici. La produzione del dominio catalitico N-terminale di CDKL5 è stata eseguita con successo in *E. coli*. Tuttavia, le caratteristiche strutturali del dominio C-terminale intrinsecamente disordinato rendono particolarmente complicata la produzione della proteina in forma integra. Attraverso i sistemi procariotici convenzionali si osserva infatti l' insorgenza di processi degradativi e di aggregazione in corpi di inclusione, mentre problemi di citotossicità e modifiche post-traduzionali indesiderate sono riscontrati in sistemi eucariotici.

Per valorizzare le miglorie ottenute dall'ingegnerizzazione di *PhTAC125*, il nuovo ceppo mutante KrPI *lacY*⁺ è stato utilizzato come ospite per la produzione ricombinante di tale proteina umana fusa all'N-terminale al peptide TATk, utilizzato per la veicolazione di farmaci attraverso la barriera ematoencefalica. I primi risultati ottenuti hanno da subito dimostrato un miglioramento nella produzione di TATk-CDKL5 con un incremento di circa 10 volte della resa proteica rispetto al ceppo *wild type*. Nonostante l'ottimizzazione della condizione di produzione, un'analisi di quantificazione del trascritto ne ha però evidenziato uno scarso accumulo nelle ore successive all'induzione dell'espressione ricombinante. Per tale motivo i successivi sforzi sono stati volti al miglioramento della scarsa efficienza di traduzione, imputata come causa di tale alterazione. Il recente sviluppo di sistemi di espressione psicrofilii bicistronici ha infatti consentito la triplicazione dei livelli di trascritto, avvalorando l'ipotesi dell' instabilità del trascritto derivante da

una scarsa copertura da parte dei ribosomi. Sorprendentemente, l'impiego dei sistemi di espressione bicistronici ha reso evidente l'insorgenza di un inizio alternativo della traduzione dovuto ad una emblematica sequenza nucleotidica del trascritto ricombinante. La costruzione della variante TATk-CDKL5-M43V, caratterizzata dalla sostituzione della Metionina 43 in Valina, ha consentito la completa conversione del trascritto nella forma integra della proteina. Altro miglioramento del sistema è poi derivato dalla concomitante disponibilità di una nuova generazione di plasmidi di espressione a medio-alto numero di copie, attraverso cui è stato raggiunto un incremento della produzione ricombinante di circa 10 volte. La successiva ottimizzazione del costrutto ricombinante ottenuta attraverso la fusione all' N-terminale di TATk-CDKL5-M43V con il tag SUMO, ha infine ridotto la suscettibilità della proteina alla degradazione proteolitica, raggiungendo livelli di produzione di circa 4 mg/ L di coltura. Inoltre, il costrutto ottimizzato di CDKL5 è stato soggetto a prove preliminari di purificazione, che si sono rese essenziali per l'ottenimento di frazioni arricchite della proteina, utilizzate poi per allestire un saggio di attività. I risultati emersi hanno chiaramente dimostrato che il ceppo ingegnerizzato *PhTAC125* KrPL *lacY*⁺ è capace di produrre la proteina umana complessa CDKL5 in forma attiva, la cui applicazione può dare un solido contributo in studi funzionali e strutturali oltre che per scopi terapeutici.

Capitolo 3: Sviluppo di un nuovo sistema di regolazione genico in *PhTAC125* basato su RNA antisense

Molte strategie di ottimizzazione ed ingegnerizzazione di ceppi batterici richiedono metodiche di manipolazione genica che siano precise ed attendibili e consentano un fine controllo di uno o più geni, anche essenziali. A tale scopo, le tecnologie basate su RNA antisense si sono largamente diffuse nella comunità scientifica, ampliando notevolmente il pannello di strategie attuabili non solo nel campo della ricerca applicata ma anche per studi fisiologici di base. Gli RNA antisense (asRNA) fanno parte di una vasta classe di RNA non codificanti, noti per il ruolo di regolazione di numerosi processi cellulari, quali risposte allo stress, virulenza, formazione di biofilm e cambi metabolici. La maggior parte degli RNA antisense caratterizzati nel dominio procariotico bersagliano uno specifico trascritto agendo attraverso appaiamento prevalentemente nella regione di inizio della traduzione. Tale interazione altera l'accessibilità del trascritto al ribosoma, bloccandone la traduzione e stimolandone la degradazione. Con un interessante approccio, Na e i suoi collaboratori hanno sviluppato un

sistema di silenziamento genico basato sulla modularizzazione dell'asRNA in una regione coinvolta nel riconoscimento ed interazione con l'mRNA target e un'altra costituita dallo scaffold di un asRNA naturale che consente il reclutamento e il legame con le proteine Hfq. Queste ultime sono degli chaperoni di RNA noti per il loro ruolo nella stabilizzazione dell'asRNA a cui si legano. È stato dimostrato che le proteine Hfq aumentano l'efficienza di silenziamento attraverso la promozione dell'interazione tra asRNA ed mRNA target ed il reclutamento dell'RNAsiE, coinvolta poi nella degradazione delle due molecole ribonucleasiche. Ispirati da questo studio eseguito in *E. coli*, abbiamo valutato la portabilità di questo sistema in *PhTAC125*. Data infatti l'elevata percentuale di identità tra la sequenza aminoacidica delle Hfq di *E. coli* e *PhTAC125*, abbiamo utilizzato la sequenza nucleotidica dello scaffold che ha mostrato maggiore efficacia in *E. coli*, derivante dall'asRNA noto come MicC, che è stata poi fusa con la sequenza complementare al trascritto target. In particolare, il gene codificante la proteasi Lon è stato scelto come target del silenziamento, dato che erano già noti gli effetti fenotipici della sua interruzione. Una volta costruito, l'asRNA-*lon* è stato espresso in KrPI, e i livelli di Lon sono stati poi misurati attraverso Western blot quantitativi. Purtroppo, tale sistema ha dimostrato una scarsa efficacia nel batterio psicrofilo, probabilmente a causa dalle differenze strutturali del dominio C-terminale delle Hfq dei due ospiti. Per tale motivo, abbiamo deciso di tentare un secondo approccio basato sui cosiddetti PTasRNA. Queste sono molecole caratterizzate da sequenze terminali invertite e ripetute che ne inducono una strutturazione a forcina. Grazie a tale caratteristica, i PTasRNA risultano estremamente stabili e capaci di accumularsi all'interno delle cellule raggiungendo livelli di repressione genica molto elevati. Seguendo il lavoro riportato da Nakashima, abbiamo costruito PTasRNA diretti contro i geni codificanti Lon e l'emoglobina trHbO di *PhTAC125*, che sono stati poi espressi in KrPI. I dati ottenuti hanno dimostrato un efficiente e duraturo silenziamento mediato dai nuovi costrutti, capaci di raggiungere livelli di repressione fino al 70%. Ulteriori analisi sono state poi volte alla comprensione ed identificazione di fattori che potessero influenzare l'efficacia della repressione genica ottenuta con i PTasRNA in *PhTAC125*, ponendo particolare attenzione alla selezione delle sequenze di riconoscimento del target sulla base della predetta forza di legame. I dati emersi hanno consentito di delineare delle indicazioni utili per la costruzione di sistemi per il controllo dell'espressione genica nei batteri psicrofili, ponendo così le basi per successivi studi nell'ambito della biologia sintetica ed ingegneria metabolica.

Summary

Pseudoalteromonas haloplanktis TAC125 (*PhTAC125*) represents a promising biological system for the recombinant production of high-quality proteins due to its profound differences in cellular physiochemical conditions in comparison to the commonly used mesophilic bacteria. The establishment of efficient constitutive and regulated gene expression systems, optimized culture media, mathematical metabolic models, and fermentative processes allowed the exploitation of this bacterium to produce complex eukaryotic proteins. In this scenario, this research project aimed to explore and extend the biotechnological capabilities of *PhTAC125* as a cell factory. In the first part of my PhD project, I focused on the development of a mutant strain engineered to boost the performance of an IPTG-inducible expression system. The obtained strain, named KrPI *lacY*⁺, proved to be able to produce the *E. coli* lactose transporter and a truncated Lon protease devoid of its catalytic domain. The improvement in recombinant production derived from KrPI *lacY*⁺ was also demonstrated at low temperatures and encouraged further optimization toward cheaper and sustainable industrial processes. As described in the second chapter of this thesis, KrPI *lacY*⁺ was exploited for the recombinant production of the human partially IDP kinase CDKL5, unsuccessfully produced in other prokaryotic systems. Different strategies were applied to overcome the bottlenecks affecting the overall production yield, taking into account the translational efficiency, the optimization of the coding sequence and fusion partners, and the increase of expression plasmid copy number. The establishment of such an improved platform allowed the achievement of high production yields of CDKL5 in a full-length and active form, enabling its application for functional, structural as well as therapeutic studies. Finally, to further strengthen the exploitation of *PhTAC125*, an asRNA-mediated regulatory system was developed. The results described in the last chapter of the present study demonstrated the feasibility of conditional gene silencing in *PhTAC125*, opening new perspectives for manipulating marine psychrophilic bacteria in basic and applicative studies.

Introduction

1. Strain engineering as a tool for enhancing recombinant protein productivity

In the last couple of decades, the engineering of microbial platforms has emerged as a robust tool for the optimization of biotechnological production processes. The overcoming of the bottlenecks affecting recombinant protein production is the main goal of the strain improvement strategies. Indeed producing a protein is a multi step process, involving transcription, translation, folding and management of stress responses, which are intricately linked to cellular physiology and strongly influence the overall flux through the biosynthetic pathway.

The availability of -omics data, predictive mathematical models and a wide variety of technologies for genome editing has led to relevant improvements in the design of host platforms for high-level recombinant expression [1, 2, 3]. Furthermore, the establishment of high throughput methods allowed such approaches to be implemented through large-scale screenings [4]. Advances in metabolic engineering also provided a tool for modulating critical metabolic pathways in competition with recombinant protein production, aiding the uncoupling of microbial growth from the product formation [5].

In this context, the RNA-based regulatory systems proved to be an excellent tool for screening and engineering purposes. Used for genome-scale identification of genes to be modified and modulation of metabolic pathways to maximize the production of desired biomolecules, this technology was widely exploited in synthetic biology and metabolic engineering [6, 7].

An explicative example of the results achieved through strain improvement strategies is the great arsenal of *E. coli* strains available nowadays. In addition to the well-known BL21(DE3) strain, carrying the T7 RNA polymerase gene and deficient in OmpT and Lon proteases [8], several derivatives can be exploited for many specific production needs. In particular, the platform has been modified to gain peculiar capabilities, such as the formation of cytoplasmic disulfide bonds (Origami strain) [9], translation of transcripts containing rare codons (Rosetta(DE3) strain) [10], stabilization of the recombinant plasmids (BLR(DE3) strain) [11], coexpression of genes encoding chaperonins (ArcticExpress (DE3) strain) [12], adjustment of the recombinant expression (Tuner strain) [13], enhancement of the mRNA stability (BL21 star strain) [14], production of membrane proteins (SuptoxD and SuptoxR strains) [15], expression of toxic genes (BL21(DE3)pLysS

strain) [16] and production of particularly troublesome proteins (C41(DE3) and C43(DE3) strains) [17]. The overall amelioration of the features of the *E. coli* derivative strains represents one reason why it is used as the first choice host for high-level protein production.

Although all these progresses, some drawbacks still limit this production platform [18]. The proteins are often heavily proteolyzed or accumulated as inclusion bodies, whose resolubilization does not necessarily allow active protein recovery. Furthermore, some mammalian proteins could be poorly expressed in the microbial system, and the endotoxin contamination greatly complicates the purification protocols for therapeutic purposes.

For this reason, the interest in developing novel and non-conventional expression systems is rising.

2. *Pseudoalteromonas haloplanktis* TAC125 as unconventional host for the recombinant protein production

The physiological diversity of microorganisms used as unconventional systems for the heterologous gene expression provides the basis for overcoming constraints limiting the harnessing of common model platforms.

Cold-adapted bacteria appear as a promising biological system for the production of high-quality recombinant products, and in this context, *Pseudoalteromonas haloplanktis* TAC125 (*PhTAC125*) represents a model in which several efficient gene expression technologies have been set up [16]. *PhTAC125* is a γ -proteobacterium isolated from Antarctic coastal seawater [17] growing in a wide range of temperatures (from -2,5°C to 30°C) [18]. The sequencing and annotation of its genome [19] allowed the analysis of two chromosomes and a small cryptic plasmid, pMtBL, whose characterization has been reported by Tutino and coworkers [20]. Recently taking advantage of the consolidation of third-generation sequencing technologies, a de novo genome assembly was performed. It highlighted the presence of a second large plasmid, pMEGA, which carries a series of genes involved in the SOS response and survival in extreme environments [21].

The capability of *PhTAC125* to reach high cell density even at lower temperatures, with optimum growth at 15°C, makes it one of the fastest-growing psychrophiles so far characterized and an attractive host as a cell factory for proteins. By the use of this non-conventional host, several proteins were efficiently produced in a soluble and active form [22, 24, 28, 29, 30] and, even when high production yields were reached, insoluble protein aggregates have never been found [22]. This

particular behaviour could be explained by the profound difference of cellular physicochemical conditions of *PhTAC125* in comparison to those described in mesophilic bacteria. Several observations seem to confirm a high capacity for translation in the cold, such as the relatively high number of rRNA and tRNA genes (up to 106) pinpointed in its genome sequence [19]. Moreover, it was demonstrated that at low temperatures the Antarctic bacterium up-regulates proteins directly related to protein synthesis (components of both transcription and translation machinery) and actively overproduces the trigger factor, whose function is the assistance to protein folding [23]. Other evidence of the relevant efficiency of translation in *PhTAC125* is the overproduction of enzymes such as RNA helicases, which may be involved in unwinding the mRNA secondary structures, and peptidyl-prolyl isomerases which promote the proline isomerization process and the folding of membrane proteins [23].

By combining genome sequencing and *in silico* and *in vivo* analyses, a collection of constitutive and inducible gene-expression vectors was set up to drive the production of recombinant proteins in *PhTAC125* [22, 24] and a cold gene expression system for the secretion of heterologous proteins was also developed [25]. The genetic analysis of the main metabolic pathways [19] and the screening of the growth performances in the presence of different amino acids allowed the establishment of a fed-batch fermentation strategy [26]. Taking a cue from these results, a synthetic medium was then formulated and used for batch cultivation, allowing for the first time the production of a recombinant protein at a subzero temperature [18]. Recently, the knowledge about the metabolic features of *PhTAC125* enabled the development of two theoretical models [27]. According to the regulation of the assimilatory pathways, these models describe the nutrients switching predicting the microbial behaviour in diverse environments. However, diverse optimizations are still necessary. Many cellular processes implicated in heterologous expression are not yet characterized at the molecular level, and the support of the available -omics data, mathematical metabolic models and genome engineering tools will be pivotal for developing superior strains of *PhTAC125* granting improved culture productivity.

References

- [1] Y. L. Sang, D. Y. Lee, and Y. K. Tae, "Systems biotechnology for strain improvement," *Trends Biotechnol.*, vol. 23, no. 7, pp. 349–358, 2005.
- [2] S. Mahalik, A.K. Sharma, K.J. Mukherjee, "Genome engineering for improved recombinant protein expression in escherichia coli," *Microb. Cell Fact.*, 2014.

- [3] R. Liu, M. C. Bassalo, R. I. Zeitoun, and R. T. Gill, "Genome scale engineering techniques for metabolic engineering," *Metab. Eng.*, vol. 32, 2015.
- [4] B. Jia and C. O. Jeon, "High-throughput recombinant protein expression in *Escherichia coli*: Current status and future perspectives," *Open Biol.*, 2016.
- [5] C. Ghosh, R. Gupta, and K. J. Mukherjee, "An inverse metabolic engineering approach for the design of an improved host platform for over-expression of recombinant proteins in *Escherichia coli*," *Microb. Cell Fact.*, vol. 11, 2012.
- [6] D. Na, S. M. Yoo, H. Chung, H. Park, J. H. Park, and S. Y. Lee, "Metabolic engineering of *Escherichia coli* using synthetic small regulatory RNAs" *Nat. Biotechnol.*, vol.31, no.2, pp.170–174, 2013.
- [7] W. Ahmed, M. A. Hafeez, and R. Ahmed, "Advances in engineered trans-acting regulatory RNAs and their application in bacterial genome engineering," *J. Ind. Microbiol. Biotechnol.*, vol. 46, no. 6, pp. 819–830, 2019.
- [8] F. W. Studier and B. A. Moffatt, "Use of bacteriophage T7 RNA polymerase to direct selective high-level expression of cloned genes," *J. Mol. Biol.*, 1986.
- [9] A. I. Derman, W. A. Prinz, D. Belin, and J. Beckwith, "Mutations that allow disulfide bond formation in the cytoplasm of *Escherichia coli*," *Science*, 1993.
- [10] R. Novy, D. Drott, K. Yaeger, and R. Mierendorf, "Overcoming the codon bias of *E. coli* for enhanced protein expression," *Innovations*, no. 12, pp. 4–6, 2001.
- [11] P. D. Philippe Goffin, "crossm," *genome Announc.*, vol. 5, no. 22, 2017.
- [12] G. L. Rosano, E. S. Morales, and E. A. Ceccarelli, "New tools for recombinant protein production in *Escherichia coli*: A 5-year update," *Protein Sci.*, 2019.
- [13] A. Khlebnikov and J. D. Keasling, "Effect of lacY expression on homogeneity of induction from the P_{tac} and P_{trc} promoters by natural and synthetic inducers," *Biotechnol. Prog.*, vol. 18, no. 3, pp. 672–674, 2002.
- [14] P. J. Lopez, I. Marchand, S. A. Joyce, and M. Dreyfus, "The C-terminal half of RNase E, which organizes the *Escherichia coli* degradosome, participates in mRNA degradation but not rRNA processing in vivo," *Mol. Microbiol.*, 1999.
- [15] D. Gialama, K. Kostelidou, M. Michou, D. C. Delivoria, F. N. Kolisis, and G. Skretas, "Development of *Escherichia coli* Strains That Withstand Membrane Protein-Induced Toxicity and Achieve High-Level Recombinant Membrane Protein Production," *ACS Synth. Biol.*, vol. 6, no. 2, pp. 284–300, 2017.
- [16] F. W. Studier, "Use of bacteriophage T7 lysozyme to improve an inducible T7 expression system," *J. Mol. Biol.*, vol. 219, no. 1, pp. 37–44, 1991.
- [17] Bruno Miroux and John E. Walker, "Over-production of Proteins in *Escherichia coli*: Mutant Hosts that Allow Synthesis of some Membrane Proteins and Globular Proteins at High Levels," *J. Mol. Biol.*, vol. 19, no. 67, 1996.
- [19] E. Parrilli, M.L. Tutino, "Heterologous protein expression in *Pseudoalteromonas haloplanktis* TAC125," in 2017 in "Psychrophiles: From Biodiversity to Biotechnology: Second Edition" (Margesin R Editor) Springer, 2017.
- [20] L. Birolo *et al.*, "Aspartate aminotransferase from the Antarctic bacterium *Pseudoalteromonas haloplanktis* TAC 125. Cloning, expression, properties, and molecular modelling," *Eur. J. Biochem.*, vol. 267, no. 9, 2000.
- [21] F. Sannino *et al.*, "A novel synthetic medium and expression system for subzero growth and recombinant protein production in *Pseudoalteromonas haloplanktis* TAC125," *Appl. Microbiol. Biotechnol.*, vol. 101, no. 2, 2017.
- [22] E. C. Medigue, Krin *et al.*, "Coping with cold: The genome of the versatile marine Antarctica bacterium *Pseudoalteromonas haloplanktis* TAC125," *Genome Res.*, 2005.
- [23] M. L. Tutino, A. Duilio, E. Parrilli, E. Remaut, G. Sannia, and G. Marino, "A novel replication element from an Antarctic plasmid as a tool for the expression of proteins at low temperature," *Extremophiles*, vol. 5, no. 4, 2001.
- [24] W. Qi *et al.*, "New insights on *Pseudoalteromonas haloplanktis* TAC125 genome organization and benchmarks of genome assembly applications using next and third generation sequencing technologies," *Sci.Rep.*, vol.9, no.1, 2019.
- [25] R. Papa, V. Rippa, G. Sannia, G. Marino, and A. Duilio, "An effective cold inducible expression system developed in *Pseudoalteromonas haloplanktis* TAC125," *J.*

- Biotechnol.*, vol. 127, no. 2, pp. 199–210, 2007.
- [26] F. Piette *et al.*, “Proteomics of life at low temperatures: Trigger factor is the primary chaperone in the Antarctic bacterium *Pseudoalteromonas haloplanktis* TAC125,” *Mol. Microbiol.*, vol. 76, no. 1, pp. 120–132, 2010.
- [27] M. Giuliani, E. Parrilli, P. Ferrer, K. Baumann, G. Marino, and M. L. Tutino, “Process optimization for recombinant protein production in the psychrophilic bacterium *Pseudoalteromonas haloplanktis*,” *Process Biochem.*, 2011.
- [28] E. Parrilli, D. De Vizio, C. Cirulli, and M. L. Tutino, “Development of an improved *Pseudoalteromonas haloplanktis* TAC125 strain for recombinant protein secretion at low temperature,” *Microb. Cell Fact.*, vol. 7, 2008.
- [29] B. Wilmes, A. Hartung, M. Lalk, M. Liebeke, T. Schweder, and P. Neubauer, “Fed-batch process for the psychrotolerant marine bacterium *Pseudoalteromonas haloplanktis*,” *Microb. Cell Fact.*, vol. 9, pp. 1–9, 2010.
- [30] E. Perrin *et al.*, “Diauxie and co-utilization of carbon sources can coexist during bacterial growth in nutritionally complex environments,” *Nat. Commun.*, vol. 11, no. 1, pp. 1–16, 2020.
- [31] M. Dragosits *et al.*, “Influence of growth temperature on the production of antibody Fab fragments in different microbes: A host comparative analysis,” *Biotechnol. Prog.*, vol. 27, no. 1, pp. 38–46, 2011.
- [32] I. Vigentini, A. Merico, M. L. Tutino, C. Compagno, and G. Marino, “Optimization of recombinant human nerve growth factor production in the psychrophilic *Pseudoalteromonas haloplanktis*,” *J. Biotechnol.*, vol.127, 2006.
- [33] U. Unzueta *et al.*, “Strategies for the production of difficult-to-express full-length eukaryotic proteins using microbial cell factories: production of human alpha-galactosidase A,” *Appl. Microbiol. Biotechnol.*, vol. 99, no. 14, 2015.

Chapter 1: Optimization of *PhTAC125* as a cell-factory

PhTAC125 proved to be a worthwhile unconventional cell factory for producing proteins unsuccessfully obtained in mainstream hosts, such as *E. coli*. A mutant strain was developed through genome-scale genetic manipulations to further improve the psychrophilic bacterium's promising capability in this field. The establishment of a new powerful expression plasmid was coupled with the strain improvement, focusing on optimising inducer internalization and controlling the deleterious proteolysis of recombinant products. The published paper below demonstrated that insertional inactivation of the proteolytic domain of Lon protease is compatible with a viable phenotype, almost indistinguishable from the wild type psychrophilic bacteria, at least in the tested conditions. Furthermore, the obtained mutant strain could also produce a mesophilic lactose transporter in functional form, even at very low temperatures. The evaluation of the recombinant production performance of this new platform validated the precious contribution of the permease to reducing the amount of IPTG used as the inducer of the recombinant expression. For the first time, the detection of a fluorescent protein was achieved in *PhTAC125*, providing a tool for various sensitive and innovative study approaches. In addition, the capacity of the engineered *PhTAC125* to internalize lactose paves the way for the development of a sustainable industrial production process since it could be used as a cost-effective inducer in our expression system.



Article

Improvement of *Pseudoalteromonas haloplanktis* TAC125 as a Cell Factory: IPTG-Inducible Plasmid Construction and Strain Engineering

Andrea Colarusso †, Concetta Lauro †, Marzia Calvanese, Ermenegilda Parrilli and Maria Luisa Tutino *

Dipartimento di Scienze Chimiche, Complesso Universitario Monte Sant'Angelo, Via Cintia, 80126 Napoli, Italy;

andrea.colarusso@unina.it (A.C.); concetta.lauro@unina.it (C.L.); marzia.calvanese@unina.it (M.C.); erparril@unina.it (E.P.) * Correspondence: tutino@unina.it; Tel.: +39-081-674317

† These authors equally contributed to this work.

Received: 22 August 2020; Accepted: 22 September 2020; Published: 24 September 2020

Abstract: Our group has used the marine bacterium *Pseudoalteromonas haloplanktis* TAC125 (*PhTAC125*) as a platform for the successful recombinant production of “difficult” proteins, including eukaryotic proteins, at low temperatures. However, there is still room for improvement both in the refinement of *PhTAC125* expression plasmids and in the bacterium’s intrinsic ability to accumulate and handle heterologous products. Here, we present an integrated approach of plasmid design and strain engineering finalized to increment the recombinant expression and optimize the inducer uptake in *PhTAC125*. To this aim, we developed the IPTG-inducible plasmid pP79 and an engineered *PhTAC125* strain called KrPL *LacY*⁺. This mutant was designed to express the *E. coli* lactose permease and to produce only a truncated version of the endogenous Lon protease through an integration-deletion strategy. In the wild-type strain, pP79 assured a significantly better production of two reporters in comparison to the most recent expression vector employed in *PhTAC125*. Nevertheless, the use of KrPL *LacY*⁺ was crucial to achieving satisfying production levels using reasonable IPTG concentrations, even at 0 °C. Both the wild-type and the mutant recombinant strains are characterized by an average graded response upon IPTG induction and they will find different future applications depending on the desired levels of expression.

1. Introduction

Over recent years, both constitutive promoters [1] and inducible cassettes [2,3] have been established for the recombinant expression in *Pseudoalteromonas haloplanktis* TAC125 (*PhTAC125*) in a wide range of temperatures. Regulatable systems are particularly desirable in industrial processes where the decoupling of the biomass accumulation from the recombinant expression could be crucial to guarantee satisfactory yields. Although they proved to be useful for a series of studies [2–6], the two inducible expression vectors used in *PhTAC125* so far showed some major drawbacks. The L-malate inducible pUCRP plasmid guaranteed a remarkable protein accumulation [2], but its efficacy resulted in be strongly influenced by the medium composition. In particular, the use of L-glutamate as carbon source negatively affected pUCRP induction, making it necessary to formulate bacterial media devoid of this amino acid [5]. Given the pivotal contribution of such a carbon source to *PhTAC125* specific growth rate and metabolic regulation [7], its depletion might limit the versatility of this recombinant system for industrial purposes. On the other hand, the D-galactose regulatable pMAV expression vector showed a good versatility in terms of the temperature range of use when *P. haloplanktis* TAE79 β -galactosidase was employed as a reporter [3]. Nevertheless, the amount of enzyme that could be accumulated in recombinant *PhTAC125* pMAV-*lacZ* was lower than the yield achievable in the nonrecombinant parental *PhTAE79* strain [8], suggesting a low strength of the used inducible promoter.

The β -galactosidase production in *PhTAE79* wt was indeed sufficiently high to guarantee its purification from *PhTAE79* extracts and its industrial exploitation for lactose treatment without the use of any recombinant technology [8,9]. This data induced us to evaluate the potential translatability of the regulatory sequences of *PhTAE79 lacZ* in *PhTAC125* for recombinant purposes. The preferable choice of *PhTAC125* rather than *PhTAE79* as a host descends from the wider available information in terms of genomic organization and annotation [10], genetic modification strategies [11], and metabolic networks [5,7,12,13] for the first bacterium.

Based on an in silico analysis of the *PhTAE79 lacZ* expression cassette and on previously published data from other authors, we were persuaded of the feasibility of the use of this regulatory system to develop a new expression vector in *PhTAC125*. This plasmid, called pP79, proved to be IPTG-inducible, to outperform our previous regulated expression vector pMAV, and to allow the detection of the production of a fluorescent protein in *PhTAC125* for the first time. To

better the performance of this system, we genetically engineered the host for the expression of a mesophilic lactose permease. Such a mutant strain guaranteed a higher recombinant production using a lower IPTG concentration range in comparison with the parental strain. Collectively, our results emphasize the remarkable flexibility of *PhTAC125*, a polar host capable of combining a heterologous psychrophilic expression system with a mesophilic inducer transporter for the recombinant production of proteins.

2. Materials and Methods

2.1. Bacterial Strains and Growth Media Formulations

The strains used in this study are listed in Table S1. *E. coli* DH5 α was used for cloning procedures, while *E. coli* S17-1(λ *pir*) was employed in intergeneric conjugations as a donor strain for KrPL transformations [14]. KrPL—a cured *PhTAC125* strain—was used in all the recombinant expression and mutagenesis experiments. *E. coli* was cultured in LB broth (10 g/L bacto-tryptone, 5 g/L yeast extract, 10 g/L NaCl) at 37 °C and the recombinant strains were treated with either 34 μ g/mL chloramphenicol or 100 μ g/mL ampicillin, depending on the selection marker of the vector. KrPL was grown in TYP (16 g/L bacto-tryptone, 16 g/L yeast extract, 10 g/L NaCl) during conjugations and precultures development, and in GG [3] in expression growths. For the propagation and culture of KrPL recombinant strains, either chloramphenicol or ampicillin was used. In detail, chloramphenicol was added to solid and liquid media at 12.5 μ g/mL and 25 μ g/mL concentrations, respectively. Ampicillin was always used with a concentration of 100 μ g/mL, instead.

2.2. Construction of pP79 and p79C Expression Plasmids

The AUTL01000130.1 contig containing *PhTAE79 lacZ* (Figure 1) was automatically annotated with RAST [15] and the annotations were refined using BlastP [16]. For all digestion/ligation reactions, NEB enzymes were used (New England Biolabs, Hitchin, UK). The restriction sites in pP79 and p79C that were hydrolyzed for cloning purposes are visible in the maps in Figure 2. The pP79 inducible expression vector was designed by cloning the DNA fragment from *PhTAE79* encompassing the *lacR* gene and the divergent *lacZ* promoter + 5' UTR into pUCLT/Rterm vector [2,17]. To this aim the pSP73- β -*gal* vector [8] was used as a template in a PCR involving the use of p79_fw and p79_rv primers (Table S2). The resulting ~1.2 kb amplified sequence covered the 18'782– 19'909 region of AUTL01000130.1 and was characterized by the addition of SphI restriction site to its 5' extremity

and NdeI, Sall and XbaI to its 3' terminus. Both pUCLT/Rterm and the p79 amplicon were double digested with SphI/XbaI and ligated. The resulting plasmid was pP79.

p79C is a variant of pP79 harboring a chloramphenicol resistance marker rather than an ampicillin selection gene. For its construction, pP79 regulatory sequences, its MCS and the *aspC* transcriptional terminator were extracted with SphI and SacI from pP79 and ligated with pUCC [4] digested in the same sites.

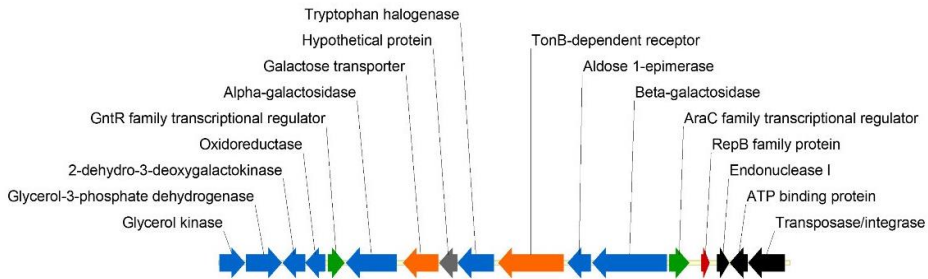


Figure 1. Disposition of genes surrounding the β -galactosidase encoding gene in *Pseudoalteromonas haloplanktis* TAE79 (*PhTAE79*) AUTL01000130.1 contig. Blue arrows indicate genes involved in metabolism, in orange receptors and transporters, while in green transcriptional regulators. Black arrows depict genes involved in DNA rearrangements, the red arrow highlights the presence of a gene involved in plasmid replication and the gray arrow indicates a coding sequence with unknown functions.

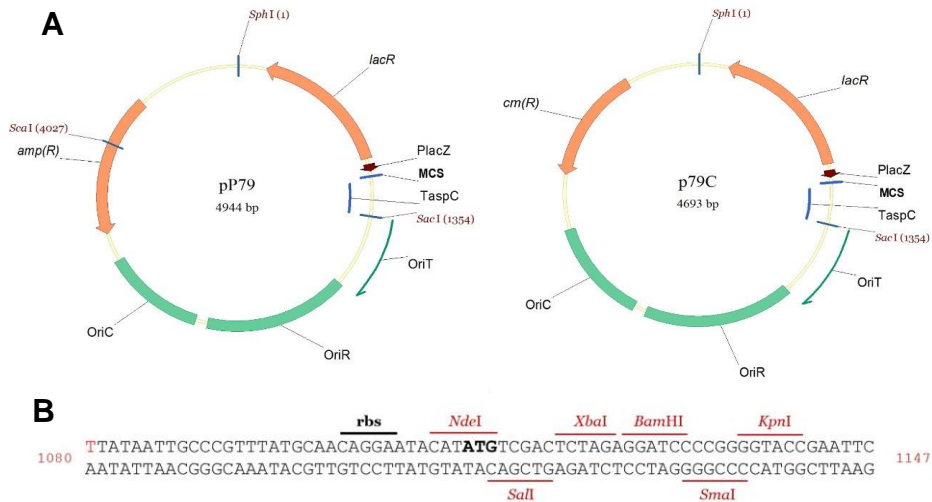


Figure 2. Maps of pP79 and p79C shuttle vectors. (A) The two plasmids differ for the selection markers, which are a β -lactamase encoding gene (*amp(R)*) in pP79 and a chloramphenicol acetyltransferase encoding sequence (*cm(R)*) in p79C. The common elements to the plasmids are *PhTAE79* regulatory gene *lacR*, the promoter of *PhTAE79 lacZ* gene (*PlacZ*), the transcriptional terminator on *PhTAC125 aspC* gene (*TaspC*), an origin of conjugative transfer (*OriT*), the pMtBLderived replication origin for the maintenance in *PhTAC125* (*OriR*) and the pUC18-derived replication origin for

the propagation in *E. coli* (OriC). Restriction sites outside the MCS that have been used for cloning purposes are indicated. (B) The sequence encompassing the 5' UTR and the MCS of the two plasmids included between *P_{lacZ}* and *TaspC* is illustrated using the coordinates of pP79. The +1 of the mRNA and the start ATG are indicated in red and bold black, respectively.

2.3. Sub-Cloning of Heterologous Genes into the Expression Plasmids

The expression plasmids used in this work are reported in Table S3. pMAV-*lacZ* was prepared in a previous study [3] and was used to isolate the psychrophilic β -galactosidase encoding gene for the construction of pP79-*lacZ*. In particular, *lacZ* was split into two different fragments: one of 1.2 kb with NdeI/NcoI extremities and the second of 2.3 kb with NcoI/XbaI extremities. The two gene fragments were ligated with pP79 opened with NdeI and XbaI restriction sites. For the conversion of pP79-*lacZ* into p79C-*lacZ*, the same approach described in Section 2.2 was employed: the regulatory *lacR* gene and *lacZ* were isolated using SphI/SacI double digestion and inserted into pUCC hydrolyzed with the same enzymes.

The *R9-gfp* gene was taken from pET-21b-*R9-gfp* [18] using NdeI and HindIII restriction sites. In the detail, the HindIII digestion was performed first and then the extremities of the hydrolyzed vector were filled by Klenow reaction. After NdeI digestion, the *R9-gfp* gene was cloned into pMAV with NdeI/filled-EcoRI extremities. pMAV-*R9-gfp* was then converted into pP79-*R9-gfp* by replacing pMAV typical expression sequences with the ones of pP79. To do so, Scal/NdeI double digestion was used to isolate the pP79 fragment encompassing its promoter and its regulatory gene (2.1 kb). This was cloned into the pMAV-*R9-gfp* backbone devoid of the *gaIT* expression sequences isolated with the same restriction sites (3.6 kb). pP79-*pGFP* was designed to drive the expression of a codon optimized version of the eGFP [19]. Composition optimization of the *pGFP* for the codon usage of *PhTAC125* was automatically performed with the Optimizer web tool using the “guided random” method [20]. The synthesized gene (Thermo Fisher Scientific, Waltham, MA, USA) was cloned into pP79 using NdeI and KpnI restriction sites.

p13C-*lacY* and pFC-*lacY* were the two constructs used for the constitutive expression of *E. coli lacY* gene. Briefly, the gene encoding the mesophilic lactose permease was synthesized by Thermo Fisher Scientific (Waltham, MA, USA) following a sequence optimization for the codon usage of *PhTAC125* [20] and adding a *c-myc* encoding sequence at its 3' extremity. The insert harbored NdeI and KpnI restriction sites at its 5' and 3' ends, respectively, and was cloned into

p13C and pFC vectors using the same sites. p13C is a plasmid containing the P13 promoter and a chloramphenicol resistance gene. It was built by fusing P13 sequence taken from pPM13 [1] using HindIII/XbaI double digestion with pUCC [4] hydrolyzed with the same enzymes. pFC contains the constitutive promoter of the *PhTAC125 aspC* gene and was already available [21].

The complete sequences of genes introduced in this study are reported in the Appendix A and Supplementary Material.

2.4. Preparation of pVS-*lon* and pVS-*lacY* Suicide Vectors

For the construction of *lon* mutant, two DNA fragments of *PhTAC125 lon* gene (A and B) were amplified by PCR using bacterial genomic DNA as the template. Two primer pairs were designed to amplify a 305 bp region at the 5' end (*lonA_SphI* fw, *lonA_SacI* rv) and a 233 bp region at the 3' end (*lonB_SacI* fw, *lonB_EcoRI* rv) of *lon* gene. The obtained amplicons were subjected to SphI/SacI and SacI/EcoRI double digestions respectively and cloned into the pVS [22] previously digested with SphI and EcoRI, resulting in pVS-*lon* vector.

The construction of pVS-*lacY* was performed starting from the recovery of the fragment P13-*lacY* from p13C-*lacY* vector through hydrolysis with HindIII and KpnI. Then two fragments (B and B') at the 3' end of *PhTAC125 lon* gene were amplified by PCR. The reactions were carried out using the genomic DNA as the template and allowed the amplification of a fragment of 233 bp (*lonB_SphI* fw, *lonB_HindIII* rv) and one of a 170 bp region (*lonB'_HindIII* fw, *lonB'_EcoRI* rv). SphI/HindIII and KpnI/EcoRI double digestions were performed on the obtained amplicons, respectively. The fragment B carrying SphI/HindIII extremities and P13-*lacY* hydrolyzed with HindIII/KpnI were cloned into pUCC vector, previously digested with SphI and KpnI. Afterward, the obtained intermediate vector pUCC-*lonB*-P13-*lacY* was digested with SphI and KpnI to extract the fragment *lonB*-P13/*lacY*. This fragment was finally cloned together with the second amplicon B' hydrolyzed KpnI/EcoRI into pVS adequately digested with SphI and EcoRI, resulting in pVS-*lacY*.

2.5. Transformation of KrPL and Selection of the *lon* and *lacY*⁺ Mutant Strains

The recombinant vectors were mobilized into KrPL by intergeneric conjugation [14]. The selection of recombinant transconjugants was performed at 15 °C in the presence of 50 µg/mL kanamycin and either 100 µg/mL ampicillin or 12.5 µg/mL chloramphenicol, depending on the specifically employed vector. As for the mutant strains, the

transconjugants were selected at 15 °C in the presence of 50 µg/mL kanamycin and 30 µg/mL carbenicillin.

2.6. *gDNA Extraction from the Mutant Strains and Sequence Analysis*

Genomic DNA extraction from KrPL mutants and *PhTAE79* was performed using the Bacterial DNA kit (D3350-02, E.Z.N.A™, OMEGA bio-tek, Norcross, GA, USA) following the manufacturer's instructions. The insertion of the suicide vectors into the cells was verified by PCR analysis with a NEB Taq DNA polymerase (New England Biolabs, Hitchin, UK). The genomic DNA was used as the template of the reactions and two couples of primers were used for the amplification of *amp(R)* (*bla_fw*, *bla_rv*) and *pheS* (*pheS_fw*, *pheS_rv*) genes. Then, further PCR analysis was performed to identify the insertion site into *lon* gene. The couples of primers used for this purpose are: *lonA_SphI fw*, *lon_rv* and *lon_fw*, *lonB_EcoRI rv*, for the analysis of *lon* mutants; *lonY_fw*, *lacY_rv* and *lacY_fw*, *lonY_rv*, for the analysis of *lacY⁺* mutants.

2.7. *Recombinant Production of the Reporter Proteins*

Glycerol stocks (-80 °C) of KrPL recombinant strains were streaked over TYP agar selective plates. After three-five days of incubation at 15 °C, a single colony was inoculated in 2–3 mL of TYP at 15 °C for one day. To grow the bacteria in GG, they were routinely trained in the same medium with two subsequent 1/100 dilutions within a time frame of 24 h. The actual inoculum was generally performed in the liquid medium filling an Erlenmeyer flask by 20% of its volume and with a starting OD600 of 0.1. For recombinant expression at 15 °C, the cells were generally induced in late exponential phase (OD600 = 1) about 13 h after the initial dilution. Strains harboring pMAV derived vectors were induced with 10 mM D-galactose, while pP79 and p79C carrying strains were treated with different concentrations of either IPTG or lactose. Expression trials were attempted also at 0 °C in a similar way as described above. In this case, Erlenmeyer flasks were filled by 35% of their volume to stem oxidative stress and the growths lasted several days considering that KrPL generation time was about 24 h at 0 °C. In most of the experiments, a Biosan PSU-20i orbital shaker was used setting the agitation at 180–220 rpm.

2.8. *Analysis of the Production of the Recombinant Proteins*

For the analysis of the β-galactosidase production, 10 OD600 pellets were harvested during the cultures by centrifugation (5000x g for 5 min

at 4 °C) and resuspended in 0.4 mL of Lysis buffer (100 mM sodium phosphate buffer pH 7.5, 2% (v/v) Triton X-100, 1 mM DTT, 5 mg/mL lysozyme). After 20 min of incubation at 15 °C, the samples were centrifuged (10,000× *g*, 15 min, 4 °C) and the supernatants were used in the following enzymatic measurements with ONPG as a substrate. The spectrophotometric assays were performed in triplicate as reported by Hoyoux et al. [8] and the data analysis was carried out using the ONPG extinction coefficient at 410 nm ($3.5 \text{ mM}^{-1} \text{ cm}^{-1}$) and the total protein concentration measured with the Bradford assay (Bio-Rad Laboratories, Hercules, CA, USA).

To monitor the production of fluorescent proteins, 1 OD600 of liquid cultures was centrifuged at 5000× *g* for 5 min at 4 °C and the pellets were resuspended in 0.5 mL PBS. Then, the samples were serially diluted to achieve the best signal to noise ratio in fluorescence measurements and the dilution factor was used for normalization. Fluorescence measurements were conducted with a JASCO FP750 spectrofluorometer at 25 °C with an excitation wavelength of 488 nm (slit 3 nm), an emission wavelength of 509 nm (slit 6 nm) and an integration time of 0.10 s.

The production of the recombinant proteins was also monitored by SDS-PAGE, by loading 20 µg of soluble cellular extracts onto the wells of 10% denaturant gels. The cellular homogenization was carried out through the chemical-enzymatic method indicated at the beginning of this section and the total protein concentration in the soluble fractions was estimated with the Bradford method. In the case of GFP producing strains, we also checked for the synthesis of the recombinant proteins in total lysates to control their solubility. Nevertheless, the presence of R9-GFP and pGFP was never visible both in the soluble and total extracts when run onto SDS-PAGE.

To verify the presence of the truncated form of Lon protease, 1 OD600 cell pellets were collected by centrifugation and solubilized in 60 µL of Laemmli buffer 4X. Then, the samples were boiled at 95 °C for 20 min, quickly cooled on ice for 5 min and finally centrifuged at 10,000× *g* for 5 min at RT. 5 µL of samples were analyzed by SDS-PAGE. 4–15% Mini-Protean TGX (Biorad) gels were used in TGS buffer setting the power supply to constant 120 V. For electroblotting, the Biorad Transblot Turbo system with Biorad PVDF mini membranes was used employing the mixed molecular weight setting. After the transfer, the membrane was blocked with PBS, 0.05% Triton X-100, 5% (*w/v*) milk for one hour. Then, an anti-Lon antiserum (ab103809) was diluted 1:1,000 in the same buffer. After one hour of incubation at RT with the primary antibody, the membrane was washed with PBS, 0.05% Triton

X-100 three times (5 min each) and incubated with an anti-rabbit antibody diluted 1:30,000 in PBS, 0.05% Triton X-100, 5% (w/v) milk for one hour at RT. Then, the membrane was washed again with PBS, 0.05% Triton X-100 three times (5 min each) and the secondary antibody was detected using the ECL method.

2.9. mRNA Extraction and qPCR

Total RNA was isolated from the cells using the Direct-zol RNA Kit (Zymo Research, Irvine, CA, USA) following the manufacturer's instructions. Contaminating genomic DNA was then removed through treatment with RNase-free DNase I (Roche, Mannheim, Germany). Total RNA was reverse transcribed using SuperScript IV (Invitrogen, Carlsbad, CA, USA) according to the recommended protocol. The primers used for this reaction are listed in Table S2. Quantitative real-time PCR was performed on cDNA from each sample by using PowerUp SYBR Green Master Mix (Applied Biosystems, Foster City, CA, USA) implemented with the specific primers (listed in Table S2) in StepOne Real-time PCR System (Applied Biosystems, Foster City, CA, USA). The housekeeping gene *PSHA_RS01090* was chosen as the normalizer. The expression level of the gene of interest was assayed for up-regulation in experimental samples in comparison to a calibrator sample (NI). The relative quantification of mRNA was expressed as fold-change and was calculated through the standard curve method [23]. Three independent sets of experiments were performed.

3. Results

3.1. Analysis and Cloning of the *PhTAE79 lacZ* Expression Sequences

The *PhTAE79* genome has been sequenced in the framework of a WGS project involving several Antarctic *Pseudoalteromonadales* [24], but it was neither assembled nor annotated. The *lacZ* gene is in the AUTL01000130.1 contig according to the GenBank notation, whose predicted genes distribution has been schematized in Figure 1. In this ~24 kb region, *lacZ* clusters with other genes involved in carbohydrates and amino acids metabolism (Figure 1, blue arrows) and, intriguingly, with three predicted CDSs involved in cut and paste mechanisms (black arrows) and a putative RepB protein involved in plasmid replication (red arrow) [25]. In particular, the RepB is highly conserved (65–95% nucleotide identity) in plasmids harbored by three marine *Pseudoalteromonadales*, *P. haloplanktis* TAC125 (MN400773.1), *P. nigrificans* KMM 661 (CP011038.1), *P. arctica* A 37-1-2 (CP011027.1), whose reciprocal similarities have been recently

examined [26]. Considering that the whole analyzed contig is almost totally conserved in *P. nigrifaciens* plasmid (88% coverage with 99% identity), it is very likely that the DNA containing the *lacZ* gene is the result of horizontal gene transfer also in *PhTAE79*.

Upstream and divergent to *PhTAE79 lacZ* is a gene predicted to encode an AraC family transcriptional regulator (one of the two green arrows in Figure 1), which probably regulates the β galactosidase mRNA synthesis and, for this reason, it will be named LacR from now on. Hoyoux et al. used a combination of lactose and IPTG to induce the production of the β -galactosidase in *PhTAE79* and reported that IPTG addition led to an increased protein yield [8]. We confirmed this outcome by inducing *lacZ* expression in *PhTAE79* using IPTG as the only inducer molecule (data not shown). This suggests that LacR is probably regulated by this small allolactose analog.

Persuaded by this preliminary data, we developed a shuttle vector, named pP79, containing *PhTAE79 lacR-lacZ* regulatory elements. In detail, a PCR was designed to amplify the LacR CDS with its putative transcriptional terminator and promoter together with the predicted *lacZ* divergent promoter, its 5' UTR and initial ATG. Then, the amplicon was cloned into the shuttle vector pUCLT/Rterm [2,17], so to have the pP79 plasmid. To make this expression system compatible with other constructs, we also developed its chloramphenicol resistant version, p79C, by ligating pP79 expression cassette with the pUCC vector (Figure 2A) [4]. The transcription start of the *lacZ* gene indicated in red in Figure 2B was identified with a primer extension assay (data not shown).

3.2. Quantification of pP79 Activity Using β -galactosidase and R9-GFP Reporters

3.2.1. Comparison between pP79 and pMAV Efficiencies

To test the usefulness of pP79, we compared its performance with our most recent inducible expression system, pMAV [3]. To this aim, we used two different reporter genes, *PhTAE79 lacZ* that has been employed for the characterization of all the expression plasmids in *PhTAC125* so far [1–3], and *R9-gfp* which encodes a GFP variant tagged with an N-terminal R9 peptide [18]. In particular, the GFP protein encoded by this construct harbors the eGFP mutations for enhanced fluorescence [19] and the Cycle 3 mutations for improved folding [27]. To ensure plasmids stability, the recombinant constructs were mobilized into KrPL, a *PhTAC125* strain cured of its endogenous plasmid pMtBL (unpublished results from this laboratory). The β -

galactosidase production in KrPL pMAV-*lacZ* was carried out by D-galactose induction in the defined medium GG at 15 °C [3]. In the case of KrPL pP79/*lacZ* strain, a 1–10 mM IPTG range was tested for induction in the same growth conditions and the levels of accumulated recombinant protein were measured after overnight expression. pP79 proved to guarantee a higher enzymatic specific activity at all the tested inducer concentrations than pMAV, reaching a 20-fold higher production when 10 mM IPTG was used (Figure 3A). This result was confirmed by assessing the fluorescence emitted by R9-GFP producing strains at 15 °C (Figure 3B). When induced with 10 mM D-galactose, pMAV-*R9-gfp* bearing cells had a fluorescence that was at the same level as the autofluorescence of non-recombinant *PhTAC125*. Conversely, KrPL pP79-*R9gfp* showed a detectable protein accumulation over time when 10 mM IPTG was added to the culture.

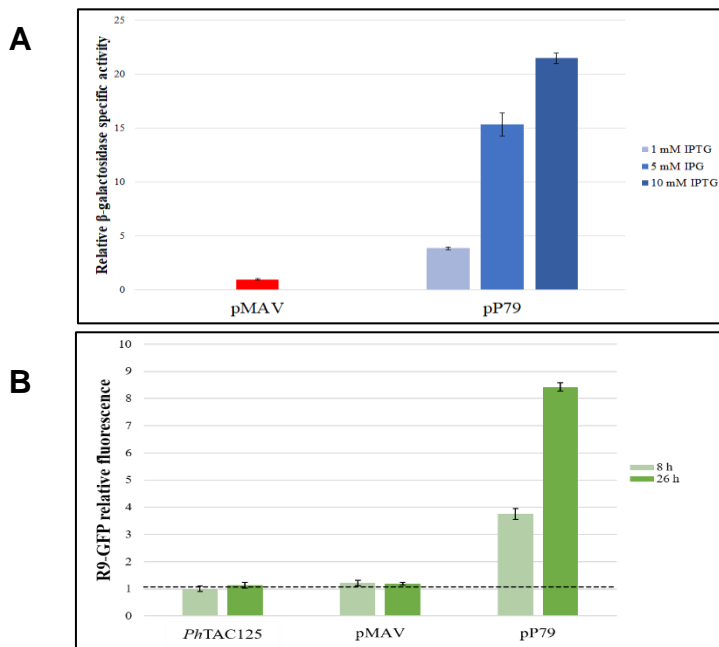


Figure 3. Quantification of the relative strengths of pMAV and pP79-driven expression of *lacZ* and *R9-gfp* genes at 15 °C. **(A)** β -galactosidase production measured with an enzymatic assay. Logarithmic cultures of KrPL pMAV-*lacZ* and KrPL pP79-*lacZ* strains were exposed to 10 mM D-galactose and 110 mM IPTG, respectively. After 26 h expression, the β -galactosidase activities were assayed. The enzymatic specific activities are reported as measures normalized by pMAV-*lacZ*. **(B)** R9-GFP synthesis was triggered with 10 mM D-galactose in the case of pMAV-*R9-gfp* bearing strain and with 10 mM IPTG in the case of KrPL pP79-*R9-gfp*. The recorded fluorescence intensities were scaled to the autofluorescence of wild-type cells (*PhTAC125* bars and horizontal dashed line). Levels of β galactosidase activity and fluorescence are expressed as mean \pm SD, $n = 3$.

3.2.2. Evaluation of the Reliability of *lacZ* and *R9-gfp* as Reporter Systems

Although the two reporter systems consistently demonstrated that pP79 guarantees a higher recombinant production than pMAV, the fluorescence-based approach suffered from lower sensitivity because pMAV-driven R9-GFP production could not be distinguished from the background noise (Figure 2B). To define if this drawback was due to the intrinsic different sensitivities of the two assays or to a discrepancy in the absolute production of the two reporters, further analyses were carried out. First, we monitored the β -galactosidase productions via SDS-PAGE, which allowed us to detect the presence of the recombinant enzyme both in KrPL pMAV-*lacZ* and KrPL pP79-*lacZ* induced strains (Figure 4A). As expected, even when the lower IPTG concentration of 1 mM was used, the intensity of the estimated 118 kDa band was higher in the cellular extract of KrPL pP79-*lacZ* than the one observable in KrPL pMAV-*lacZ* induced lysate (lanes 2 and 4 in Figure 4A, respectively). However, no protein band was visible in induced KrPL strains producing R9-GFP at the expected molecular weight of 28 kDa, regardless of the employed plasmid and inducer concentration (Lanes 5 and 6 in Figure 4A). To define if this different accumulation of the two recombinant proteins was related to transcriptional issues, *lacZ* and *R9-gfp* mRNAs produced by pP79 were quantified through quantitative real-time PCR. The results were expressed as foldchanges to compare the relative amount of *lacZ* and *R9-gfp* mRNA produced both in the presence and in the absence of IPTG. As reported in Figure 4B, a rapid increase of mRNA and a significant accumulation during the time were observed for both the reporters.

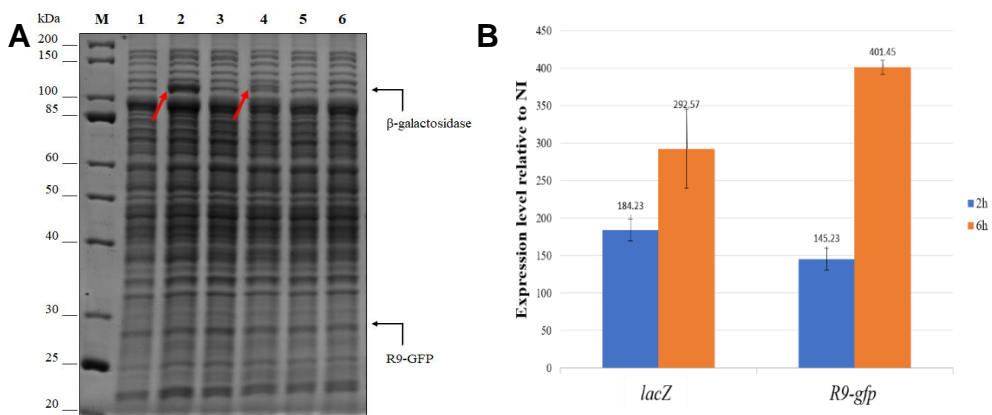


Figure 4. β -galactosidase and R9-GFP proteins productions (panel A) and their respective mRNA transcriptions (panel B). (A) SDS-PAGE analysis of cell extracts of KrPL strains producing the β galactosidase (lanes 1–4) and R9-GFP (lanes 5–6). The

induction was performed with 10 mM Dgalactose for pMAV carrying strains and with 1 mM IPTG for pP79 bearing cells and protracted for 26 h. M, molecular weight marker; 1, non-induced pP79-*lacZ*; 2, induced pP79-*lacZ*; 3, non-induced pMAV-*lacZ*; 4, induced pMAV-*lacZ*; 5, induced pP79-*R9-gfp*; 6, induced pMAV-*R9-gfp*. Black arrows on the right of the gel represent the expected molecular weights of the recombinant proteins. Red arrows inside the gel highlight the bands of the β -galactosidase. **(B)** Relative quantification by RTqPCR of mRNA expression levels of *lacZ* and *R9-gfp*. Two genes under the control of the PlacZ promoter were analyzed for their mRNA expression levels after 2 and 6 h from the induction in comparison to the non-induced condition. The reported results are the mean of three independent experiments.

Taken together, these results prove that R9-GFP production is considerably less efficient than the one of the psychrophilic β -galactosidase in *PhTAC125* and that this phenomenon is unrelated to transcriptional issues. To determine if the N-terminal polyarginine moiety of R9-GFP and its Cycle 3 mutations were the cause of such a low protein yield, we designed an automatically codon optimized gene encoding the eGFP devoid of any N-terminal tag and sequence mutations other than the ones needed for increased fluorescence. This protein was named pGFP and its fluorescence levels were compared with the ones of R9-GFP using pP79 plasmid. The fluorescence of KrPL cultures was significantly higher when R9-GFP was produced (Figure S1), suggesting that this construct is characterized by improved properties in comparison to the canonical eGFP also at low temperatures.

3.2.3. Influence of Medium Composition on pP79 Efficiency

We performed all our expression trials in GG, a defined medium whose only carbon sources are D-gluconate and L-glutamate [3]. The uptake of substrates is hierarchical in *PhTAC125* [7,28] and specific amino acid combinations had to be formulated in the past to guarantee the optimal induction of another psychrophilic expression plasmid in this bacterium [5]. To understand if this kind of interference could be experienced also using pP79, we measured the achievable levels of β galactosidase production when KrPL pP79-*lacZ* was grown in TYP, a complex medium containing yeast extract and bacto-tryptone. The growth curves of the recombinant bacteria cultivated in GG and TYP at 15 °C are reported in Figure S2A,B, respectively. As observable in Figure S2C, the performance of the expression plasmid was similar in the two media when the lower IPTG concentration (1 mM) was reached in the cultures. On the other hand, at the two higher tested IPTG concentrations the β -galactosidase production was less efficient in the

complex broth, indicating that in those conditions some negative effects took place.

3.3. Optimization of IPTG Transport Mechanism

3.3.1. Attempts in the Plasmidic Expression of a Lactose Permease

For an in-depth study of the pP79 system, the influence of the IPTG transport mechanism was evaluated in relationship to protein expression. The requirement of a high concentration of IPTG (10 mM) to reach full induction and the absence of the lactose metabolic pathway in *PhTAC125* [29] suggest the potential absence of high-affinity IPTG transporters in this bacterium. If so, the mechanism by which the inducer penetrates within the cells is supposed to be either simple or facilitated diffusion.

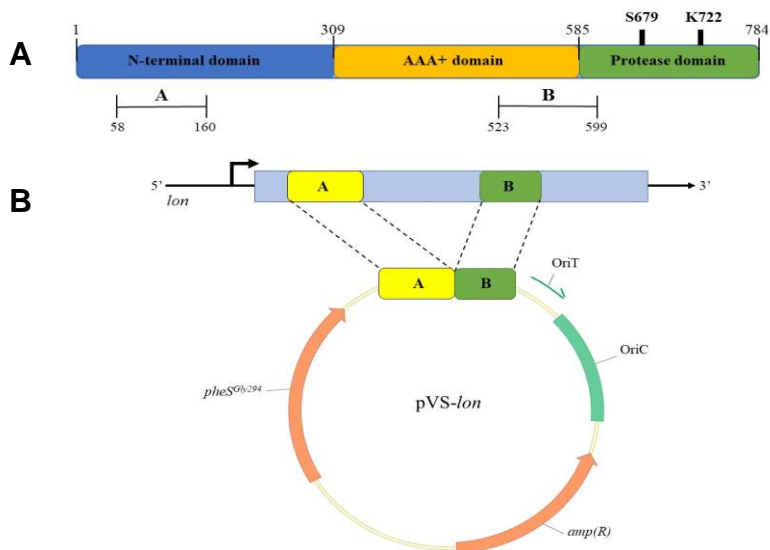
This observation led us to examine whether the heterologous expression of a suitable lactose permease could deliver a significant contribution to the optimization of the pP79 system. Since the *E. coli* LacY transporter has already been successfully used in other Gram negative bacteria [30], its encoding gene was optimized for the codon usage of *PhTAC125* and cloned into pFC [21] and p13C, a pPM13 derivative [1]. These constitutive psychrophilic expression plasmids possess a medium and a strong promoter, respectively [1]. However, no transconjugant clones resulted from the mobilization of both plasmids into KrPL, probably due to toxic effects on the cell membrane deriving from the excessive production of the permease (data not shown). An alternative strategy was then applied through the integration of *E. coli lacY* gene into the genome of KrPL.

3.3.2. Construction of KrPL *lon* and *lacY*⁺ Mutant Strains

To ensure a subtoxic level of LacY in KrPL a mutant strain was developed so that the production of the permease derived from a single copy of *lacY*, integrated within the host genome.

Firstly, we focused on the selection of the target gene for the integration of *lacY*. To obtain a mutant strain displaying improved features as a host for recombinant protein production, the centerpiece of our analysis was the set of genes coding for proteases that are constitutively expressed in *PhTAC125* and are involved in the proteolytic process of recombinant proteins. The Lon protease encoding gene (*PSHA_RS10175*) was chosen as the target of mutagenesis because it represents the major protein quality control protease and, as such, is responsible for most of the ATP-dependent degradation of misfolded proteins in bacteria [31]. Despite this protease is involved in a wide

range of cellular functions (from proteins degradation to DNA replication and recombination, stress response, motility and biofilm formation), it is not an essential enzyme in many bacterial species such as *E. coli* [32]. To evaluate the consequence of *lon* disruption in *PhTAC125*, a first mutant strain was constructed through a two-step integration–segregation approach using pVS, a suicide vector suitably constructed for *PhTAC125* [22]. Two internal gene fragments of *lon* were chosen as homologous sequences for the recombination event, amplified by PCR and cloned into pVS, resulting in pVS-*lon*. The first fragment (named A) is located into the sequence encoding the N-terminal domain of Lon, while the second fragment (named B) includes the sequence encoding the region straddling the ATPase domain and the proteolytic domain (Figure 5A). Since two different crossingover events could occur, depending on which fragment underwent recombination, the two homologous regions were selected in order to provide the disruption of the whole Lon protease in the case of recombination of fragment A or the deletion of its proteolytic domain in the case of recombination of fragment B (Figure 5B). Once obtained, pVS-*lon* was mobilized into KrPL by intergeneric conjugation and a single recombination event allowed the vector insertion on the genome. PCR analyses demonstrated that the insertion occurred in fragment B of the gene (data not shown) resulting in a mutant that contains two non-functional copies of the *lon* gene. The first one encodes a truncated form of the Lon protease because it is devoid of the fragment B downstream sequence, coding for the active site domain of the protease. The second copy is not transcribed because it lacks its promoter and the 5'-encoding region (Figure 5C).



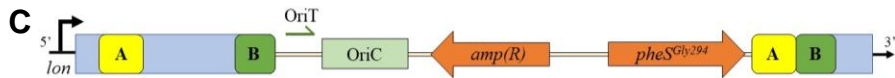


Figure 5. Construction of KrPL *lon* mutant strain. **(A)** Domain organization of Lon protease. The N-domain is involved in substrate recognition and binding; the AAA+ domain contains the ATPase module; the Protease domain is responsible for proteins degradation. S679 and K722 represent the catalytic dyad of the proteolytic domain. Fragments A and B encoding sequences were chosen as recombination regions. **(B)** Schematic representation of pVS-*lon* vector. **(C)** Genetic organization of KrPL *lon* selected mutant.

The presence of the truncated form of Lon was evaluated through Western blot analysis carried out on total KrPL cellular extracts with a polyclonal anti-Lon antiserum. As shown in Figure 6, the Lon band signal was detected at different heights in the wild-type and the mutant strains: the first one exhibited a band compatible with the expected molecular weight of the full-length protein (87.4 kDa, lane 1 in Figure 6), whereas the lower band of the mutant strain was clearly the truncated form (lane 2 in Figure 6). Indeed, the partial deletion of the first copy of the *lon* gene caused the loss of 564 bp at the 3'-region, generating a truncated protein with a theoretical size of 66 kDa.

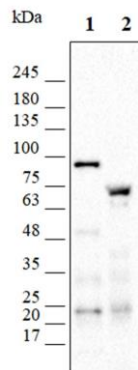


Figure 6. Western blot analysis carried out with anti-Lon antiserum. Total cellular extracts of KrPL wt and *lon* mutant were analyzed through Western blot analysis. Lane 1 shows a signal corresponding to the full-length form of Lon protease (expected size 87.4 kDa) in the wt strain. A lower band (theoretical size of 66 kDa) is detected in the selected *lon* mutant strain corresponding to the truncated form of the protein.

The growth behavior and the fitness of *lon* mutant were then compared to the wt strain and no deleterious effects took place (Figure S3). Thus, *lon* was confirmed as the target of insertion of *EclacY* gene and the strain mutated in *lon* was used as its isogenic control. With this purpose, an expression cassette—consisting of the strong constitutive psychrophilic promoter P13 [1] and the *E. coli lacY* gene—was

designed and included between two intragenic fragments of the *lon* gene. The entire construct was then cloned into pVS resulting in pVS-*lacY*. With a similar strategy used for the obtaining of the *lon* mutant strain, pVS-*lacY* was designed to obtain a truncated Lon protease devoid of its proteolytic domain. To do this, the fragment B, already used for the construction of KrPI *lon*, and the fragment B', including the upstream region of the active site of Lon, were chosen as target sequences (Figure 7A).

The obtained pVS-*lacY* was then mobilized into KrPL through interspecies conjugation and the genomes of the mutant clones were analyzed by PCR to define the presence and the orientation of the insertion (data not shown). Here too, the recombination event occurred in fragment B, succeeding in the disruption of *lon* and insertion of *lacY*. The obtained KrPL *lacY*⁺ mutant strain is potentially capable of producing a lactose permease and a truncated form of Lon protease (Figure 7C).

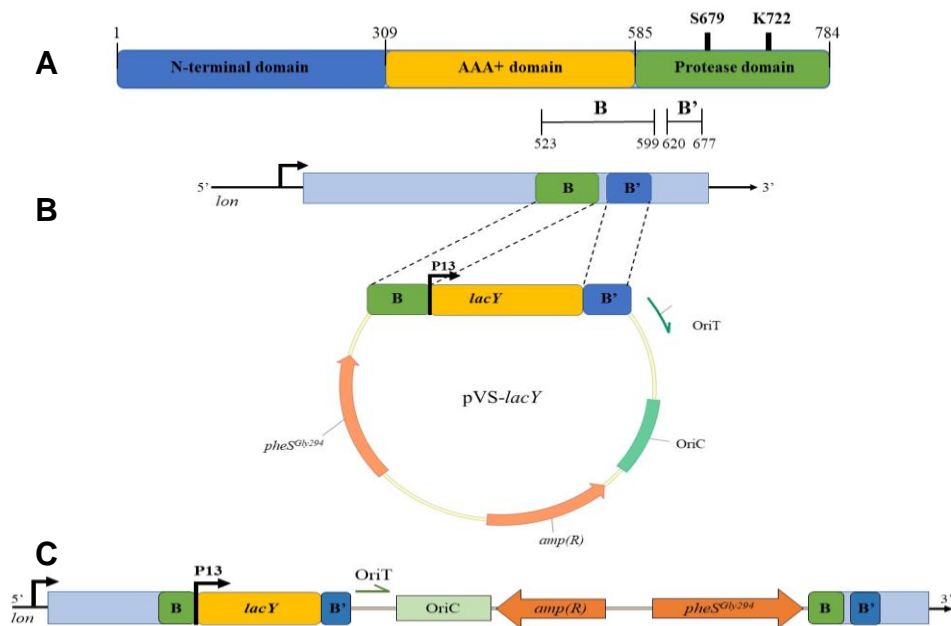


Figure 7. Construction of KrPL *lacY*⁺ mutant strain. **(A)** Domain organization of Lon protease. The Ndomain is involved in substrate recognition and binding; the AAA+ domain contains the ATPase module; the Protease domain is responsible for proteins degradation. S679 and K722 represent the catalytic dyad of the proteolytic domain. Fragments B and B' encoding sequences were chosen as recombination regions. **(B)** Schematic representation of pVS-*lacY* vector. **(C)** Genetic organization of KrPL *lacY*⁺ selected mutant.

3.4. Comparison between the Performance of *KrPL lon* and *KrPL lacY⁺* Strains

3.4.1. Evaluation of the Production Improvement at Different Temperatures

To study whether the lactose permease provides an improvement to the transport of IPTG within the cell, the recombinant production of β -galactosidase was performed in *lacY⁺* in comparison to its isogenic control, *lon* mutant. Both strains were transformed with the expression vector p79C*lacZ* and grown in GG medium at 15 °C. During the middle exponential growth phase, the induction was performed with different concentrations of IPTG. In particular, 0.05 mM, 0.1 mM, 0.5 mM, 1 mM IPTG was added to the culture to examine the difference in β -galactosidase production. The β galactosidase activity was then assayed in the soluble cellular extracts recovered 8, 24, 32 and 48 h after the induction. As shown in Figure 8A, the highest production was achieved with the *lacY⁺* mutant and proved to be about 5-fold superior to *lon* strain. In the tested range of IPTG concentration, a direct proportionality between the inducer amount and production level was observed in both strains, but with a higher slope in *lacY⁺* mutant. As an example, Figure 8B highlights the linear correlation between β -galactosidase activity and IPTG concentration for the last data points. Bacterial cells containing the lactose permease yielded high levels of production both with 0.5 mM and 1 mM IPTG. However, the increase of inducer concentration in this range only drove a slight improvement in recombinant production. This is probably due to the decrease in the contribution of the lactose permease in the IPTG uptake when its concentration is relatively high, compatibly with its saturation. Furthermore, these results highlight that the minimum concentration of IPTG needed for the induction of expression in the strain containing the LacY transporter is 10-fold lower in comparison with the strain lacking the permease. When the induction of *lacZ* expression was performed with 0.05 mM and 0.1 mM IPTG in *lon* mutant, no difference in β -galactosidase activity is observed in comparison to the non-induced cells (NI). Hence, the lactose permease is a very important contributor in transporting IPTG across the *PhTAC125* membrane.

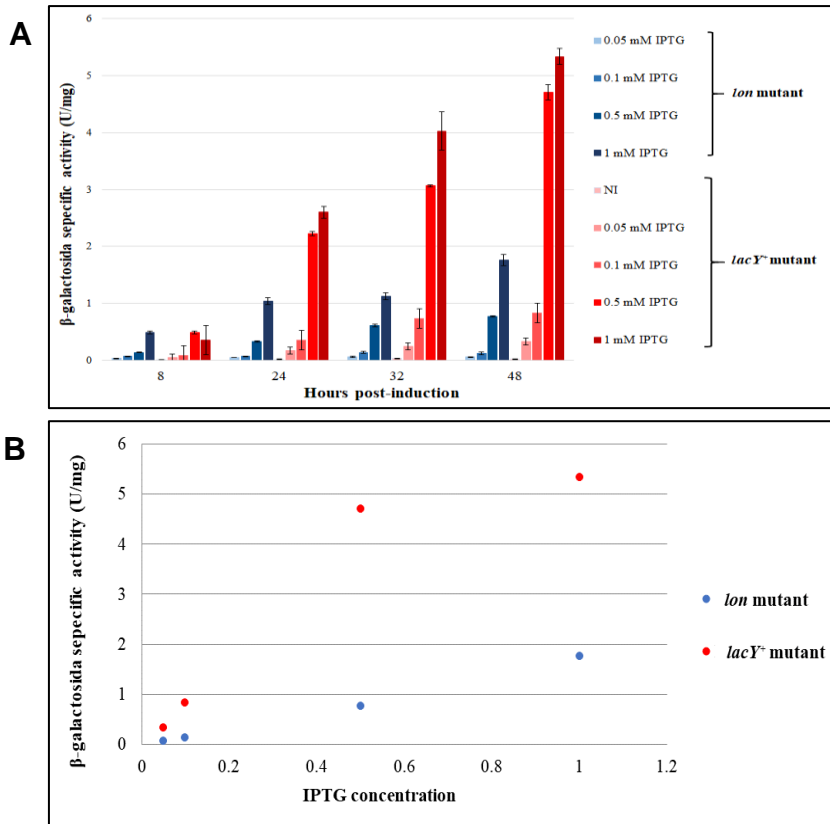


Figure 8. Evaluation of production performance of KrPL *lon* and *lacY*⁺ mutant strains. **(A)** β galactosidase specific activity (U/mg) in *lacY*⁺ and *lon* mutant cells harboring p79C-*lacZ*, collected after progressive times of induction, in GG medium at 15 °C using different concentrations of inducer. Levels of β -galactosidase activity are expressed as mean \pm SD, $n = 3$. **(B)** Analysis of the relationship between IPTG concentrations and β -galactosidase specific activity measured after 48 h of expression in *lacY*⁺ and *lon* strains.

To verify that the mesophilic membrane protein is produced and functioning in the psychrophilic bacterium even at ultra-low temperatures, the recombinant production of β galactosidase was performed at 0 °C using 0.5–1 mM IPTG. The levels of the reporter protein were then assayed after 24, 48 and 72 h from the induction. The specific activity of β -galactosidase measured in *lon* mutant highlights a poor accumulation of the protein, suggesting that the response of the system is owing to the basal expression of the protein (Figure 9). On the contrary, the effect of LacY in the transport of IPTG is noticeable already after 24 h of expression, with an enhancement of the production in *lacY*⁺ strain of about 1.5-fold in comparison to *lon* cells treated with the same inducer concentration. As with the expression trials at 15 °C,

0.5 and 1 mM IPTG triggered the same expression levels in *lacY*⁺ mutant also at 0 °C, except for the first time point where a higher recombinant production was guaranteed by increasing amounts of inducer.

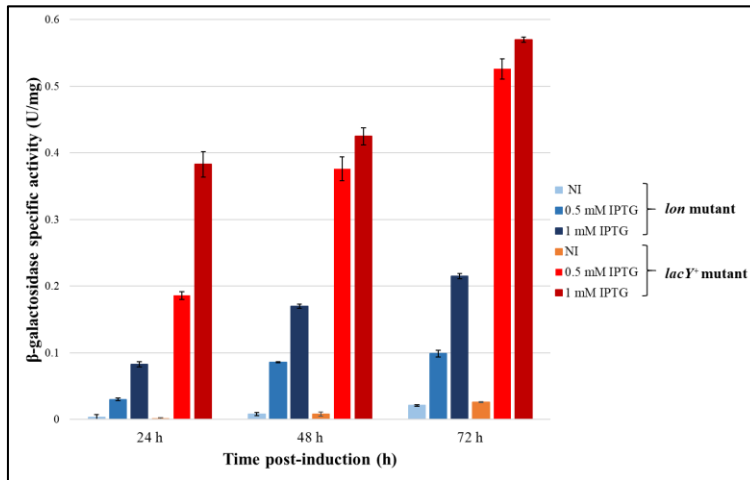


Figure 9. Evaluation of production performance of KrPL *lon* and *lacY*⁺ mutant strains at 0 °C. βgalactosidase specific activity (U/mg) in *lacY*⁺ and *lon* mutant cells harboring p79C-*lacZ*, collected after progressive times of induction, in GG medium at 0 °C using different concentrations of inducer. Levels of β-galactosidase activity are expressed as mean ± SD, *n* = 3.

3.4.2. Evaluation of β-galactosidase Production Using Lactose as an Inducer

A further demonstration of the functioning of *EcLacY* transporter in the mutant strain was performed through the recombinant expression of *lacZ* by using 2% (w/v) lactose as an inducer. As shown in Figure 10A, a rapid increase in β-galactosidase activity was observed in *lacY*⁺ strain after the first 4 h of expression, while no production was detected in *lon* mutant. Nonetheless, after 8 h of induction, the amount of recombinant protein took a decreasing trend. This can be traced back to a toxic effect observed when the cells can transport the lactose within the cells (Figure 10B). To better understand the reason for this occurrence, the growth behavior of the cells bearing pP79-*lacZ* and pP79 in the presence of lactose was compared. As reported in Figure 10B, only the cells capable of producing β-galactosidase showed cell death, suggesting that this effect was potentially caused by the metabolism and degradation of the disaccharide.

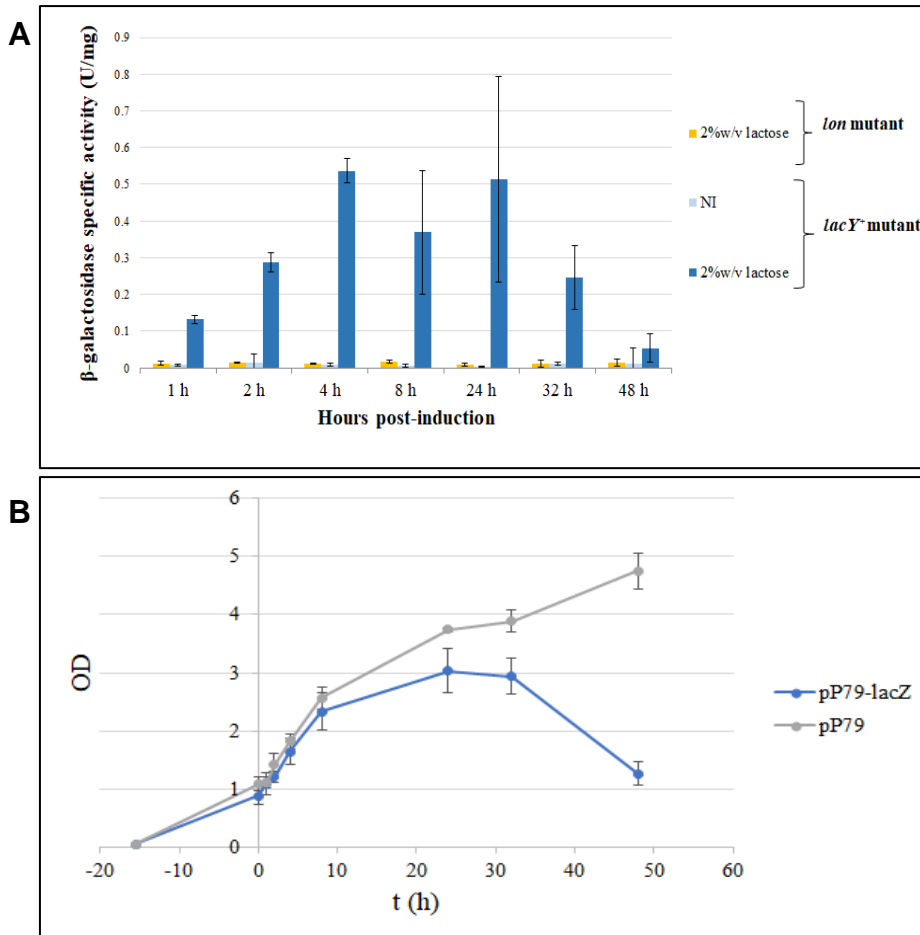


Figure 10. (A) Evaluation of β -galactosidase production in KrPL *lacY*⁺ strain using lactose as the inducer. β -galactosidase specific activity (U/mg) in *lacY*⁺ and *lon* mutant cells harboring p79C-*lacZ* collected after progressive times of induction in GG medium at 15 °C using 2% (w/v) lactose as inducer. Levels of β -galactosidase activity are expressed as mean \pm SD, $n = 3$. (B) Growth curves of KrPL *lacY*⁺ harboring p79C-*lacZ* and pP79 in the presence of 2% (w/v) lactose. The growth was performed at 15 °C in GG medium. The moment of the induction is represented by the intersection of the axes. The measures of optical density are expressed as mean \pm SD, $n = 2$.

4. Discussion

The ability to produce heterologous proteins with high yields is a prerequisite for the exploitation of a microorganism as a cell factory [33]. The psychrophilic bacterium *PhTAC125* represents a model as a non-conventional host for the production of difficult to express proteins in a soluble and active form [2,5,34,35]. In the present paper, the set of plasmids for controlled gene expression in *PhTAC125* and KrPL—a pMtBL deficient strain—has been expanded with the IPTG inducible

plasmid pP79. Moreover, the usability of this plasmid for different purposes has been widened by the development of an engineered KrPL strain. All our experiments were carried out in the cured *PhTAC125* strain to avoid instability issues possibly arising from the coexistence of pMtBL and pP79 or pMAV.

In our selection of a new expression system, we looked for characterized psychrophilic genes involved in carbohydrate catabolism with a clear regulator-catabolic gene asset. In this sense, the choice of the *lacR-lacZ* gene couple of *PhTAE79* was immediate, considering the high levels of β galactosidase produced by this bacterium [8] and the lack of *lacZ*-based inducible plasmids in other prokaryotes [33]. Rather than a disadvantage, the lack of lactose metabolism in the chosen host *PhTAC125* [29] can be seen as a possible prerequisite for a more predictable and tunable expression. As a matter of fact, the integration of a heterologous regulatory network in a new context can provide the basis to avoid undesired autocatalytic phenomena as the ones due to uneven and uncontrollable inducer transport [36] causing either bistable or “all-or-none” responses [37–39]. The main prerequisite needed for the functioning of *lacZ* induction in KrPL was the possibility of the internalization of its inducer. Both Hoynoux et al. [8] and our group demonstrated that IPTG could be used as a molecule regulating LacR activity. This reinforced our idea of implementing this recombinant system in KrPL, given the capability of this inducer to penetrate biological membranes in a diffusive manner also in transporter-deficient strains [30,36,40].

The pP79 vector proved to be more efficient than pMAV—a D-galactose inducible plasmid previously used in *PhTAC125* [3]. In particular, with the new system, we could accumulate a 20-fold higher quantity of β -galactosidase than pMAV-*lacZ* and we could detect the production of a fluorescent reporter for the first time in this bacterium. Moreover, we demonstrated that the growth broth composition had an impact on the levels of expression, i.e., a rich medium caused partial repression of the IPTG mediated induction of pP79. Understanding the underlying mechanisms of this negative regulation (e.g., inducer exclusion or repression of the regulator) will be important in the future to increase the extent of fine regulation that can be applied to pP79 [41,42]. However, it is worth noting that the deeply different formulations of the two used media gave rise to drastic different behaviors of the bacterial growths in general (Figure S2A,B). In particular, the use of TYP guaranteed the doubling of the specific growth rate and the final biomass concentration, suggesting that diversified metabolic networks are activated in this “feast” condition. Hence, to dissect the processes

that interfere with pP79 activity, slighter progressive modifications of the medium composition must be applied in the future.

Despite their promising features, KrPL pP79 recombinant strains needed high IPTG concentrations to reach maximal expression, a demand that could be prohibitive in large scale applications requiring induction levels as high as possible.

To approach this problem, we applied a strain engineering strategy based on the combination of the psychrophilic regulatory elements derived from *PhTAE79* with the mesophilic lactose permease LacY from *E. coli*. Despite the use of plasmids with a low copy number [26] and two different constitutive promoters with medium and high strength, the accumulation of the permease and the alteration of membrane properties probably caused serious toxic phenomena in *PhTAC125* [43]. This led to the failure of the first attempt of heterologous expression of LacY.

A further effort was made to modify the host cell to accommodate the production of the membrane protein through the integration of the *lacY* gene into the KrPL genome. Emphasis was concomitantly given to the control of the deleterious proteolysis of recombinant products with the final aim to design a more robust cell factory with improved features for various biotechnological applications. The novel mutant strain *lacY*⁺, constructed through a genome-scale manipulation, was characterized by a deletion in the proteolytic domain of Lon protease and the capability to produce the lactose transporter LacY in a functional form (Figure 7).

Previous analyses performed to characterize the truncated Lon protease suggest that it could act as a molecular chaperone [44]. Indeed, mutations in the active site abolish proteolysis but not ATPase activity, resulting in a protease that is still able to bind its substrates without degrading them [44]. The occurrence of the same phenomenon in KrPL mutant strains has to be proved by analyzing the production of more complex and unstable proteins than the ones studied in this work. The functional characterization of the *lacY*⁺ mutant highlighted great differences in the levels of the reporter protein produced in comparison to its isogenic control, *lon* strain (Figure 8A). Despite no changes in the growth behavior and kinetics were observed between the two strains (Figure S3), a 5fold increased protein accumulation was observed for *lacY*⁺, showing a higher slope of the direct proportionality between the production level and the inducer concentration. Owing to the cost and the possible cytotoxic effect of high concentrations of IPTG, this feature remarks the potentiality of *lacY*⁺ strain as a cell factory given the

advantage to use less inducer to reach the same level of recombinant production.

Furthermore, our novel mutant succeeded in the production of the mesophilic membrane protein in a functional form also at 0 °C, allowing the enhancement of the production levels of a reporter in comparison to its counterpart *lon* strain (Figure 9). This result is quite impressive, considering that the expressed lactose permease is naturally used to work at 37 °C and the known effects of the low temperatures on the membrane structure and composition [45].

Additional evidence to support the functionality of the transporter in *lacY*⁺ strain was then gained by inducing the recombinant production of the β -galactosidase with lactose. This experiment confirmed that little or no lactose molecule penetrates inside *lon* cells by either other facilitated transport systems or diffusion and LacY is required for the disaccharide internalization (Figure 10A). However, a deleterious effect on cell viability was observed in *lacY*⁺ cells, resembling a “lactose killing” phenomenon [46]. Surprisingly, the comparison of the growth behaviors of recombinant KrPL *lacY*⁺ bearing pP79-*lacZ* and pP79 highlights that the cause of the observed stress is not related to the de-energization caused by elevated transmembrane lactose transport. Instead, a toxic accumulation of its catabolic products likely takes place (Figure 10B). As a matter of fact, the only difference between the two used strains consists of the production of the β -galactosidase which is causative of the conversion of lactose to catabolic intermediates. For this reason, these experiments carried out with lactose must be taken as proof of LacY functioning in KrPL, rather than as an example of its actual use for induction purposes. *PhTAE79* LacR is predicted to be an AraC-type protein and we experimentally demonstrated that its activity is regulated by IPTG, an allolactose analog. Considering that we used a β -galactosidase as a reporter and that allolactose is a product of the reaction catalyzed by this enzyme [47], it is very likely that part of the observed lactose-mediated induction is due to the peculiar activity of this protein (see Appendix A and Figure A1). Accordingly, when we used the same approach for the expression of other genes than *lacZ* in KrPL *lacY*⁺ pP79, we could observe a lactose-mediated induction, but it was considerably lower than the one achievable with IPTG (data not shown), suggesting again that allolactose is probably the main inducer of this system. Our analysis of KrPL mutants demonstrated that LacY contributes to improving the recombinant production yield in *PhTAC125* when the *lacZ* promoter is employed. This finding is in agreement with most studies performed in *E. coli* and other Gram negative bacteria [30] and is noteworthy given that the IPTG uptake mechanism can be

mediated by lactose permease, passive diffusion, or other types of permeases [40].

Altogether, our data certify that in both KrPL *lon* and KrPL *lacY*⁺ strains an average graded production is possible upon IPTG induction (Figure 8B). Depending on the particular application, the two strains can be differently employed. As with the *E. coli* Tuner(DE3) strain (Novagen, [33]), either KrPL or KrPL *lon* could be successfully used for those studies requiring low production levels with a clear linear response over a wide IPTG concentration range, as in the case of metabolic engineering and of the production of toxic proteins. On the other hand, KrPL *lacY*⁺ can be useful for those processes where an average graded response is still guaranteed, though not always linear (Figure 8B), and high production is triggered by a low concentration of the inducer [39]. This might be the case of the synthesis of non-problematic proteins and of low added value products requiring the containment of the production costs. However, one has to keep in mind that all our studies recorded the average expression levels of the cultures, and certain conclusions about the homogeneity of the induction cannot be deduced. Nevertheless, the introduction of the GFP as a reporter in *PhTAC125* for the first time opens to the possibility of single-cell studies as FACS screenings that can address this question.

Finally, although it is beyond the scope of this study, it is worth drawing some considerations about the selection of reporter genes to study promoter strengths at 15 °C. The *PhTAE79* βgalactosidase and R9-GFP were the main tools used to study pP79. Despite they both demonstrated a higher protein accumulation in pP79 recombinant strains than pMAV bearing cells, the production of the fluorescent reporter was way more inefficient than the β-galactosidase and this phenomenon was not related to transcriptional efficiency. More reasons can justify this difference. First, in pP79 the β-galactosidase encoding sequence is directly fused to its natural 5' UTR, while the R9-GFP CDS is artificially joined with the psychrophilic 5' UTR. Different groups have widely reported how the 5' UTR composition and the fusion with heterologous translated sequences can cause translational issues [48–50]. In this sense, even the comparison of pMAV and pP79 relative strengths might be partially biased by the fact that they harbor the *galT* and *lacZ* 5' UTR sequences, respectively.

Nevertheless, in the past a similar disparity in terms of protein accumulation was also observed when the production of the psychrophilic β-galactosidase and a mesophilic α-glucosidase were compared in recombinant *PhTAC125* pUCRP strains [2]. Also, in that case the synthesis of the coldadapted enzyme was higher than the

mesophilic one, indicating that even when fused to a heterologous 5' UTR, the *lacZ* CDS is efficiently translated. Hence, the remarkable accumulation of *PhTAE79* β -galactosidase may be strictly related to either a high translation efficiency or protein stability at low temperatures. This hypothesis is corroborated by a study effectively demonstrating that the *PhTAE79* β -galactosidase showed a particularly high activity when produced in a heterologous bacterium at low temperatures, despite the low levels of transcription [51]. Collectively, these observations may suggest that even if *PhTAE79 lacZ* can be a useful tool for comparative studies, as done in this work, it might not reliably represent the absolute achievable amounts of other proteins at low temperatures using the same system, especially in the case of mesophilic proteins.

On the other hand, the production of fluorescent reporters in KrPL was so low not to allow the detection of the expression starting from weak promoters, as the one of pMAV vector. Originally, we used an R9-GFP variant, possessing an N-terminal oligoarginine peptide and the mutations characteristic of the eGFP [19] and of Cycle 3 GFP [27]. We intended to combine the enhanced fluorescence of eGFP and improved folding features of Cycle 3 mutations to the aggregation-prone polyarginine peptide [18,52]. In this way, we wanted to confer an increased in vivo stability to the protein, typical of full-protein nanoparticles [53]. However, all these modifications were predicted to improve the GFP properties at 37 °C with no further information about their consequences at lower temperatures. That is why we also produced a plain codon optimized eGFP—called pGFP—with neither R9 nor Cycle 3 mutations. The R9-gfp gene has a Codon Adaptation Index (CAI) of 0.66, while the *pGFP* gene has a CAI equal to 0.73 [20], but R9-GFP derived fluorescence was considerably higher. This indicates that at least some of the modifications introduced in R9-GFP had a positive effect. Nevertheless, the actual necessity to use the R9 peptide has still to be tested, considering the translational and degradation issues possibly deriving from N-terminal oligoarginines [50,54] and that GFP nanoparticles can sometimes show worsened fluorescent properties [55]. To make this fluorescent system more sensitive, other approaches have to be pursued, such as the shift of the emission spectrum to a wavelength for which *PhTAC125* experiences a lower autofluorescence and the application of protein mutations that improve the fluorophore maturation at low temperatures. However, both pGFP and R9-GFP are already detectable in combination with pP79, allowing for new kinds of study.

5. Conclusions

There is still a significant number of predicted protein products whose recombinant production in conventional gene expression systems is unsuccessful, making their structural/functional characterization and their biotechnological application impossible. Almost 20 years ago, our research group suggested the use of *PhTAC125* and its derived genetic tools for the setup of a novel cell factory working at low temperatures [14]. Till then, much evidence highlighted the notable skills of the Antarctic bacterium in the high quality production of human and/or eukaryotic complex proteins, reinforcing our original idea [2,3,5,6,11,34,35].

In this paper, we achieved a further considerable improvement toward the actual application of *PhTAC125* as an industrial cell factory. Based on the study of the regulated genetic elements in the psychrophilic bacterium *PhTAE79*, we developed pP79, a novel IPTG-inducible plasmid. By using this expression system, we obtained about 20-fold higher production of the recombinant β galactosidase in comparison to pMAV, the previous best inducible genetic system exploited in *PhTAC125* [3]. For the first time, the detection of a fluorescent protein was achieved in *PhTAC125* pP79 recombinant cells, paving the way for a variety of sensitive and innovative approaches of study.

Another essential aim of this work was to demonstrate the feasibility of a rational approach toward the host improvement. The inducer internalization and the control of proteolytic events were addressed, constructing the engineered strain *lacY*⁺ capable of producing a mesophilic lactose permease and a truncated form of Lon protease. This mutant strain allowed a 5-fold higher production than its isogenic *lon* mutant using a lower IPTG concentration. Furthermore, the heterologous permease showed its positive contribution to induction at 0 °C, widening the applicability of KrPL *lacY*⁺ also as a host for the recombinant protein production at ultra-low temperatures.

Supplementary Materials: The following are available online at www.mdpi.com/2076-2607/8/10/1466/s1, Figure S1: Production levels of R9-GFP and pGFP using pP79 expression plasmid, Figure S2: Growths of KrPL pP79*lacZ* and β -galactosidase production in GG and TYP, Figure S3: Growths curves of KrPL wt, *lon* and *lacY*⁺ strains, Table S1: Strains used in this study, Table S2: Oligonucleotides used in this study, Table S3: Plasmids used in this study.

Author Contributions: A.C. had the idea of using the IPTG-inducible gene expression system in *PhTAC125*, set up the gene expression systems; C.L. constructed the genome inserted mutants, and tested their growth and production performance; M.C. constructed the psychrophilic gene expression vectors for the production of the reporter proteins, and tested the production performance; E.P. and

A.C. were responsible for data curation; A.C. and C.L. wrote the original draft; all the authors contributed to reviewing and editing of the final version; M.L.T. had the supervision and was responsible for funding acquisition. All authors have read and agreed to the published version of the manuscript.

Funding: This research was funded by two grants from Progetto Nazionale di Ricerca in Antartide, number PNRA 2013/B1.04 and PNRA18_00335.

Acknowledgments: The generous contribution of the Italian parent's association "La fabbrica dei sogni 2-New developments for Rett Syndrome" is warmly acknowledged.

Conflicts of Interest: The authors declare no conflict of interest

References

- [1] Duilio, A.; Madonna, S.; Tutino, M.L.; Pirozzi, M.; Sannia, G.; Marino, G. Promoters from a cold-adapted bacterium: Definition of a consensus motif and molecular characterization of UP regulative elements. *Extremophiles* 2004, 8, doi:10.1007/s00792-003-0371-2.
- [2] Papa, R.; Rippa, V.; Sannia, G.; Marino, G.; Duilio, A. An effective cold inducible expression system developed in *Pseudoalteromonas haloplanktis* TAC125. *J. Biotechnol.* 2007, 127, 199–210, doi:10.1016/j.jbiotec.2006.07.003.
- [3] Sannino, F.; Giuliani, M.; Salvatore, U.; Apuzzo, G.A.; De Pascale, D.; Fani, R.; Fondi, M.; Marino, G.; Tutino, M.L.; Parrilli, E. A novel synthetic medium and expression system for subzero growth and recombinant protein production in *Pseudoalteromonas haloplanktis* TAC125. *Appl. Microbiol. Biotechnol.* 2016, 725–734, doi:10.1007/s00253-016-7942-5.
- [4] Parrilli, E.; Giuliani, M.; Tutino, M.L. General Secretory Pathway from marine Antarctic *Pseudoalteromonas haloplanktis* TAC125. *Mar.Genom.* 2008, 1, 123–128, doi:10.1016/j.margen.2009.01.002.
- [5] Giuliani, M.; Parrilli, E.; Ferrer, P.; Baumann, K.; Marino, G.; Tutino, M.L. Process optimization for recombinant protein production in the psychrophilic bacterium *Pseudoalteromonas haloplanktis*. *Process. Biochem.* 2011, 46, 953–959, doi:10.1016/j.procbio.2011.01.011.
- [6] Giuliani, M.; Parrilli, E.; Sannino, F.; Apuzzo, G.A.; Marino, G.; Tutino, M.L. Recombinant production of a single-chain antibody fragment in *Pseudoalteromonas haloplanktis* TAC125. *Appl. Microbiol. Biotechnol.* 2014, 98, doi:10.1007/s00253-014-5582-1.
- [7] Wilmes, B.; Hartung, A.; Lalk, M.; Liebeke, M.; Schweder, T.; Neubauer, P. Fed-batch process for the psychrotolerant marine bacterium *Pseudoalteromonas haloplanktis*. *Microb. Cell Factories* 2010, 9, 72, doi:10.1186/1475-2859-9-72.
- [8] Hoyoux, A.; Jennes, I.; Dubois, P.; Genicot, S.; Dubail, F.; François, J.M.; Baise, E.; Feller, G.; Gerday, C. Cold-Adapted β -Galactosidase from the Antarctic Psychrophile *Pseudoalteromonas haloplanktis*. *Appl. Environ. Microbiol.* 2001, 67, 1529–1535, doi:10.1128/aem.67.4.1529-1535.2001.
- [9] Van De Voorde, I.; Goiris, K.; Syryn, E.; Bussche, C.V.D.; Aerts, G. Evaluation of the cold-active *Pseudoalteromonas haloplanktis* β -galactosidase enzyme for lactose hydrolysis in whey permeate as primary step of d-tagatose production. *Process. Biochem.* 2014, 49, 2134–2140, doi:10.1016/j.procbio.2014.09.010.
- [10] Médigue, C.; Krin, E.; Pascal, G.; Barbe, V.; Bernsel, A.; Bertin, P.N.; Cheung, F.; Cruveiller, S.; D'Amico, S.; Duilio, A.; et al. Coping with cold: The genome of the versatile marine Antarctica bacterium *Pseudoalteromonas haloplanktis* TAC125. *Genome Res.* 2005, 15, 1325–1335, doi:10.1101/gr.4126905.
- [11] Parrilli, E.; De Vizio, D.; Cirulli, C.; Tutino, M.L. Development of an improved *Pseudoalteromonas haloplanktis* TAC125 strain for recombinant protein secretion at low temperature. *Microb. Cell Factories* 2008, 7, 2, doi:10.1186/1475-2859-7-2.

- [12] Wilmes, B.; Kock, H.; Glagla, S.; Albrecht, D.; Voigt, B.; Markert, S.; Gardebrecht, A.; Bode, R.; Danchin, A.; Feller, G.; et al. Cytoplasmic and Periplasmic Proteomic Signatures of Exponentially Growing Cells of the Psychrophilic Bacterium *Pseudoalteromonas haloplanktis*TAC125. *Appl. Environ. Microbiol.* 2010, doi:10.1128/aem.01750-10.
- [13] Fondi, M.; Maida, I.; Perrin, E.; Mellera, A.; Mocali, S.; Parrilli, E.; Tutino, M.L.; Lió, P.; Fani, R. Genomescale metabolic reconstruction and constraint-based modelling of the Antarctic bacterium *Pseudoalteromonas haloplanktis* TAC125. *Environ. Microbiol.* 2014, 17, 751–766, doi:10.1111/1462-2920.12513.
- [14] Tutino, M.L.; Duilio, A.; Parrilli, E.; Remaut, E.; Sannia, G.; Marino, G. A novel replication element from an Antarctic plasmid as a tool for the expression of proteins at low temperature. *Extremophiles* 2001, 5, 257–264, doi:10.1007/s007920100203.
- [15] Brettin, T.; Davis, J.J.; Disz, T.; Edwards, R.A.; Gerdes, S.; Olsen, G.J.; Olson, R.; Overbeek, R.; Parrello, B.; Pusch, G.D.; et al. RASTtk: A modular and extensible implementation of the RAST algorithm for building custom annotation pipelines and annotating batches of genomes. *Sci. Rep.* 2015, 5, 8365, doi:10.1038/srep08365.
- [16] Altschul, S.F.; Gish, W.; Miller, W.; Myers, E.W.; Lipman, D.J. Basic local alignment search tool. *J. Mol. Biol.* 1990, 215, 403–410, doi:10.1016/s0022-2836(05)80360-2.
- [17] Tutino, M.L.; Parrilli, E.; Giaquinto, L.; Duilio, A.; Sannia, G.; Feller, G.; Marino, G. Secretion of α -Amylase from *Pseudoalteromonas haloplanktis* TAB23: Two Different Pathways in Different Hosts. *J. Bacteriol.* 2002, doi:10.1128/jb.184.20.5814-5817.2002.
- [18] Vázquez, E.; Roldán, M.; Diez-Gil, C.; Unzueta, U.; Domingo-Espín, J.; Cedano, J.; Conchillo, O.; Ratera, I.; Veciana, J.; Daura, X.; et al. Protein nanodisk assembling and intracellular trafficking powered by an arginine-rich (R9) peptide. *Nanomedicine* 2010, 5, 259–268, doi:10.2217/nnm.09.98.
- [19] Zhang, G.; Gurtu, V.; Kain, S.R. An Enhanced Green Fluorescent Protein Allows Sensitive Detection of Gene Transfer in Mammalian Cells. *Biochem. Biophys. Res. Commun.* 1996, 227, 707–711, doi:10.1006/bbrc.1996.1573.
- [20] Puigbo, P.; Guzmán, E.; Romeu, A.; Garcia-Vallve, S. OPTIMIZER: A web server for optimizing the codon usage of DNA sequences. *Nucleic Acids Res.* 2007, 35, W126–W131, doi:10.1093/nar/gkm219.
- [21] Cusano, A.M.; Parrilli, E.; Duilio, A.; Sannia, G.; Marino, G.; Tutino, M.L. Secretion of psychrophilic α -amylase deletion mutants in *Pseudoalteromonas haloplanktis* TAC125. *FEMS Microbiol. Lett.* 2006, 258, 67–71, doi:10.1111/j.1574-6968.2006.00193.x.
- [22] Giuliani, M.; Parrilli, E.; Pezzella, C.; Rippa, V.; Duilio, A.; Marino, G.; Tutino, M.L. A Novel Strategy for the Construction of Genomic Mutants of the Antarctic Bacterium *Pseudoalteromonas haloplanktis* TAC125. *Adv. Struct. Saf. Stud.* 2011, 824, 219–233, doi:10.1007/978-1-61779-433-9_11.
- [23] Pfaffl, M.W. A new mathematical model for relative quantification in real-time RT-PCR. *Nucleic Acids Res.* 2001, 29, e45, doi:10.1093/nar/29.9.e45.
- [24] Bosi, E.; Fondi, M.; Orlandini, V.; Perrin, E.; Maida, I.; De Pascale, D.; Tutino, M.L.; Parrilli, E.; Giudice, A.L.; Filloux, A.; et al. The pangenome of (Antarctic) *Pseudoalteromonas* bacteria: Evolutionary and functional insights. *BMC Genom.* 2017, 18, 93, doi:10.1186/s12864-016-3382-y.
- [25] Lu, S.; Wang, J.; Chitsaz, F.; Derbyshire, M.K.; Geer, R.C.; Gonzales, N.R.; Gwadz, M.; Hurwitz, D.I.; Marchler, G.H.; Song, J.S.; et al. CDD/SPARCLE: The conserved domain database in 2020. *Nucleic Acids Res.* 2020, 48, D265–D268, doi:10.1093/nar/gkz991.
- [26] Qi, W.; Colarusso, A.; Olombrada, M.; Parrilli, E.; Patrignani, A.; Tutino, M.L.; Toll-Riera, M. New insights on *Pseudoalteromonas haloplanktis* TAC125 genome organization and benchmarks of genome assembly applications using next and third generation sequencing technologies. *Sci. Rep.* 2019, 9, 16444, doi:10.1038/s41598-019-52832-z.

- [27] Cramer, A.; Whitehorn, E.A.; Tate, E.; Stemmer, W.P. Improved Green Fluorescent Protein by Molecular Evolution Using DNA Shuffling. *Nat. Biotechnol.* 1996, *14*, 315–319, doi:10.1038/nbt0396-315.
- [28] Perrin, E.; Ghini, V.; Giovannini, M.; Di Patti, F.; Cardazzo, B.; Carraro, L.; Fagorzi, C.; Turano, P.; Fani, R.; Fondi, M. Diauxie and co-utilization of carbon sources can coexist during bacterial growth in nutritionally complex environments. *Nat. Commun.* 2020, *11*, 3135, doi:10.1038/s41467-020-16872-8.
- [29] Mocali, S.; Chiellini, C.; Fabiani, A.; Decuzzi, S.; De Pascale, D.; Parrilli, E.; Tutino, M.L.; Perrin, E.; Bosi, E.; Fondi, M.; et al. Ecology of cold environments: New insights of bacterial metabolic adaptation through an integrated genomic-phenomic approach. *Sci. Rep.* 2017, *7*, 839, doi:10.1038/s41598-017-00876-4.
- [30] Hansen, L.H.; Knudsen, S.; Sørensen, S.J. The effect of the lacY gene on the induction of IPTG inducible promoters, studied in *Escherichia coli* and *Pseudomonas fluorescens*. *Curr. Microbiol.* 1998, *36*, 341–347, doi:10.1007/s002849900320.
- [31] Tsilibaris, V.; Maenhaut-Michel, G.; Van Melderen, L. Biological roles of the Lon ATP-dependent protease. *Res. Microbiol.* 2006, doi:10.1016/j.resmic.2006.05.004.
- [32] Van Melderen, L.; Aertsen, A. Regulation and quality control by Lon-dependent proteolysis. *Res. Microbiol.* 2009, *160*, 645–651, doi:10.1016/j.resmic.2009.08.021.
- [33] Rosano, G.L.; Ceccarelli, E.A. Recombinant protein expression in *Escherichia coli*: Advances and challenges. *Front. Microbiol.* 2014, *5*, 1–17, doi:10.3389/fmicb.2014.00172.
- [34] Vigentini, I.; Merico, A.; Tutino, M.L.; Compagno, C.; Marino, G. Optimization of recombinant human nerve growth factor production in the psychrophilic *Pseudoalteromonas haloplanktis*. *J. Biotechnol.* 2006, doi:10.1016/j.jbiotec.2006.05.019.
- [35] Unzueta, U.; Vázquez, F.; Accardi, G.; Mendoza, R.; Toledo-Rubio, V.; Giuliani, M.; Sannino, F.; Parrilli, E.; Abasolo, I.; Schwartz, S.; et al. Strategies for the production of difficult-to-express full-length eukaryotic proteins using microbial cell factories: Production of human alpha-galactosidase A. *Appl. Microbiol. Biotechnol.* 2015, *99*, 5863–5874, doi:10.1007/s00253-014-6328-9.
- [36] Khlebnikov, A.; Keasling, J. Effect of lacY Expression on Homogeneity of Induction from the Ptac and Ptrc Promoters by Natural and Synthetic Inducers. *Biotechnol. Prog.* 2002, *18*, 672–674, doi:10.1021/bp010141k.
- [37] Özbudak, E.M.; Thattai, M.; Lim, H.N.; Shraiman, B.I.; Van Oudenaarden, A. Multistability in the lactose utilization network of *Escherichia coli*. *Nature* 2004, *427*, 737–740, doi:10.1038/nature02298.
- [38] Afroz, T.; Biliouris, K.; Kaznessis, Y.N.; Beisel, C.L. Bacterial sugar utilization gives rise to distinct singlecell behaviours. *Mol. Microbiol.* 2014, doi:10.1111/mmi.12695.
- [39] Afroz, T.; Biliouris, K.; Boykin, K.E.; Kaznessis, Y.N.; Beisel, C.L. Trade-offs in Engineering Sugar Utilization Pathways for Titratable Control. *ACS Synth. Biol.* 2014, *4*, 141–149, doi:10.1021/sb400162z.
- [40] Fernández-Castané, A.; Vine, C.E.; Caminal, G.; López, C. Evidencing the role of lactose permease in IPTG uptake by *Escherichia coli* in fed-batch high cell density cultures. *J. Biotechnol.* 2012, *157*, 391–398, doi:10.1016/j.jbiotec.2011.12.007.
- [41] Guzman, L.M.; Belin, D.; Carson, M.J.; Beckwith, J. Tight regulation, modulation, and high-level expression by vectors containing the arabinose PBAD promoter. *J. Bacteriol.* 1995, *177*, 4121–4130, doi:10.1128/jb.177.14.4121-4130.1995.
- [42] Stülke, J.; Hillen, W. Carbon catabolite repression in bacteria. *Curr. Opin. Microbiol.* 1999, *2*, 195–201, doi:10.1016/s1369-5274(99)80034-4.
- [43] Gubellini, F.; Verdon, G.; Karpowich, N.K.; Luff, J.D.; Boël, G.; Gauthier, N.; Handelsman, S.K.; Ades, S.E.; Hunt, J.F. Physiological Response to Membrane Protein Overexpression in *E. coli*. *Mol. Cell. Proteom.* 2011, *10*, 10, doi:10.1074/mcp.m111.007930.

- [44] Van Melderen, L.; Gottesman, S. Substrate sequestration by a proteolytically inactive Lon mutant. *Proc. Natl. Acad. Sci. USA* 1999, *96*, 6064–6071, doi:10.1073/pnas.96.11.6064.
- [45] D'Amico, S.; Collins, T.; Marx, J.-C.; Feller, G.; Gerday, C. Psychrophilic microorganisms: Challenges for life. *EMBO Rep.* 2006, *7*, 385–389, doi:10.1038/sj.embor.7400662.
- [46] Grube, M.; Dimanta, I.; Gavare, M.; Strazdina, I.; Liepins, J.; Juhna, T.; Kalnenieks, U. Hydrogen-producing *Escherichia coli* strains overexpressing lactose permease: FT-IR analysis of the lactose-induced stress. *Biotechnol. Appl. Biochem.* 2014, *61*, 111–117, doi:10.1002/bab.1128.
- [47] Juers, D.H.; Matthews, B.W.; Huber, R.E. LacZ β -galactosidase: Structure and function of an enzyme of historical and molecular biological importance. *Protein Sci.* 2012, *21*, 1792–1807, doi:10.1002/pro.2165.
- [48] Mutalik, V.K.; Guimaraes, J.C.; Cambray, G.; Lam, C.; Christoffersen, M.J.; Mai, Q.-A.; Tran, A.B.; Paull, M.; Keasling, J.D.; Arkin, A.P.; et al. Precise and reliable gene expression via standard transcription and translation initiation elements. *Nat. Methods* 2013, *10*, 354–360, doi:10.1038/nmeth.2404.
- [49] Mirzadeh, K.; Martinez, V.; Toddo, S.; Guntur, S.; Herrgård, M.J.; Elofsson, A.; Nørholm, M.H.H.; Daley, D.O. Enhanced Protein Production in *Escherichia coli* by Optimization of Cloning Scars at the Vector– Coding Sequence Junction. *ACS Synth. Biol.* 2015, *4*, 959–965, doi:10.1021/acssynbio.5b00033.
- [50] Boel, G.; Letso, R.; Neely, H.; Price, W.N.; Wong, K.-H.; Su, M.; Luff, J.D.; Valecha, M.; Everett, J.K.; Acton, T.B.; et al. Codon influence on protein expression in *E. coli* correlates with mRNA levels. *Nature* 2016, *529*, 358–363, doi:10.1038/nature16509.
- [51] Welsch, N.; Homuth, G.; Schweder, T. Suitability of different β -galactosidases as reporter enzymes in *Bacillus subtilis*. *Appl. Microbiol. Biotechnol.* 2011, *93*, 381–392, doi:10.1007/s00253-011-3645-0.
- [52] Tesei, G.; Vazdar, M.; Jensen, M.R.; Cragnell, C.; Mason, P.E.; Heyda, J.; Skepö, M.; Jungwirth, P.; Lund, M. Self-association of a highly charged arginine-rich cell-penetrating peptide. *Proc. Natl. Acad. Sci. USA* 2017, doi:10.1073/pnas.1712078114.
- [53] Verma, D.; Gulati, N.; Kaul, S.; Mukherjee, S.; Nagaich, U. Protein Based Nanostructures for Drug Delivery. *J. Pharm.* 2018, *2018*, 1–18, doi:10.1155/2018/9285854.
- [54] Tasaki, T.; Sriram, S.M.; Park, K.S.; Kwon, Y.T. The N-end rule pathway. *Annu. Rev. Biochem.* 2012, *81*, 261– 89, doi:10.1146/annurev-biochem-051710-093308.
- [55] Favaro, M.T.P.; Sánchez-García, L.; Sánchez-Chardi, A.; Roldan, M.; Unzueta, U.; Serna, N.; Cano-Garrido, O.; Azzoni, A.R.; Ferrer-Miralles, N.; Villaverde, A.; et al. Protein nanoparticles are nontoxic, tuneable cell stressors. *Nanomedicine* 2018, *13*, 255–268, doi:10.2217/nnm-2017-0294.
- [56] Hartman, A.H.; Liu, H.; Melville, S.B. Construction and Characterization of a Lactose-Inducible Promoter System for Controlled Gene Expression in *Clostridium perfringens*. *Appl. Environ. Microbiol.* 2011, *77*, 471– 478. doi:10.1128/AEM.01536-10.
- [57] Caron, K.; Trowell, S.C. Highly Sensitive and Selective Biosensor for a Disaccharide Based on an AraC-Like Transcriptional Regulator Transduced with Bioluminescence Resonance Energy Transfer. *Anal. Chem.* 2018, doi:10.1021/acs.analchem.8b03689.
- [58] Newman, J.; Caron, K.; Nebl, T.; Peat, T.S. Structures of the Transcriptional Regulator BgaR, a Lactose Sensor. *Acta Crystallogr. Sect. D* 2019, doi:10.1107/S2059798319008131.
- [59] Wheatley, R.W.; Lo, S.; Jancewicz, L.J.; Dugdale, M.L.; Huber, R.E. Structural Explanation for Allolactose (Lac Operon Inducer) Synthesis by LacZ β -Galactosidase and the Evolutionary Relationship between Allolactose Synthesis and the Lac Repressor. *J. Biol. Chem.* 2013, *288*, 12993–13005. doi:10.1074/jbc.M113.455436.

Chapter 2: A multiparametric approach to exploit the full-length and active recombinant production of the human protein CDKL5 in the engineered strain *Pseudoalteromonas haloplanktis* TAC125 KrPI *lacY*⁺

To exploit the improvements obtained from the engineering of *PhTAC125*, the new mutant strain KrPI *lacY*⁺ was used for recombinantly producing the human serine/threonine protein kinase CDKL5. Due to its structural features, the heterologous production of this enzyme in the full-length and active form in conventional bacterial hosts, such as *E. coli*, is impaired by extensive proteolytic degradation and the formation of insoluble aggregates and inclusion bodies.

The first trials of recombinant production of CDKL5 fused at a cell-penetrating peptide TATk performed in KrPI *lacY*⁺ showed exciting results but highlighted some limiting factors. Subsequent efforts aimed to improve the poor translation efficiency, which was attributed as a cause of a low accumulation of recombinant transcript, also succeeding in overcoming an alternative translation initiation issue.

In addition, the boosting of the recombinant productivity achieved with the implementation of high copy number psychrophilic expression systems and the optimization of the N-terminal fusion tag allowed us to reach high production levels of about 4mg/L of culture.

The results that emerged from the activity assay performed with enriched fractions of CDKL5 undeniably demonstrated that KrPL *lacY*⁺ is suitable to produce the complex human protein in full-length and active form. The application of such an enzyme can give a solid contribution in functional and structural studies as well as for therapeutic purposes.

A manuscript is in preparation for these results

A multiparametric approach to exploit the full-length and active recombinant production of the human protein CDKL5 in the engineered strain *Pseudoalteromonas haloplanktis* TAC125 KrPI *lacY*⁺

Andrea Colarusso, Concetta Lauro, Marzia Calvanese, Ermenegilda Parrilli and Maria Luisa Tutino *

Dipartimento di Scienze Chimiche, Complesso Universitario Monte Sant'Angelo, Via Cintia, 80126 Napoli, Italy; concetta.lauro@unina.it (C.L.); andrea.colarusso@unina.it (A.C.); marzia.calvanese@unina.it (M.C.); erparril@unina.it (E.P.) * Correspondence: tutino@unina.it; Tel.: +39-081-674317

2.1 Introduction

2.1.1 Human Cyclin-dependent kinase-like 5

Human Cyclin-dependent kinase-like 5 (CDKL5) is a serine/threonine kinase belonging to the CMGC family (cyclin-dependent kinases CDKs; mitogen-activated protein kinases, MAP kinases; glycogen synthase kinases, GSK; and CDK-like kinases) encoded by a gene located on the short arm of the X-chromosome at position 22 (Xp22). *hCDKL5* gene is 240 kb in length and is characterised by the presence of 27 exons (Figure 2.1A), which generate multiple transcripts arising from events of (1) alternative splicing, (2) alternative promoter and (3) first exon usage [1]. Five different coding isoforms of *hCDKL5* result from this regulation [1]. The first four isoforms are widely expressed in the brain, heart, liver, lung, muscle, spleen and kidney with a different relative abundance, while *hCDKL5_5* is mainly expressed in testis [1]. No evidence for the functional significance of these alternative isoforms has been reported far now. However, the catalytic domain of CDKL5 is preserved across all isoforms while the diversity occurs within the C-terminal domain (containing signals of nuclear translocation), suggesting that they occur as a regulation mechanism for the subcellular distribution of the protein [2]. Indeed, in neurons, CDKL5 seems to be localized both in the nucleus [3] and different cytoplasmatic compartments, such as growth cone [2], dendritic spines [4] and centrosomes [5].

hCDKL5_1 is a 9.7 kb transcript composed of 22 exons with a large 6.6 kb 3'-UTR, which is the predominant brain isoform. For this reason, the present study will be focused on this variant (from now on called CDKL5). CDKL5 (Figure 2.1B) is characterized by an N-terminal catalytic domain (aa 13–297), containing an ATP-binding region (aa 19-

43), a serine/threonine protein kinase active site (aa 131-143) and a Thr–Xaa–Tyr motif (TEY) (aa 169-171), involved in the autophosphorylation and consequent activation of the protein [6, 7, 8]. The large C-terminal domain contains two putative nuclear localization signals (NLS) (NLS₁, aa 312-315; NLS₂, aa 784-789) and a nuclear export signal (NES) (aa 836-845), which regulate the intracellular localization of CDKL5 [9]. Furthermore, it seems to negatively regulate the kinase activity of the protein [10].

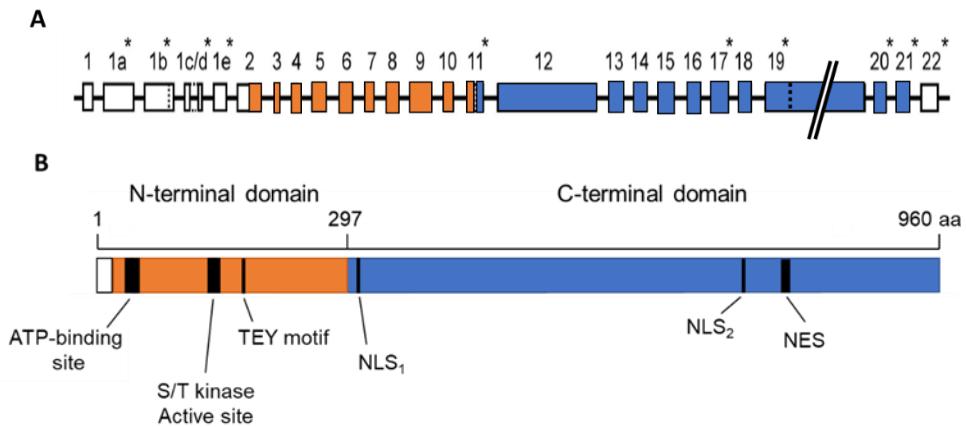


Figure 2.1. Schematic representation of CDKL5 and its encoded gene. **(A)** Representation of hCDKL5 gene. The exons are depicted with boxes and introns with lines. Asterisks indicate the sites wherein the difference in the transcript isoforms were found. Dotted lines denote alternative splicing sites. **(B)** Representation of the functional domains of the isoform hCDKL5_1. ATP-binding region (aa 19-43), serine/threonine kinase active site (aa 131-143) and Thr–Xaa–Tyr motif (TEY) (aa 169-171) belong to the N-terminal catalytic domain (aa 13-297) (orange box). Two putative nuclear localization signals (NLS) (NLS₁ aa 312-315, NLS₂ aa 784-789) and a nuclear export signal (NES) (aa 836-845) are placed in the C-terminal domain (blue box).

Despite the structural feature of the catalytic domain has been determined through a crystallographic analysis [11], the C-terminal domain structure is still unknown. Its aminoacidic sequence characterized by high net charge and low hydrophobicity makes this domain prone to adopt an unstructured conformation. This phenomenon is known as intrinsic disorder and is quite common in eukaryotic proteins, especially associated with signalling and regulation [12]. Although spontaneously unable to fold, the intrinsically disordered region (IDR) of CDKL5 can participate in the interaction with diverse binding partners and contributes to the functional versatility of the protein [9,13]. However, it is still unclear if the IDR assumes a folded state in its physiological environment, where it coexists with its

interactors, according to a folding-upon-binding model or retains a disordered or not full structured state even after the binding [13]. The multiple subcellular localizations and the potentiality of the IDR to interact with a broad spectrum of molecules partially justify the roles of CDKL5 in the brain. Although recent studies extensively focused on this aspect, the functions of CDKL5 are still far from being fully characterized. The recent availability of suitable study models such as cultured neurons, knockout animals, human iPSC-derived neurons and organoids [15, 16, 17, 18, 19] allowed to gain important evidence of the critical role of CDKL5 in neuronal development and maturation. During the early neuronal morphogenesis, CDKL5 has been demonstrated to act as a modulator of cell proliferation [5], axon outgrowth [19] and dendrite growth and phenotype [2]. The suggested molecular mechanisms behind these processes include the regulation of BDNF-Rac1, AKT/mTOR and AKT/GSK-3 β signalling pathways [21, 2, 22, 23]. Furthermore, CDKL5 was supposed to be involved in synapse development and function due to its localization in this neuronal compartment [4, 24]. In the adult brain, it is involved in the stabilization and maintenance of mature spines through the regulation of the expression and targeting of glutamate receptors NMDAR [20]. Through the action of these receptors, it was also supposed to regulate the dendritic microtubule dynamics by acting on some microtubules-associated proteins [24]. However, all the above mentioned biological processes are regulated and influenced by numerous factors, and the identification of new substrates and interactors of CDKL5 could have great relevance in the full understanding of its function.

2.1.2 CDKL5 deficiency disorder and therapeutic strategies

The characterization of the biological function of CDKL5 sparks great interest because of its involvement in neurological disorders. CDKL5 deficiency disorder (CDD; OMIM entry #300203, #300672) is a rare developmental encephalopathy caused by mutations in the CDKL5 encoding gene [25]. The typical symptoms of CDD include early-onset epilepsy (often drug-refractory), hypotonia, psychomotor developmental delay, intellectual disability, and vision disorders. Moreover, CDD patients are frequently affected also by other comorbidities such as autistic features, sleep abnormalities or vegetative, gastrointestinal and orthopaedic illnesses [26]. Since the genetic basis of this pathology (X-linked), the phenotype observed in the male patients seems to be much more severe than in the female. The incidence of the disorder is indeed four times higher in female,

suggesting that in males the aberration is mainly lethal [27]. However, the clinical picture of CDD is very heterogeneous and this could derive from the nature of the alteration behind the pathological phenotype. The analysis of the mutations reported in the literature highlighted that those occurring in the catalytic domain of CDKL5 are generally associated with more severe impairments, especially if they consist of missense mutations. On the other hand, alterations of the C-terminal region, wherein nonsense mutations are more frequent, are identified in patients with milder symptoms [29, 30]. Importantly, other aspects to consider in the genetics of CDD are deletions, frameshifts, aberrant splicing of the transcripts and epigenetic factors, i.e. random X-inactivation [6, 31]. Thus, further studies will be pivotal to clarify the genotype-phenotype correlation of CDD and to elucidate its molecular biology, paving the way for the development of effective therapies for this pathology. Indeed, to date no specific therapy for CDD is available. The current treatments adopted for CDD patients act basically on symptomatology aiming at the control of pathological manifestations. Great attention is placed on the treatment of epilepsy, which often manifests drug resistance. In addition to the conventional anti-epileptic therapy, nonpharmacological approaches are used, such as ketogenic diet, vagus nerve stimulation and callosotomy [25].

Additionally, the constant commitment in the research field has led to the development of potential therapeutic approaches for CDD, targeting its biological, metabolic and genetic basis. Nowadays, the attention is focused on modulators of NMDA receptor system, such as Ganaxolone (a synthetic derivative of allopregnanolone able to restore the correct microtubule morphology and that successfully completed a phase 3 clinical trial, <https://www.themarigoldstudy.com/it/>), insulin-like growth factor IGF-1 (which activates the AKT/mTOR pathway acting on the serotonergic receptor 5-HT₇R with a partial rescue of the mitochondrial brain dysfunction and dendritic spine instability) and tianeptin (antidepressant directed against AMPA receptors) [25, 5, 32, 33]. Other interesting drugs proposed for CDD therapy are the inhibitors of the transduction pathway altered in the CDKL5 knockout mouse model, i.e. tideglusib, which inhibit AKT/GSK3- β signalling with an improvement of hippocampal development and function [33].

Promising therapeutic strategies also derive from novel techniques of genome editing and gene therapy. A recent study reported by Gao and coworkers demonstrates that the Adeno-associated virus (AAV) serotype PhP.B vector allows high efficiency of transduction in the cerebellum, wherein the replacement of the isoform 1 of CDKL5 significantly enhances the motor coordination in knockout mice [34]. An

RNA-based therapeutic has also been established by using the spliceosomal U1 small nuclear RNA (U1snRNA) to correct exon skipping and aberrant splicing events characterizing some pathological mutations in CDD [35].

Finally, great expectations are addressed to enzyme replacement therapy, which was described by Trazzi and coworkers (2018). Their study demonstrated that a protein transduction domain (TAT) could be used as a fusion partner of CDKL5 to deliver the protein in neurons retaining its wild-type activity [36]. The protein administration through intracerebroventricular infusions compensates for the dendritic alterations in terms of architecture, length and spine density. An improvement in the behavioural disturbance in CDD model mice was observed without side effects and the benefits were also observed in mature neurons. Furthermore, the efficiency of delivery in the brain cells and therapeutic effects are conserved after vascular infusion, demonstrating the feasibility of this strategy in humans.

2.2 Aim of the study

Full-length human CDKL5 is a difficult-to-produce enzyme for two main reasons: i) almost two-thirds of its sequence is predicted to be intrinsically disordered, and the lack of a precise 3D structure makes this region more susceptible to proteolytic attack by host encoded protease in conventional prokaryotic and eukaryotic cell factories; ii) the cytoplasmic accumulation of the enzyme in eukaryotic production hosts is associated to considerable toxicity, and the only permissive production strategy is its extracellular secretion, often ending up with unwanted glycosylation.

This study aimed to demonstrate the feasibility of the exploitation of *PhTAC125* as a cell factory for the production of the recombinant CDKL5 in full-length and active form. The establishment of a suitable production process will pave the way for functional and structural studies as well as for the therapeutic application of this enzyme.

2.3 Results

The improved features of *PhTAC125* KRPL *lacY*⁺ strain [37] were challenged with the recombinant production of the most abundant isoform of CDKL5 in the human brain, *hCDKL5_1* [1]. The codon-optimized sequence encoding the human protein was cloned into the psychrophilic vector p79C [37] fused at the 5'-region with the leader sequence coding for a slightly modified TATk (*HIV-1 Transactivator of*

Transcription) peptide, used as a drug delivery system through the blood brain barrier for therapeutic purposes [37, 39]. At the 3'-end of the fusion construct a 3xFlag and a 6xHis tag coding sequences were added for purification purposes. The affinity tags are interspaced by the regions of recognition of Tobacco Etch Virus protease (TEV) and Enterokinase (EK) (Figure 2.2).

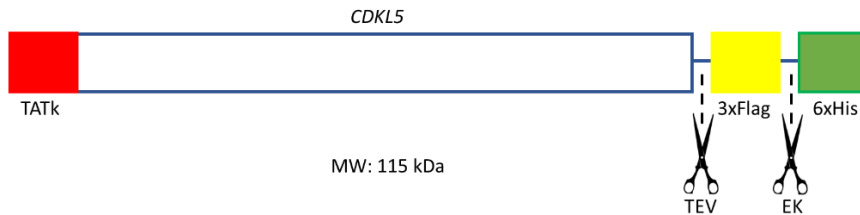


Figure 2.2. Schematic representation of CDKL5 construct. A sequence encoding an N-terminal TATk peptide (red box) was added for translational purposes. C-terminal 3xFlag (yellow box) and 6xHis (green box) tags were used both for antibody detection and purification trials. Two proteases recognition sequences were added between the CDKL5 sequence and each affinity tag (indicated with scissors). These consisted of Tobacco Each Virus protease (TEV) and Enterokinase (EK) recognition sequences.

2.3.1 Optimization of the production condition

The first trials were spent on the optimization of the production conditions. Variables like the temperature and the inducer concentration were taken into account to improve the yields and the overall quality of the recombinant product (data not shown). The best production condition was obtained when KrPI *lacY*⁺ was grown in GG medium at 15°C with the induction performed in the late-exponential growth phase (about 2 OD/mL) with 5 mM IPTG. Figure 2.3 shows the level of recombinant CDKL5 (115 kDa) obtained in KrPI *lacY*⁺ in comparison to its isogenic control *lon* and wt strains. The production was evaluated through SDS-PAGE and Western blot analysis. As shown in panel A, recombinant KrPI *lacY*⁺ produced ten-fold more protein than the wt strain when the induction of expression was performed with 5 mM IPTG (lanes 3 and 1, respectively). The amount of protein obtained in recombinant KrPI wt was indeed very similar to that achieved when the production was induced with 0.5 mM IPTG in KrPI *lacY*⁺ strain (lanes 1 and 2). In Panel B, the comparison of recombinant CDKL5 produced in KrPI *lacY*⁺ (lane 2) and KrPI *lon* (lane 1) is reported. The lactose transporter contribution in the engineered strain can be appreciated with an increase of CDKL5 production of about 2.5- fold.

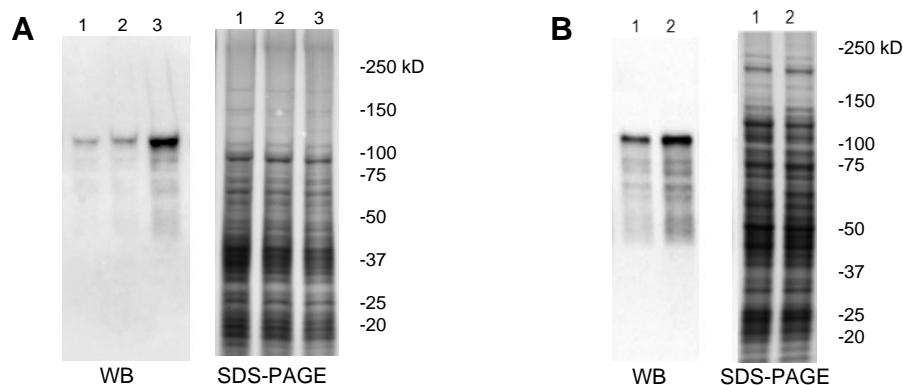


Figure 2.3. Optimization of the production performance of *PhTAC125* KrPI *lacY*⁺-*p79C-CDKL5* evaluated through SDS-PAGE and Western blot analysis. Total cellular extracts of *PhTAC125* KrPI *lacY*⁺ mutant harbouring *p79C-CDKL5* were analyzed through SDS-PAGE and Western blot with the anti-CDKL5 antibody in comparison with the KrPI wt strain (panel A) and the *lon* mutant strain (panel B). The recombinant production was evaluated after 8 hours of induction in GG medium at 15 °C. Panel A shows the production level obtained with 5mM IPTG in the KrPI wt strain (lane 1) in comparison to that obtained in the *lacY*⁺ mutant with 0.5 and 5 mM IPTG (lanes 2 and 3 respectively). Panel B represents the recombinant protein obtained with 5mM IPTG in the KrPI *lon* (lane 1) and KrPI *lacY*⁺ strains (lane 2).

2.3.2 Optimization of the psychrophilic expression vectors

2.3.2.1. Analysis of gene expression level in *p79C* system

Despite the optimization of the production conditions in the engineered strain, the low recombinant yield was still quite evident. In most of the tested conditions, the recombinant protein diminished over time upon the induction (data not shown) without observing some changes in the proteolytic pattern. Hence, an investigation about the gene expression in *p79C* starting from the quantification of transcribed mRNA of the *CDKL5* gene was conducted. Quantitative real-time PCR was performed on reverse-transcribed cDNA from recombinant cells grown in the presence and absence of IPTG. The housekeeping gene *PSHAa0221* was chosen as the normalizer for variations of mRNA amounts, cDNA synthesis efficiency and plasmid DNA contamination. The expression level of the *CDKL5* gene was assayed for up-regulation in the experimental samples (induction of expression) in comparison to the calibrator sample (noninduced cells, NI). The relative quantification of mRNA was expressed as fold-change and was calculated through the standard curve method (Pfaffl method) [39]. The data demonstrated that mRNA coding *CDKL5* did not accumulate and resulted in only 5x

enhancement after 2 hours following the induction (Figure 2.4). Moreover, the mRNA concentration tended to remain constant in the following hours (6 hours). Interestingly, this issue was observed only when *CDKL5* gene expression was carried out. Indeed, When relative transcript quantification was performed on the expression of two reporter genes (*lacZ* and *egfp*) by the same expression vector, a rapid increase of mRNA was observed with a significant accumulation during the same observed time. This data demonstrated that the production limit of the system is not attributable to the expression vector and its promoter rather it is specifically related to the *CDKL5* gene.

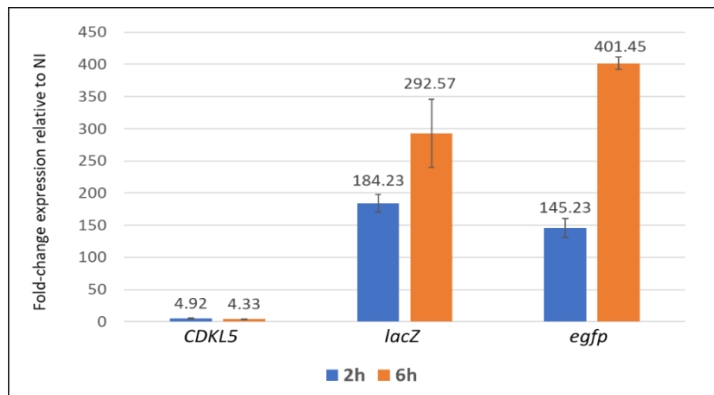


Figure 2.4. Relative quantification by RT-qPCR of mRNA expression levels of *CDKL5*, *lacZ* and *egfp*. Three genes under the control of the p79 promoter were analysed for their mRNA expression levels after 2 and 6 hours from the induction in comparison to the non-induced condition. The housekeeping gene *PSHAa0221* was chosen as a normalizer. The relative quantification results were obtained using the Pfaffl method. The reported results are the mean of three independent experiments.

2.3.2.2 Evaluation of a bicistronic system for gene expression in the psychrophilic system

The temporal changes in mRNA abundance typically measured during a recombinant gene expression are the result of a balance between transcription rate -in terms of production of mRNA transcript- and mRNA degradation. These processes can be regulated at both the transcriptional and post-transcriptional levels through mRNA stability regulation. There are some possible strategies for shaping gene expression and the first that was investigated is the enhancement of the efficiency of translation in order to reduce mRNA degradation. When the recombinant expression is performed with a monocistronic system- in which the gene of interest is directly fused to the transcriptional promoter- the expression levels may not be reproducible due to the presence of several other structural elements that may interfere with

translation initiation and ribosome speed on the recombinant mRNA [40]. The attention was thus focused on the ribosome coverage and translation efficiency of the transcript since it constitutes the main factor influencing mRNA stability in prokaryotes [41]. Indeed, a highly translated transcript is efficiently protected from degradation by RNAses. According to what reported in the literature, the translational coupling is the main strategy to enhance the translation of a specific transcript and the bicistronic expression systems seemed to be a valid instrument to reach this purpose [42]. The bicistronic constructs are small operons in which the gene coding for the protein of interest is cloned in the second position. If the first ORF is small and rapidly translated, this event efficiently attracts ribosomes to protect the mRNA. As the two ORFs are translationally coupled, every time ORF1 is translated, ORF2 is translated as well. A bicistronic design (BCD) may improve the translation of the distal gene with two possible mechanisms: the first is related to the increasing of recruitment of ribosomes by the ORF1 close to the ribosome binding site (RBS) of the ORF2; on the other hand, the translational coupling could act through the disruption of mRNA secondary structures at 5' UTR/TIR region of ORF2 during the translation of the first cistron, given the helicase activity of 70S ribosome [42].

Some bicistronic constructs were already available in the laboratory where my PhD project was carried out (Colarusso A., personal communication). These systems differed in the Shine-Dalgarno (SD) sequences upstream of each ORF and the most promising one was evaluated into the engineered psychrophilic cell factory. In detail, the chosen bicistronic operon (BCD2) is constituted by the first ORF derived from the *PhlacZ* gene and the second one from *PhtrpA*, whose SD sequence is perfectly complementary to the *PhTAC125* 16S rRNA sequence (Figure 2.5). The length of the ORF1 had a minimum of 17 amino acids, avoiding a similarity of the encoding sequence with the SD2. Furthermore, a stop codon was located upstream of the SD2 sequence and overlapping- with 1bp frameshift- the start codon of the ORF2 to avoid the ribosome displacement from the bicistronic transcript before the ORF2 translation. The 6xHis and a 3xFlag tag coding sequences were fused at the 5' and 3' region of the *CDKL5* gene, respectively, using Enterokinase and TEV protease recognition sequences as spacers (Figure 2.5).

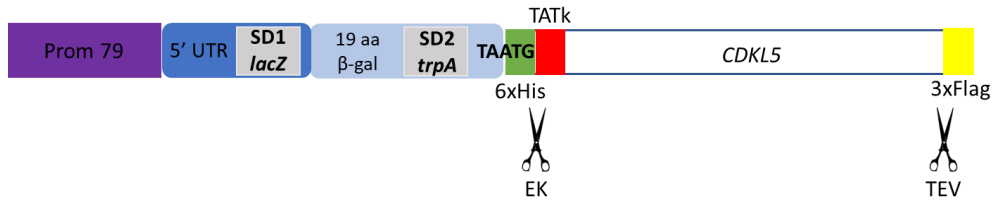


Figure 2.5. Schematic representation of bicistronic system BCD2 for *CDKL5* gene expression. *P79*, psychrophilic promoter inducible by IPTG (purple box); ORF1 and its 5' UTR/TIR region, derived from *PhlacZ* gene (blue box); 19 amino acids derived from the psychrophilic β -Galactosidase coding sequence containing SD of ORF2 from *PhtrpA* operon (light blue box); *CDKL5*, the gene encoding the human CDKL5 (white box) fused to TATk (red box), 6xHis tag (green box) and 3xFlag tag (yellow box) at the N-terminal and C-terminal domains, respectively. Tobacco Each Virus protease (TEV) and Enterokinase (EK) recognition sequences were added between the CDKL5 sequence and each affinity tag (indicated with scissors). 1-bp frameshift between the stop codon of the first cistron and the start codon of the second one is highlighted in bold.

The gene was then cloned through the Golden Gate assembly strategy into the available bicistronic expression cassette BCD2 under the control of the P79 promoter. The resulting construct pBCD2_79C-*CDKL5* (Figure 2.6A) was mobilized into *PhTAC125* KrPI *lacY*⁺ by intergeneric conjugation. A qPCR analysis was carried out to define if the enhancement in translational efficiency allows an increment in the transcript levels of the *CDKL5* gene. The quantification of mRNA detected in the bicistronic system was expressed as fold-change relative to the levels detected in the monocistronic one. The result demonstrated an increase of about 2.8-fold in *CDKL5* mRNA obtained from the BCD2 asset, confirming that the translation rate in p79C impaired the protein recombinant production. Then, the effects of this amelioration were evaluated via Western blotting using the anti-*CDKL5* antibody (Figure 2.6B). Compared to the protein obtained with the monocistronic system (lanes 1,2,3,4), the analysis pointed out an extra immunoreactive band apparently corresponding to a higher molecular weight of *CDKL5* when the production was performed with the BCD2 system (lanes 5,6,7,8).

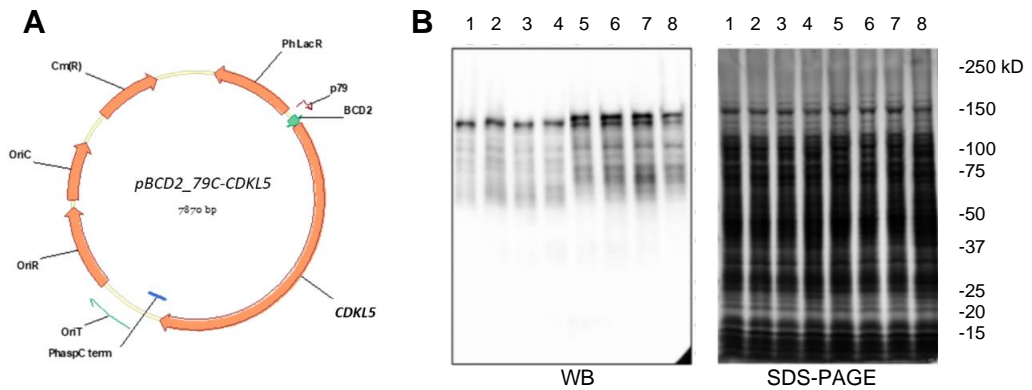


Figure 2.6. Evaluation of the recombinant CDKL5 production using monocistronic and bicistronic expression systems in *PhTAC125 KrPI lacY⁺*. (A) Schematic map of the pBCD2_79C-CDKL5 expression vector. *OriC*, pUC18-derived origin of replication; *OriR*, pMtBL-derived autonomous replication sequence; *OriT*, conjugational DNA transfer origin; *P.h.aspC term*, transcriptional terminator; *P79* and *Ph LacR*, psychrophilic promoter inducible by IPTG and its regulator, respectively; *BCD2*, bicistronic expression cassette derived from *lacZ* and *trpA* genes; *CDKL5*, gene coding the human CDKL5. (B) Evaluation of the recombinant production of CDKL5 using the pBCD2_79C expression system in comparison with p79C. Total cellular extracts of *PhTAC125 KrPI lacY⁺* harbouring the bicistronic expression system and the monocistronic one were analysed after different times from the induction by SDS-PAGE and Western blot analysis. Lanes 1, 2, 3 and 4 show the protein expression in the monocistronic system after 1.5, 3, 6 and 24 hours after the induction. Lanes 5, 6, 7, and 8 display the production profile of CDKL5 in BCD2 design after 1.5, 3, 6 and 24 hours of expression.

In order to understand if the signal visible in the analyses carried out with the monocistronic asset might be a truncated form of the protein, a Western blot analysis was performed using the anti-His antibody for the detection of the full-length form of the protein. As shown in Figure 2.7B, the monocistronic design did not allow the preservation of the N-terminal extremity of CDKL5 (lane 2), while the translational coupling promoted the true full-length form production (lane 1). Furthermore, Western blotting with anti-Flag antibody verified the integrity at the C-terminal of the protein produced with both expression systems (Figure 2.7C). In panels A and D were shown Coomassie staining and Western blotting with the anti-CDKL5 antibody, which were used as normalization controls.

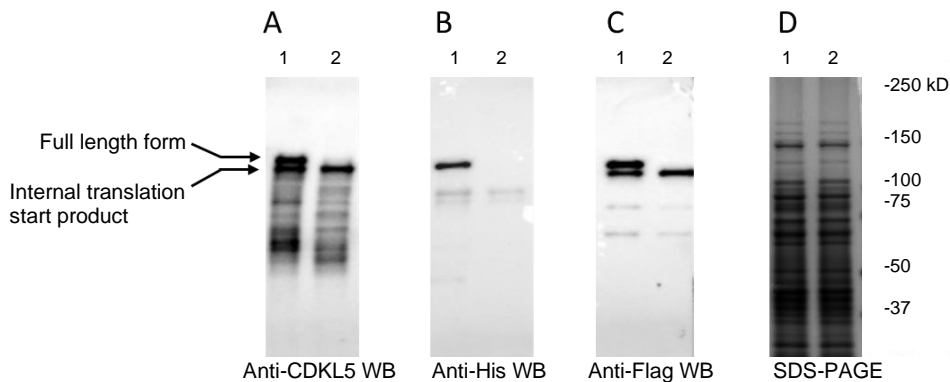


Figure 2.7. Evaluation of extremity integrity of recombinant CDKL5 produced using monocistronic and bicistronic expression systems in *PhTAC125* KrPI *lacY*⁺. Total cellular extracts of *PhTAC125* KrPI *lacY*⁺ harbouring the bicistronic and monocistronic expression system were analysed by SDS-PAGE and Western blot analysis using different antibodies. **(A)** Western blotting with the anti- CDKL5 antibody. **(B)** Western blotting with the anti- His antibody. **(C)** Western blotting with the anti- Flag antibody. **(D)** Coomassie staining. Lane 1 shows the protein produced in the BCD2 vector; Lane 2 displays the production profile of CDKL5 in the monocistronic system.

2.3.2.3 Assessment of different translation initiation sites on the production of CDKL5

The observation that the protein in the bicistronic system was produced as two main forms and a reanalysis of the CDKL5 gene coding sequence suggested that the possible reason for this translational issue could be the existence of an internal ATG triplet in position 43 of the protein, which could act as alternative initiation translation site. Indeed, an atypical Shine Dalgarno sequence in the upstream region of this triplet was identified (Figure 2.8A). Following this hypothesis, two CDKL5 variants were generating through the QuickChange site-directed mutagenesis kit. In detail, a first variant- named M43V- was obtained by changing the Methionine in position 43 into Valine. As a complement of this variant, CDKL5-M11/G2Stop was established by substituting the first Methionine with Isoleucine and the second amino acid (Glycine) with a stop codon (Figure 2.8B).



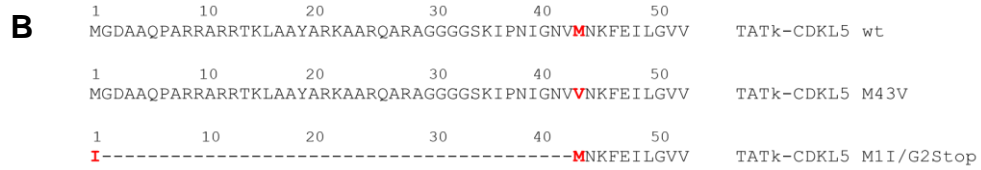


Figure 2.8. Analysis of different translation initiation sites in CDKL5 construct. (A) Nucleotide and aminoacidic sequence of CDKL5. The atypical SD sequence is highlighted in red. The internal ATG triplet is reported in bold. (B) Schematic representation of CDKL5 variants. CDKL5-M43V carried the mutation of the methionine 43 in valine. CDKL5-M1I/G2Stop presented the methionine 1 converted in isoleucine and the second amino acid (glycine) in a stop codon.

Both constructs were expressed in TAC125 KrPI *lacY*⁺ harbouring BCD2-79C expression system, performing a typical culture at 15°C. The SDS-PAGE and Western blot analysis (Figure 2.9A,B) on total cellular extracts recovered after 3, 8 and 24 hours from the induction turned up a significant difference in molecular weight between the recombinant protein starting at its authentic ATG codon with respect to the internal one. As shown in lanes 1,2, and 3, the elimination of the internal translation start in the CDKL5-M43V variant allowed the production of the real full-length protein (117 kDa). On the other hand, CDKL5-M1I/G2Stop variant gave proof of an internal translation initiation site since the translation at the first methionine was prevented by the replacement of the Methionine with Isoleucine and the insertion of a stop codon. Lanes 4,5, and 6 indeed showed a band of 111 kDa attributable to a truncated form of the protein. As expected, both bands (117 kDa and 111 kDa) were observed in CDKL5 wt produced in the same conditions (lanes 7,8 and 9). The mutation in position Methionine 43 effectively allowed the production of true full-length form only, and for this reason, the CDKL5-M43V variant was selected for the following experiments.

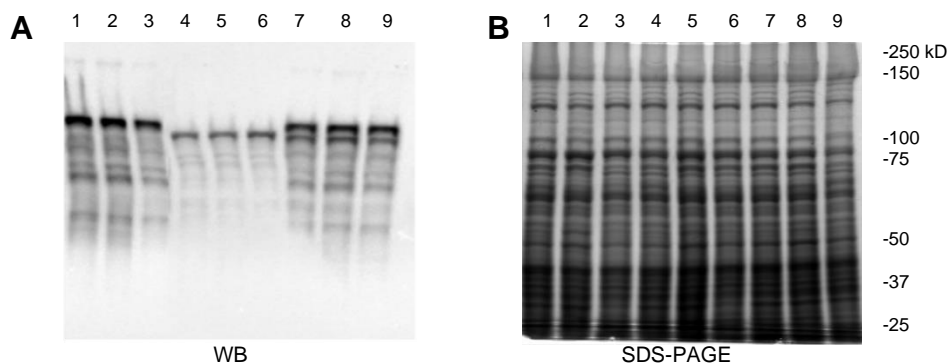


Figure 2.9. Assessment of different translation initiation sites on the production of CDKL5. (A) Western blotting with the anti-CDKL5 antibody. (B) Coomassie

staining. Lanes 1, 2, and 3 show CDKL5-M43V variant produced after 3, 8 and 24 hours of expression. Lanes 4, 5 and 6 display the production of CDKL5-M11/G2Stop after 3, 8 and 24 hours from the induction. Lanes 7, 8 and 9 represent the production profile of CDKL5 wt after 3, 8 and 24 hours of expression.

2.3.2.4 Improvement of recombinant protein production through the exploitation of psychrophilic vectors with enhanced copy number

A recent study unlocking some cryptic features of pMtBL endogenous plasmid of *PhTAC125* revealed a not negligible limit of all its derivative shuttle vectors [43]. A qPCR analysis indeed demonstrated a very low plasmid copy number (PCN) of this plasmid, equal to about 1. Since all the expression vectors till now implemented in *PhTAC125* contain the autonomous replication origin (OriR) of pMtBL [44], a strategy to enhance the PCN and consequently the production performance was applied. Very recent experiments performed by Dr Tutino's research group aimed to construct a library of OriR mutants. Since the molecular mechanism of replication of OriR has not yet been defined, random mutagenesis of this regulatory sequence was performed through an error-prone PCR. Then the mixture of the mutant amplicons was cloned into a suitable P79-based psychrophilic vector containing the eGFP coding sequence. Once the plasmid library was mobilized in KrPI by intergeneric conjugation [45], the production of eGFP was carried out in GG medium at 15°C using as inducer 10mM IPTG added at the exponential growth phase. After 24 hours from the induction, the bacterial culture was subjected to different rounds of fluorescence activated cell sorting (FACS) to isolate the clones associated with higher fluorescence intensity in comparison to the progenitor based on wt OriR (manuscript in preparation).

During these preliminary screenings, the fluorescence measurement was indirectly correlated to the PCN of each sorted population, and three mutated OriRs (called B40, K5, M8), derived from the clones with higher fluorescence intensity, were selected for the construction of as many expression systems for the production of CDKL5-M43V in the bicistronic arrangement. KrPL *lacY*⁺ was again used as the platform for recombinant production by using the resulting vectors. The experiment was performed as described in paragraph 2.3.1 and the different recombinant clones were evaluated by SDS-PAGE and Western blot analysis. Despite a metabolic burden that occurred after the induction of the recombinant production with an inhibition of cellular growth (data not shown), the exploitation of the expression vectors with mutated OriRs succeeded in ameliorating the production yield (Figure 2.10A,B). In particular, K5 (lanes 4, 5 and 6) and M8 (lanes 7, 8 and 9) contributed

to an enhancement of about 2.5-fold in the production levels in comparison to the original plasmid (lanes 10, 11 and 12). An extraordinary increase of CDKL5 signal (of about 10-fold) was instead observed when B40 replication origin (lanes 1, 2 and 3) was substituted to the wt (lanes 10, 11 and 12). Furthermore, the Coomassie staining showed for the first time the accumulation of the protein over the phase of induction (3, 8 and 24 hours). This experiment confirmed the evidence supported by Dr Tutino and coworkers about the crucial role of the plasmid copy number in the production yield and, for this reason, the expression vector containing B40 replication origin was selected for further recombinant productions.

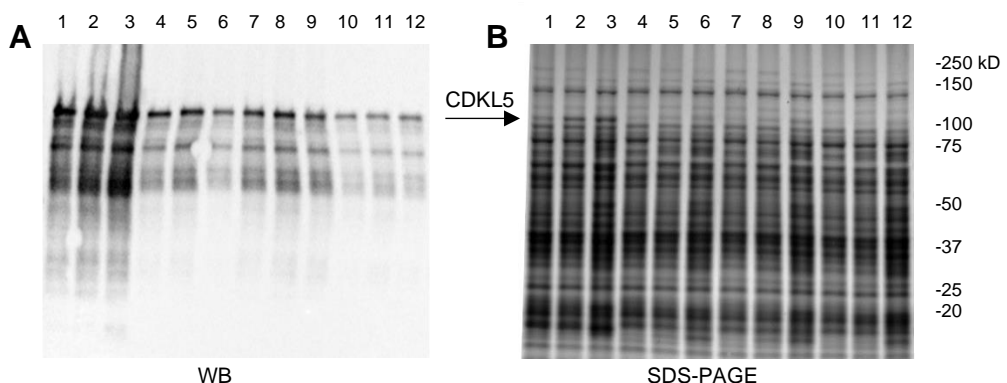


Figure 2.10. Exploitation of psychrophilic vectors with enhanced copy number for the production of CDKL5-M43V. (A) Western blotting with the anti-CDKL5 antibody. (B) Coomassie staining. Lanes 1, 2, and 3 show CDKL5-M43V produced after 3, 8 and 24 hours of expression with the B40-based vector. Lanes 4, 5 and 6 display the production of CDKL5-M43V after 3, 8 and 24 hours from the induction obtained using the K5-based vector. Lanes 7, 8 and 9 represent the production profile of CDKL5-M43V after 3, 8 and 24 hours of induction with the M8-based vector. Lanes 10, 11 and 12 represent the production profile of CDKL5-M43V after 3, 8 and 24 hours of induction with the original expression plasmid.

2.3.2.5 Assessment of different N-terminal tag on the expression level of CDKL5

Another aspect considered to improve recombinant production is protein fusion technology. Fusion systems are commonly used to enhance recombinant yield, improve protein solubility and folding, reduce proteolytic degradation of the recombinant products and simplify purification and detection. Since the high heterogeneity of fusion tags features, predicting which one will enhance the production of a difficult-to-express protein remains empirical [46]. Several comparative studies are reported in the literature, and the SUMO tag seems to be a

promising technological advancement to enhance expression and solubility in comparison to other commonly used tags [47]. Indeed, the tight, rapidly folding soluble structure of SUMO provides a nucleation site for the proper folding of fused partner proteins. Furthermore, one distinguishing feature of this fusion system is the ability of its associated SUMO protease to cleave a variety of fusion partners with remarkable fidelity and efficiency, generating native proteins with no extra amino acids at their N-terminal end [48].

Given the reported advantages in using the SUMO tag as a fusion system, a further variant of CDKL5 was designed. In detail, the SUMO tag was fused to CDKL5-M43V between the 6xHis tag and CDKL5 encoding sequences (Figure 2.11).

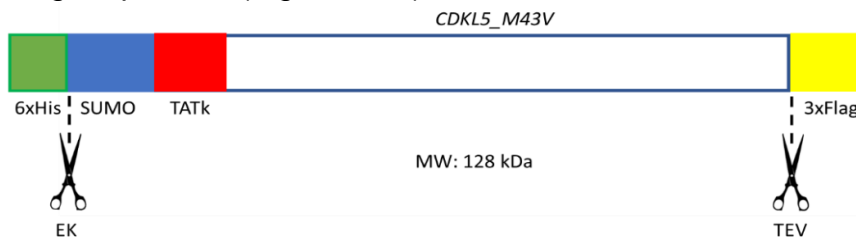


Figure 2.11. Construction of a new construct of CDKL5 with a different N-terminal tag. Schematic representation of SUMO-CDKL5-M43V variant. *CDKL5-M43V*, gene encoding CDKL5-M43V variant (blank box) fused to 6xHis tag (green box), SUMO tag (blue box) and TATk peptide (red box) coding sequences at 5' region. 3xFlag tag sequence (yellow box) was fused at the 3' domain.

The obtained construct was cloned in the B40-based vector containing the BCD2 asset and expressed in TAC125 KrPI *lacY*⁺. The recombinant production was then evaluated through SDS-PAGE and Western blotting in comparison with the CDKL5-M43V variant. No evident enhancement in expression level was detected by the anti-CDKL5 antibody (data not shown) but, interestingly, the analysis performed with the anti-His antibody revealed a higher chemiluminescent signal of the version of the protein fused to the SUMO-tag (128 kDa) (lane 2, Figure 2.12). This suggested that SUMO allowed the protection of the N-terminal extremity of the protein from the proteolysis, which was most predominant in the CDKL5-M43V variant (lane 1), resulting in a higher accumulation of integral protein.

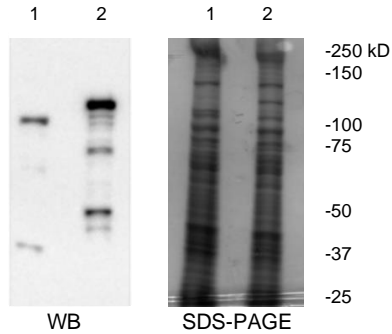


Figure 2.12. Assessment of different N-terminal tag on the production of CDKL5. SUMO-CDKL5-M43V variant was produced in *PhTAC125* KrPI *lacY⁺*-pB40-BCD2-79C and analysed by SDS-PAGE and Western blotting on total cellular extracts in comparison to CDKL5-M43V. (Left panel) Western blotting with the anti-HIS antibody. (Right panel) Coomassie staining. 1, CDKL5-M43V variant; 2, SUMO- CDKL5-M43V variant.

2.3.2.6 Estimation of the production yield achieved through the overall optimization of the expression platform

Each of the ameliorations appointed both to the bacterial strain and the expression cassette contributed to a step by step increase of the final recombinant product. The estimation of the production yield obtained with the optimized expression platform was performed through Western blotting. The analysis was conducted comparing CDKL5 detected in the total cellular extract of recombinant *PhTAC125* with scalar amounts of a commercial standard (His-Neuropilin-2, 115 KDa) (Figure 2.13). The densitometric analysis of the anti-His signals revealed a yield of about 4 mg of recombinant SUMO-CDKL5-M43V per Liter of culture. This data confirmed the effectiveness of the overall optimization efforts, which allowed to obtain a cytosolic production yield of recombinant proteins in *PhTAC125* now more than enough for the subsequent downstream process, a fundamental step required for structural, functional and therapeutic applications.

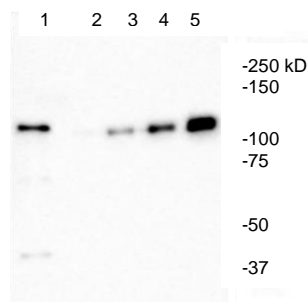


Figure 2.13. Estimation of production yields of SUMO- CDKL5-M43V produced in KrPI *lacY⁺* harbouring pB40-79C-BCD2-*sumo-CDKL5-m43v*. An anti-His

Western Blotting was performed for the analysis of the total cellular extract of KrPI *lacY*⁺ harbouring pB40-79C-BCD2-*sumo*-*CDKL5-m43v* in comparison to scalar quantities of commercial His-Neuropilin-2. 1, Total cellular extract (1/120 OD); 2, His-Neuropilin-2 (2 ng); 3, His-Neuropilin-2 (4 ng); 4, His-Neuropilin-2 (8 ng); 5, His-Neuropilin-2 (16 ng).

2.3.3 In vitro evaluation of the biological activity of recombinant CDKL5

An activity assay for CDKL5 was developed to demonstrate the high quality of the recombinant proteins produced in the psychrophilic microorganism. It is based on the kinase activity of CDKL5 on human EB2, a microtubule-associated protein recently reported to be a specific CDKL5 phosphorylation substrate [49]. The method takes advantage of the recent availability of an antibody recognizing the phosphorylation of EB2 at the Ser222 site [50]. To develop the activity assay, EB2 was recombinantly produced in *E. coli* and purified (as described in Supplementary Materials). Defined amounts of this substrate were then incubated in the presence of a CDKL5-enriched fraction and the phosphorylation of EB2 was evaluated by western blotting using the anti-EB2pSer222 antibody.

2.3.3.1 Setting up the activity assay of CDKL5 and biochemical characterization

To establish the activity assay, a purified form of the enzyme (provided by Amicus Therapeutics Inc.) was incubated with EB2 in kinase buffer for 30 minutes at 30°C. The reaction was then stopped through denaturation of the samples and the substrate phosphorylation was detected by Western blot analysis carried out with the anti-EB2pS222 antibody, as above described. In particular, the enzymatic activity of CDKL5 in different assay conditions was evaluated. The kinase activity was tested changing the enzyme concentration, ionic strength and additives known to stabilize proteins. As shown in Figure 2.14A, EB2 (200ng) is highly efficiently phosphorylated in a CDKL5 concentration-dependent manner (in a range of enzyme quantity of 5-50 ng). Furthermore, the kinase proved to be active in a wide range of NaCl (from 0.05 to 1M) and glycerol (from 2.5 to 20% v/v) concentrations even when a low quantity (5 ng) of CDKL5 was assayed (Figure 2.14B). This data paved the way for the in vitro assay set up on a partially purified fraction of CDKL5 produced in the KrPI *lacY*⁺ p79C-BCD2 expression system.

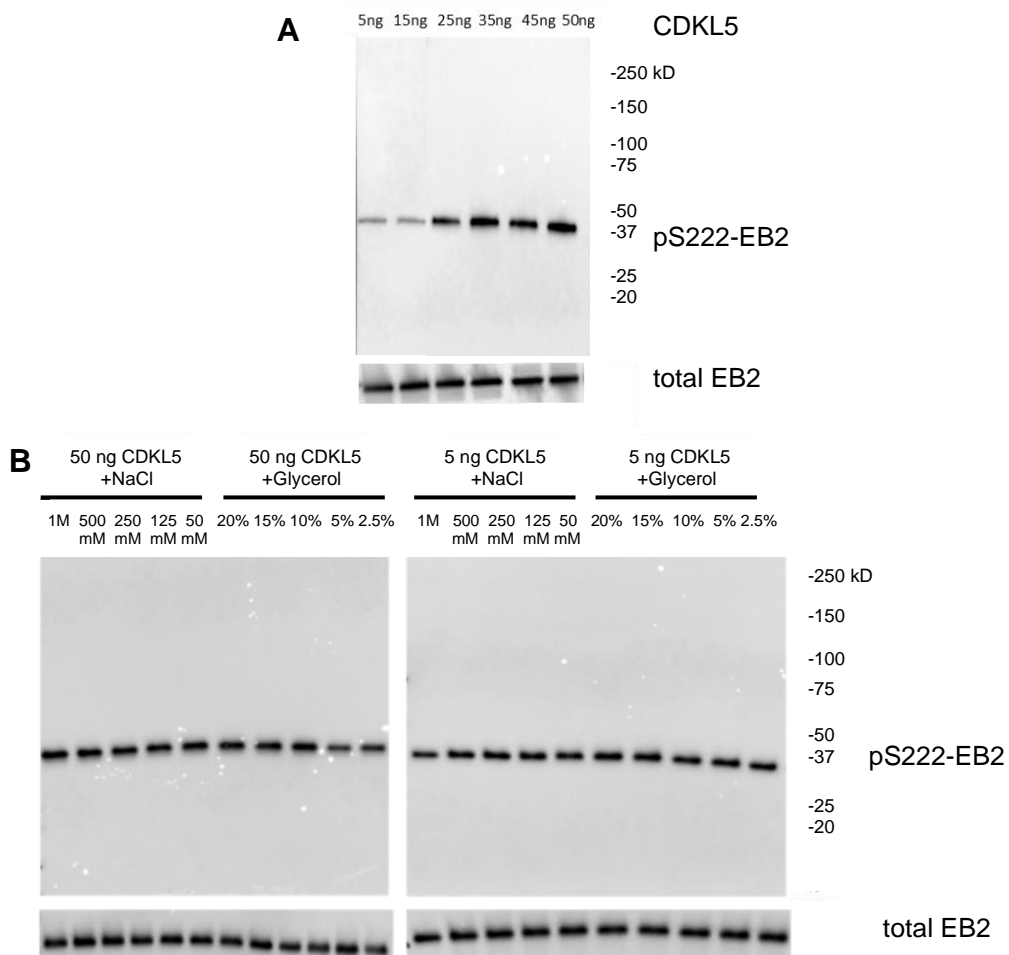


Figure 2.14. In vitro kinase assays of CDKL5 and its biochemical characterization. Purified CDKL5 (provided by Amicus Therapeutics Inc.) was incubated with 200ng EB2 in kinase buffer at 30°C for 30 minutes. The phosphorylation of EB2 at the Ser222 site was assessed by Western blotting. The substrate phosphorylation was normalized for EB2 protein level. **(A)** In vitro kinase assay performed with an increasing quantity of CDKL5 from 5ng to 50 ng. **(B)** Assessment of kinase activity of CDKL5 (50ng and 5ng) with increasing concentration of NaCl (50mM- 1M) and glycerol (2.5%- 20% v/v). The experimental conditions are reported in the upper panel of each figure.

2.3.3.2 Partial purification of CDKL5

Sumo-CDKL5-M43V was produced in KrPI *lacY*⁺ harbouring p79C-BCD2 expression system and subjected to a preliminary purification screening (data not shown). Below the better trial is described. The recombinant cells were lysed through sonication, and the soluble fraction was loaded on Sartobind S MA75 membrane adsorber to

perform a batch cationic exchange chromatography. After a washing step with equilibration buffer, the elution was directly performed by increasing the ionic strength of the buffer solution. The harvested fractions were then analysed through SDS-PAGE and Western blot with anti-CDKL5 antibody (Figure 2.15). A CDKL5-enriched fraction was obtained, but several contaminants could be observed by SDS-PAGE (left panel). Furthermore, the full-length protein was co-eluted with different proteolyzed forms, as shown in Western blot (right panel). Overall, the eluted fraction (about 2 mg) seemed suitable for setting up an *in vitro* activity assay since the full-length form of the protein constituted about the tenth part of the total protein content.

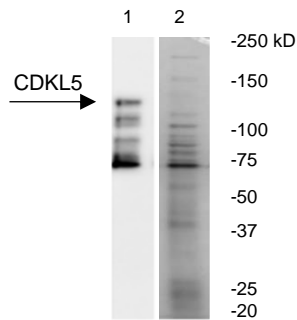


Figure 2.15. Small scale purification trial of CDKL5 through cationic exchange chromatography CEX. Analysis of the fraction obtained from CEX performed on membrane adsorber of KrPI-*lacY*⁺ soluble cellular fraction after Sumo-CDKL5-M43V production using p79C-BCD2 as the expression system. 1, SDS-PAGE; 2, Western blot.

2.3.3.3 Sumo-CDKL5-M43V kinase activity assay

Once obtained, 100µg CEX fraction containing CDKL5 were incubated with 5.4µg EB2 to test the kinase activity of the recombinant human protein produced in the psychrophilic host. The reaction was conducted as described above and the phosphorylation of EB2 was assessed by Western blot analysis (Figure 2.16). The recombinant protein obtained from the CEX chromatography resulted clearly active against its substrate. As detected by the pS222-EB2 antibody, EB2 was phosphorylated when incubated with Sumo-CDKL5-M43V in the presence of ATP (lane 1) while no signal was observed when the reaction was set up without ATP and EB2 (lanes 2 and 3, respectively). The substrate phosphorylation was normalized for the EB2 protein level.

This experiment demonstrated that the recombinant kinase is produced in an active form in the engineered psychrophilic expression system and that its activity is ATP-dependent.

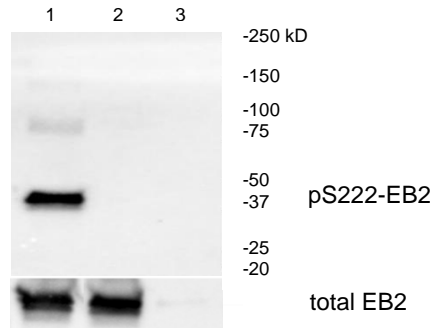


Figure 2.16. In vitro kinase assays showing efficient EB2 phosphorylation by Sumo-CDKL5-M43V produced in KrPI *lacY*⁺. 100 µg Sumo-CDKL5-M43V enriched-fraction was incubated with 5.4µg EB2 in kinase buffer at 30°C for 30 minutes. Western blot of activity assay reaction mixes showed the phosphorylation of EB2 at the pSer222 site. The substrate phosphorylation was normalized for the EB2 protein level. 1, kinase assay set up in the presence of Sumo-CDKL5-M43V, EB2 and ATP; 2, kinase assay set up in the absence of ATP; 3, kinase assay set up in the absence of EB2.

2.4 Discussion

The human X-linked gene *cyclin-dependent kinase-like 5 (CDKL5)* encodes a serine/threonine protein kinase abundantly expressed in the brain [51]. CDKL5 plays important roles in brain development and function and is involved in several cellular processes. Mutations in its coding gene have been associated with CDKL5 deficiency disorder (CDD) [25], a neurodevelopmental disorder characterized by early-onset epileptic encephalopathy and severe intellectual disability [53, 21].

Although the complete characterization of the functional pathways of CDKL5 and pathogenesis in CDD is still undefined, different therapeutic approaches based on small molecules, gene therapy, genome editing and RNA-based therapeutics are currently under development [26]. In this context, Enzyme Replacement Therapy (ERT) presents great potentiality as an effective treatment for CDD. Recently, the best characterized viral protein transduction domain (TAT) was fused to CDKL5 and used as a therapeutic agent in the murine CDD model [36]. The treatment resulted in the resolution of some impairments of brain functions without cytotoxic and immunogenic effects. The production of CDKL5 in full-length, soluble and active form is thus pivotal for developing this therapy. Furthermore, the availability of the enzyme represents an essential milestone in understanding its physiological function and the underlying cause of the dysfunctions associated with CDD.

Although the recombinant production of truncated active forms of the protein was obtained using the conventional bacterial host *E. coli* [53], the structural features of CDKL5 as intrinsically disordered protein (IDP) make this enzyme production very difficult. The main issues of extensive proteolysis and systematic aggregation in inclusion bodies often resulted in totally insoluble and inactive protein [54, 55], while the recombinant production in eukaryotic cells is limited by cytotoxicity and undesired post-translational modifications.

Given the above, CDKL5 represented an appropriate candidate to demonstrate the feasibility of the psychrophilic bacterium *PhTAC125* as a cell factory for the production of difficult to express proteins. In particular, a step-by-step optimization of the recombinant production was performed, managing different bottlenecks.

Promising preliminary results were obtained using KrPL *lacY*⁺ to produce TATk-CDKL5, with an increment of about 10-fold in protein yield compared with the wt strain, but a weak accumulation of *CDKL5* transcript affected the recombinant production.

Different factors might critically alter the overall expression level, such as promoter strength, the translation speed, the fusion between the untranslated region and the translation initiation region (UTR/TIR), and all of them contribute to the mRNA stability and efficiency of transcription and translation [56, 57]. Since the qRT-PCR analysis demonstrated that the P79 promoter induced the rapid accumulation of transcripts of two reporter genes, the hypothesis of a limited promoter efficiency was ruled out. Hence, we evaluated the benefit of improving the translation efficiency, considering that the shortage of a recombinant transcript could be a consequence of inadequate ribosome coverage. This objective was accomplished by implementing the psychrophilic vector of a bicistronic design, conceived to reduce the transcript degradation, presumably through higher ribosomal occupancy and steric protection of potential cleavage sites [42]. As expected, this adjustment resulted in the triplication of the transcript level detected after gene expression induction, also suggesting a translation efficiency enhancement.

However, our data suggest still low recombinant mRNA abundance, and further studies about the intrinsic stability, effects of secondary structures at the distal ends and codon bias could gain more insights [59, 56].

Notably, the most relevant result that emerged from the translational coupling was the identification of an internal initiation translation site at the Methionine 43. The replacement of this residue by Valine gave birth

to the variant TATk-CDKL5-M43V, which allowed the transcript conversion into the true integral form of the protein.

In this respect, it should not be overlooked that the remarkable translation capabilities of the psychrophilic bacterium may have shed light on a regulative mechanism also occurring in the biological context of CDKL5. Since a considerable number of eukaryotic transcripts possesses multiple initiation codons [59,60], it could be of great interest to examine if the two isoforms of CDKL5 coexist in human tissues and their functional relevance. Given the several regulations since now described for this protein [1], studies regarding the spatial and temporal expression profiles could be performed to determine whether these isoforms are localised into different cellular compartments or possess different tissue-specificity. The abundance of destabilising residues in the N-terminus of the short CDKL5 form could also suggest a different rate of degradation and a potential short half-life [61,62]. Furthermore, if on the one hand, this region is highly conserved across many species [64], suggesting an important functional role, on the other, the structural studies carried out on the catalytic domain failed in the resolution of the first 12 residues of the protein [11], complicating the advancement of a hypothesis. In this scenario, the variants of CDKL5 designed to demonstrate the existence of the internal initiation site in *PhTAC125* could be helpful to deepen our observation.

Since no experimental evidence has demonstrated so far which Methionine is the effective initiator in the human cells, we focused on the full-length construct to optimise its recombinant production.

One of the most significant improvements in terms of enhancement of recombinant protein productivity, was finally achieved when a new generation of psychrophilic expression vectors with a high copy number was available in Dr Tutino laboratory. The highest recombinant gene dosage correlated to the highest plasmid copy number triggered an increase in protein production yield of about 10-fold.

Furthermore, the need to obtain recombinant constructs less susceptible to transcriptional and translational issues led us to evaluate other fusion tags. Since a highly expressed N-terminal tag could stabilize the mRNA of a poorly expressing partner [65], the SUMO tag was chosen as the fusion partner of TATk-CDKL5-M43V. Interestingly, the main advantage gained with this new construct was the improved protection of the N-terminal domain from proteolytic degradation. This result led us to postulate that TATk may critically induce a protein conformation prone to proteolysis, and the presence of SUMO as a spacer between the N-terminal His-tag and TATk exerts a beneficial protective effect.

Finally, preliminary purification trials demonstrated that the protein produced in KrPI *LacY*⁺ is enough soluble to obtain an enriched fraction in just one chromatographic step. This outcome was essential to set up an in vitro activity assay which unquestionably demonstrated the capability of the recombinant CDKL5 to phosphorylate its natural substrate EB2.

In conclusion, the overall successful completion of translational issues, proteolytic stability and the proper arrangement of recombinant gene dosage managed the construction of a robust cell factory quite proficient in producing the human difficult to express protein CDKL5 with high production yield (about 4 mg/L culture) in an active form. It is reasonable to expect that most other foreign genes may be expressed at high levels in *PhTAC125* and that the production process will be amenable to scale-up, paving the way for its application also in the industrial field.

2.5 Materials and methods

2.5.1. Bacterial strains and growth media formulations

The strains used in this study are listed in Table 2.1. *E. coli* DH5 α was used for cloning procedures. The intergeneric conjugations [44] were performed by using *E. coli* S17-1(λ pir) as the donor strain and KrPL, KrPL *lon* and KrPL *lacY*⁺ as the recipient strains. *E. coli* BL21 (DE3), KrPL, KrPL *lon* and KrPL *lacY*⁺ [37] were used for the recombinant productions. *E. coli* was cultured in LB broth (10 g/L bacto-tryptone, 5 g/L yeast extract, 10 g/L NaCl) at 37 °C and the recombinant strains were treated with either 34 μ g/mL chloramphenicol and 50 μ g/mL kanamycin depending on the selection marker of the vector. KrPL and its derivative strains were grown in TYP (16 g/L bacto-tryptone, 16 g/L yeast extract, 10 g/L NaCl) during conjugations and precultures development, and in GG (10 g/L L-glutamic acid monosodium salt monohydrate, 10 g/L D-gluconic acid sodium salt, 10 g/L NaCl, 1 g/L NH₄NO₃, 1 g/L K₂HPO₄, 200 mg/L MgSO₄·7H₂O, 5 mg/L FeSO₄·7H₂O, 5 mg/L CaCl₂) [66] during the expression experiments. The growths of recombinant psychrophilic strains were performed in the presence of chloramphenicol, used at 12.5 μ g/mL in solid media and 25 μ g/mL in liquid media.

Bacterial strain	Relevant features
<i>E. coli</i> strains	
DH5 α	<i>supE44</i> , Δ <i>lacU169</i> (ϕ 80 <i>lacZ</i> Δ M15) <i>hsdR17</i> , <i>recA1</i> , <i>endA1</i> , <i>gyrA96</i> , <i>thi-1</i> , <i>relA1</i>

S17-1(λ pir)	<i>thi, pro, hsd (r- m+) recA::RP4-2-TCr::Mu Kmr::Tn7, Tpr, Smr, λpir</i>
BL21(DE3)	<i>F-ompT hsdSB(rB- mB-) gal dcm (DE3) pLysS (CamR)</i>
PhTAC125 strains	
Krpl	<i>PhTAC125 cured strain without pMtBL plasmid</i>
Krpl <i>lon</i>	<i>PhTAC125 cured strain without pMtBL plasmid lon::pVS-lon</i>
Krpl <i>lacY</i> ⁺	<i>PhTAC125 cured strain without pMtBL plasmid lon::pVS -lacY</i>

Table 2.1. Bacterial strains used in this study.

2.5.2 Construction of the plasmids

The plasmids and primers used in this study are reported in Table 2.2. The gene sequence for TATk-CDKL5-Flag-His with optimized codon usage for *PhTAC125* was synthesized by Thermo Fisher Scientific and cloned within p79C [37] using NdeI and EcoRI restriction sites.

For the construction of pBCD2-79C-*CDKL5*, p79C was converted in p79BsC to remove undesired restriction sites and introduce PstI and BsaI sites immediately downstream to the P79 promoter. The obtained vector was hydrolyzed with PstI and SacI restriction enzymes and ligated with one synthetic fragment of 5' region of *CDKL5* gene (the sequence was optimized using the “guided random” method of Optimizer web tool [67] and synthesized by Thermo Fisher Scientific) digested with PstI/HindIII and the second fragment of 3' region of *CDKL5* gene extracted from pMAVdH-TATk-*CDKL5* with HindIII/SacI digestion. The resulting vector (named pBEC_79C-*CDKL5*) presents BsaI-PstI restriction sites at the end of the P79 promoter followed by a second divergent BsaI site located at the upstream region of the *CDKL5* gene. The hydrolysis of pBEC_79C-*CDKL5* with BsaI enzyme generated extremities compatible with the synthetic fragment containing the BCD2 cassette (synthesized by Thermo Fisher Scientific) digested with the same restriction enzyme. The ligation of these two fragments allowed the obtaining of pBCD2-79C-*CDKL5*.

The generation of pBCD2-79C-*CDKL5-m43v* and pBCD2-79C-*CDKL5-m1i/g2stop* was accomplished using QuikChange Site-Directed Mutagenesis Kit following the manufacturer's protocol (Agilent Technologies). The mutagenic primers (listed in Table 2.2) were designed using the online QuikChange Primer Design Program.

The replacement of the OriR with its derivative mutants B40, K5 and M8 was performed cloning the fragment derived from the hydrolysis of pBCD2-79C-*CDKL5-m43v* performed with SphI/SacI into the pMAI-79C vector (a derivative of p79C vector containing NotI-Ascl restriction sites flanking the OriR) previously digested with the same enzymes. The

resulting pMAI-79C-BCD2-*CDKL5-m43v* was hydrolyzed with NotI/AscI and ligated to the mutated OriR extracted through the same digestion. pB40-BCD2-79C-*sumo-CDKL5-m43v* was obtained starting from the digestion of pBEC_79C-*CDKL5* with BsaI. Then, the fragment containing the sequence encoding SUMO tag (synthesized by Thermo Fisher Scientific) and the synthetic fragment containing the BCD2 cassette were hydrolyzed with the same enzyme. The complementarity of the extremities of the generated fragments allowed their ligation, resulting in the pBCD2-79C-*sumo-CDKL5-m43v* vector. Finally, B40 mutated OriR was replaced through SphI/SacI digestion of pBCD2-79C-*sumo-CDKL5-m43v* and ligation of the derived insert with pB40-BCD2-79C-*CDKL5-m43v* previously hydrolyzed with the same enzymes.

The gene sequence encoding His-EB2 with optimized codon usage for *E. coli* was synthesized by Thermo Fisher Scientific and cloned within pET40b using NdeI and BamHI restriction sites.

Plasmid	Features
p79C	Expression vector with <i>PhTAE79 lacZ</i> regulative sequences and Cm resistance
p79C- <i>CDKL5</i>	p79C vector producing codon optimized <i>hCDKL5_1</i> fused to TATk at the N-terminal domain and 3xFlag and 6xHis tags at the C-terminus
pBCD2-79C- <i>CDKL5</i>	p79C vector containing the bicistronic asset BCD2 and producing codon optimized <i>hCDKL5_1</i> fused to 6xHis tag and TATk at the N-terminal domain and 3xFlag at the C-terminus
pBCD2-79C- <i>CDKL5-m43v</i>	pBCD2-79C vector producing His-TATk- <i>hCDKL5_1</i> -Flag variant carrying the replacement of Methionine 43 with Valine
pBCD2-79C- <i>CDKL5-m1i/g2stop</i>	pBCD2-79C vector producing His-TATk- <i>hCDKL5_1</i> -Flag variant carrying the replacement of Methionine 1 with Isoleucine and Glycine 2 with a stop codon
pB40-BCD2-79C- <i>CDKL5-m43v</i>	pBCD2-79C- <i>CDKL5</i> containing B40 mutated OriR
pK5-BCD2-79C- <i>CDKL5-m43v</i>	pBCD2-79C- <i>CDKL5</i> containing K5 mutated OriR
pM8-BCD2-79C- <i>CDKL5-m43v</i>	pBCD2-79C- <i>CDKL5</i> containing M8 mutated OriR
pB40-BCD2-79C- <i>sumo-CDKL5-m43v</i>	pB40-BCD2-79C producing codon optimized His-TATk- <i>hCDKL5_1</i> -Flag fused to SUMO tag at the N-terminal domain

pET40b- <i>eb2</i>	pET40b producing codon optimized EB2 fused to 6xHis tag at the N-terminal domain
Primer	Sequence (5' – 3')
<i>PSHA_RS01090_fw</i> <i>PSHA_RS01090_rv</i>	CTAAAGACCAAATCCTTGACGCA GACCAGCTACCATAACCAGCA
<i>CDKL5_fw</i> <i>CDKL5_rv</i>	ACTCGTTGGTATCGCAGCCC TGGCCGTCAGAAAGTTCACCA
<i>lacZ_fw</i> <i>lacZ_rv</i>	ATTCGTTGGAGTGATGGCAGTT GCGTATTTGGCTTTGCGGTTT
<i>egfp_fw</i> <i>egfp_rv</i>	GGAGAGGGTGAAGGTGATGCT GGTCAGAGTAGTGACAAGTGTGG
<i>CDKL5-M43V_fw</i> <i>CDKL5-M43V_rv</i>	CCCTAACATTGGTAATGTAGTAAACAAATTCTGA AATTCTTGGTG CACCAAGAATTTCTGAATTTGTTTACTACATTACC AATGTTAGGG
<i>CDKL5-M1_G2Stop_fw</i> <i>CDKL5- M1_G2Stop _rv</i>	GAAAATAAGGAGGTCAAATAATTTGAGATGCG GCACAACCTGCAC GTGCAGTTGTGCCGCATCTCAAATTATTTGAC CTCCTATTTTC

Table 2.2. Plasmids and primers used in this work. Fw: forward. Rv: reverse.

2.5.3 Growth conditions

Glycerol stocks (- 80 °C) of Krpl, Krpl *lon* and Krpl *lacY*⁺ strains were streaked on TYP agar plates and incubated at 15°C. A single colony was inoculated in 1-2 mL TYP at 15 °C for 24-48 hours. Then, the cultures were diluted 1/100 in 10 mL GG medium and after 24 hours of incubation at 15°C, were diluted again at 0.3 OD/mL for 8 hours. The inoculum was finally performed at 0.1 OD/mL in the liquid medium filling an Erlenmeyer flask by 20% of its capacity. The induction of the recombinant expression was generally carried out in the late exponential phase (2 OD/mL) with 5 mM IPTG. Biosan PSU-20i orbital shaker was used setting the agitation to 180 rpm.

2.5.4 mRNA Extraction and qPCR

Total RNA was isolated using the Direct-zol RNA Kit (Zymo Research, Irvine, CA, USA) adopting the manufacturer's instructions, followed by treatment with RNase-free DNase I (Roche, Mannheim, Germany) to avoid genomic DNA contamination. Total RNA was reverse transcribed using SuperScript IV (Invitrogen, Carlsbad, CA, USA) according to the recommended protocol. 1 µL cDNA from each sample was used as the template for quantitative real-time PCR by using 1X PowerUp SYBR Green Master Mix (Applied Biosystems, Foster City, CA, USA) in the

presence of 400 nM of specific primers. The reactions were run by a StepOne Real-time PCR System (Applied Biosystems, Foster City, CA, USA) and three independent sets of experiments were performed.

The thermal cycling protocol was set up as follows: UDG activation for 2 min at 50 °C; initial denaturation for 10 min at 95 °C; 40 cycles of denaturation for 15 sec at 95 °C alternated with annealing/extension steps for 1 min at 60 °C. At the end of each reaction, melting curves were performed to verify the presence of a specific and unique amplification product. Each couple of primers was designed using the Primer 3 web tool and is reported in Table 2.2.

2.5.5 Analysis of the production of the recombinant proteins

To verify the expression levels, 1 OD cell pellets were collected during the production experiments by centrifugation and solubilized in 60 µL of Laemmli buffer 4X. Then, the samples were boiled at 95 °C for 20 min, quickly cooled on ice for 1 minute and finally centrifuged at 10,000 x g for 5 min at RT. The equivalent of 1/20 OD and 1/12 OD (3-5 µL of total protein extract samples, respectively) were analyzed by SDS-PAGE using 4 - 15% Mini-Protean TGX (Biorad) gels in TGS buffer, setting the power supply to constant 120 V. For electroblotting, the Biorad Transblot Turbo system with Biorad PVDF mini membranes was used. After the transfer, the membrane was blocked with PBS, 0.05% v/v Triton X-100, 5% w/v milk for one hour and incubated with a specific primary antibody.

For the detection of CDKL5, the anti-CDKL5 antibody was diluted 1:1,000 in the same buffer. After one hour of incubation at RT with the primary antibody, the membrane was washed with PBS, 0.05% v/v Triton X-100 three times (5 min each) and incubated with an anti-mouse antibody diluted 1:10,000 in PBS, 0.05% v/v Triton X-100, 5% w/v milk for one hour at RT. Then, the membrane was washed again with PBS, 0.05% v/v Triton X-100 three times (5 min each) and the secondary antibody was detected using the ECL method.

The 3xFlag peptide was detected using Monoclonal ANTI-FLAG M2, Clone M2 (F1804, Sigma) antibody diluted 1:1,000 in PBS, 0.2% v/v Tween 20, 5% w/v milk. After overnight incubation at 4 °C with the primary antibody, the membrane was washed with PBS, 0.2% v/v Tween 20 three times (5 min each) and incubated with an anti-mouse antibody diluted 1:5,000 in PBS, 0.2% v/v Tween 20, 5% w/v milk for one hour at RT. Then, the membrane was washed again with PBS, 0.2% v/v Tween 20 three times (5 min each) and the secondary antibody was detected using the ECL method.

The 6xHis tag was highlighted with Monoclonal Anti-polyHistidine-Peroxidase clone HIS-1 antibody (A7058, Sigma) diluted 1:2,000 in PBS, 0.05% v/v Tween 20, 5% w/v milk. After one hour of incubation at RT with the antibody, the membrane was washed with PBS, 0.05% v/v Tween 20 three times (5 min each) and it was developed using the ECL method. For the quantification of the production yield, Western blotting with anti-His antibody was performed using His-Neuropilin-2 (Immunological Sciences) as the reference standard.

For the detection of EB2, the membrane was blocked after the transfer with TBST (20 mM Tris, 137 mM NaCl, 0.1% Tween-20 pH 7.6), 5% w/v milk for one hour. Then, MAPRE2/EB2: 00109234 (Covalab) antibody was diluted 1:4000 in the same buffer. After overnight incubation at 4 °C with the primary antibody, the membrane was washed with TBST three times (5 min each) and incubated with an anti-mouse antibody diluted 1:10000 in PBS, 0.05% v/v Triton X-100, 5% w/v milk for one hour at RT. Then, the membrane was washed again with PBS, 0.05% v/v Triton X-100 three times (5 min each) and the secondary antibody was detected using the ECL method.

The detection of the phosphorylated EB2 was instead performed as follows. The membrane was blocked with TBST, 5% w/v milk for one hour. Then, EB2 pS222: 00117739 (Covalab) antibody was diluted 1:4000 in the same buffer. After overnight incubation at 4 °C with the primary antibody, the membrane was washed with TBST three times (5 min each) and incubated with an anti-rabbit antibody diluted 1:2000 in TBST and 5% w/v milk for one hour at RT. Then, the membrane was washed again with TBST three times (5 min each) and the secondary antibody was detected using the ECL method.

2.5.6. EB2 recombinant production and purification

EB2 was produced in *E. coli* BL21(DE3) bearing the pET40b-*eb2* vector. The recombinant cells were grown as reported in section 2.5.1. During the first production screening, the induction of expression was performed at the exponential growth phase (0.5 OD/mL) with 0.1 and 1mM IPTG. Then the cells were incubated at 15°C, 25°C and 37°C for the entire duration of the production phase. Once the best production condition was defined, the recombinant cells were grown in LB medium in the presence of 50 µg/mL of kanamycin at 37°C. At 0.5 OD/mL, 0.1 mM IPTG was supplemented and the temperature was shifted to 15°C overnight. Then the bacterial cells were harvested by centrifugation at 10,000 x *g* for 30 min at 4°C.

Afterwards, 500 OD cell pellet was resuspended in 20mL Lysis buffer (50mM Tris-HCl pH8.0, 500mM NaCl, 20mM Imidazole, 5% v/v glycerol, 10mM MgCl₂, 50U/mL DNAsil) supplemented with Complete EDTA-free protease inhibitor cocktail (Roche). The suspension was subjected to disruption by sonication (MS72 probe, 20% Amplitude with 30 seconds pauses) (Sonopuls Ultrasonic Homogenisers HD, Bandelin) and the soluble and insoluble fractions were separated by centrifugation (13,000 x *g* for 45 min at 4°C). The clarified lysate was applied to IMAC using a 1mL HisTrap HPcolumn (GE Healthcare) and an Akta purifier system (GE Healthcare). The bound fractions were washed and eluted using IMAC Wash buffers (50mM Tris-HCl pH8.0, 500mM NaCl, 5% v/v glycerol, 50mM and 100mM Imidazole) and IMAC Elution buffer (50mM Tris-HCl pH8.0, 500mM NaCl, 500mM Imidazole, 5% v/v glycerol), respectively. The eluted fractions were further subjected to a size exclusion chromatography (Superdex 75 prep grade, GE Healthcare) performed using 50mM Tris-HCl pH8.0, 100mM NaCl, 5% v/v glycerol as running buffer. About 500 µg of purified protein was collected from a 1 L culture and it was finally stored at -20 °C.

2.5.6. CDKL5 partial purification

120 OD cell pellet of KrPI *lacY*⁺ harbouring pB40-BCD2-79C-*sumo-cdkl5-M43V* was resuspended in 2mL Lysis buffer (50 mM Hepes pH 7.8, 25 mM NaCl, 1 mM DTT, 10% v/v Glycerol, 5 mM EDTA, 10mM MgCl₂, 50U/mL DNAsil) supplemented with Complete ULTRA mini EDTA-free protease inhibitor cocktail (Roche). The suspension was sonicated for 20 minutes (with 30 seconds pauses) with MS72 probe at 10% Amplitude by using Sonopuls Ultrasonic Homogenisers HD, Bandelin. Then the soluble and insoluble fractions were separated by centrifugation (13,000 x *g* for 60 min at 4°C). The clarified lysate was applied to a Sartobind S MA75 membrane adsorber, and the bound proteins were washed with the equilibration buffer (50 mM Hepes pH 7.8, 25 mM NaCl, 1 mM DTT, 10% v/v Glycerol). Then, the elution was performed with 50 mM Hepes pH 7.8, 1 M NaCl, 1 mM DTT, 10% v/v Glycerol. About 2 mg of CDKL5-enriched fraction was obtained, and it was finally stored at -20 °C.

2.5.7. CDKL5 activity assay

The experiment was performed as described by Baltussen et al. [50]. In particular, purified CDKL5 (provided by Amicus Therapeutics Inc.) and CDKL5-enriched CEX fraction were incubated with EB2 in 20 mM Tris-HCl pH 7.7, 10 mM MgCl₂, 1 mM DTT, 0.8 mM ATP, 1x cComplete

EDTA-free protease inhibitor, 1x phosphatase inhibitor cocktail (Halt, Thermo Scientific) in a final volume of 30 μ L. The reactions set up in the absence of ATP and EB2 were used as the negative controls. After incubation at 30°C for 30 min, the assay was stopped by adding 10 μ L Laemmli buffer 4X. Then, the samples were denatured through incubation at 75°C for 20 minutes and 10 μ L of each mixture were analysed by SDS-PAGE and Western blotting.

2.6 References

- [1] R. D. Hector *et al.*, 'Characterisation of CDKL5 Transcript Isoforms in Human and Mouse', *PLoS One*, vol. 11, no. 6, pp. 1–22, 2016.
- [2] Q. Chen *et al.*, 'CDKL5, a protein associated with Rett syndrome, regulates neuronal morphogenesis via Rac1 signaling', *J. Neurosci.*, vol. 30, no. 38, pp. 12777–12786, 2010.
- [3] L. Rusconi *et al.*, 'CDKL5 expression is modulated during neuronal development and its subcellular distribution is tightly regulated by the C-terminal tail', *J. Biol. Chem.*, vol. 283, no. 44, pp. 30101–30111, 2008.
- [4] Y. C. Zhu *et al.*, 'Palmitoylation-dependent CDKL5-PSD-95 interaction regulates synaptic targeting of CDKL5 and dendritic spine development', *Proc. Natl. Acad. Sci. U. S. A.*, vol. 110, no. 22, pp. 9118–9123, 2013.
- [5] I. Barbiero *et al.*, 'CDKL5 localizes at the centrosome and midbody and is required for faithful cell division', *Sci. Rep.*, vol. 7, no. 1, pp. 1–12, 2017.
- [6] C. Kilstrup-Nielsen *et al.*, 'What we know and would like to know about CDKL5 and its involvement in epileptic encephalopathy', *Neural Plast.*, vol. 2012, 2012.
- [7] I. M. Muñoz *et al.*, 'Phosphoproteomic screening identifies physiological substrates of the CDKL 5 kinase', *EMBO J.*, vol. 37, no. 24, pp. 1–19, 2018.
- [8] S. Katayama, N. Sueyoshi, T. Inazu, and I. Kameshita, 'Cyclin-Dependent Kinase-Like 5 (CDKL5): Possible Cellular Signalling Targets and Involvement in CDKL5 Deficiency Disorder', *Neural Plast.*, vol. 2020, 2020.
- [9] A. Oi, S. Katayama, N. Hatano, Y. Sugiyama, I. Kameshita, and N. Sueyoshi, 'Subcellular distribution of cyclin-dependent kinase-like 5 (CDKL5) is regulated through phosphorylation by dual specificity tyrosine-phosphorylation-regulated kinase 1A (DYRK1A)', *Biochem. Biophys. Res. Commun.*, vol. 482, no. 2, pp. 239–245, 2017.
- [10] I. Bertani *et al.*, 'Functional Consequences of Mutations in CDKL5, an X-linked Gene Involved in Infantile Spasms and Mental Retardation', *J. Biol. Chem.*, vol. 281, no. 42, pp. 32048–32056, 2006.
- [11] P. Canning *et al.*, 'CDKL Family Kinases Have Evolved Distinct Structural Features and Ciliary Function', *Cell Rep.*, vol. 22, no. 4, pp. 885–894, 2018.
- [12] V. N. Uversky, 'Intrinsically disordered proteins and their "Mysterious" (meta)physics', *Front. Phys.*, vol. 7, no. FEB, pp. 8–23, 2019.
- [13] M. J. Suskiewicz, J. L. Sussman, I. Silman, and Y. Shaul, 'Context-dependent resistance to proteolysis of intrinsically disordered proteins', *Protein Sci.*, vol. 20, no. 8, pp. 1285–1297, 2011.
- [14] E. Amendola *et al.*, 'Mapping pathological phenotypes in a mouse model of CDKL5 disorder', *PLoS One*, vol. 9, no. 5, pp. 5–16, 2014.
- [15] K. Okuda, K. Takao, A. Watanabe, T. Miyakawa, M. Mizuguchi, and T. Tanaka, 'Comprehensive behavioral analysis of the Cdkl5 knockout mice revealed significant enhancement in anxiety- and fear-related behaviors and impairment in both acquisition and long-term retention of spatial reference memory', vol. 13, no. 4, 2018.
- [16] M. Amenduni *et al.*, 'IPS cells to model CDKL5-related disorders', *Eur. J. Hum. Genet.*, vol. 19, no. 12, pp. 1246–1255, 2011.
- [17] G. Livide *et al.*, 'GluD1 is a common altered player in neuronal differentiation from both

- MECP2-mutated and CDKL5-mutated iPSC cells', *Eur. J. Hum. Genet.*, vol. 23, no. 2, pp. 195–201, 2015.
- [18] I. T. J. Wang *et al.*, 'Loss of CDKL5 disrupts kinome profile and event-related potentials leading to autistic-like phenotypes in mice', *Proc. Natl. Acad. Sci. U. S. A.*, vol. 109, no. 52, pp. 21516–21521, 2012.
- [19] M. S. Nawaz *et al.*, 'CDKL5 and shootin1 interact and concur in regulating neuronal polarization', *PLoS One*, vol. 11, no. 2, 2016.
- [20] Y. C. Zhu and Z. Q. Xiong, 'Molecular and Synaptic Bases of CDKL5 Disorder', *Dev. Neurobiol.*, vol. 79, no. 1, pp. 8–19, 2018.
- [21] Y. Jin *et al.*, 'Atorvastatin enhances neurite outgrowth in cortical neurons in vitro via up-regulating the Akt/mTOR and Akt/GSK-3B signaling pathways', *Acta Pharmacol. Sin.*, vol. 33, no. 7, pp. 861–872, 2012.
- [22] V. Kumar, M. X. Zhang, M. W. Swank, J. Kunz, and G. Y. Wu, 'Regulation of dendritic morphogenesis by Ras-PI3K-Akt-mTOR and Ras-MAPK signaling pathways', *J. Neurosci.*, vol. 25, no. 49, pp. 11288–11299, 2005.
- [23] S. Ricciardi *et al.*, 'CDKL5 ensures excitatory synapse stability by reinforcing NGL-1-PSD95 interaction in the postsynaptic compartment and is impaired in patient iPSC-derived neurons', *Nat. Cell Biol.*, vol. 14, no. 9, pp. 911–923, 2012.
- [24] I. Barbiero, R. De Rosa, and C. Kilstrup-Nielsen, 'Microtubules: A key to understand and correct neuronal defects in CDKL5 deficiency disorder?', *Int. J. Mol. Sci.*, vol. 20, no. 17, 2019.
- [25] H. E. Olson *et al.*, 'Cyclin-Dependent Kinase-Like 5 Deficiency Disorder: Clinical Review', *Pediatr. Neurol.*, vol. 97, pp. 18–25, 2019.
- [26] E. Encephalopathy, M. Jakimiec, and J. Paprocka, 'brain sciences CDKL5 Deficiency Disorder — A Complex', pp. 1–9, 2020.
- [27] J. S. Liang, H. Huang, J. S. Wang, and J. F. Lu, 'Phenotypic manifestations between male and female children with CDKL5 mutations', *Brain Dev.*, vol. 41, no. 9, pp. 783–789, 2019.
- [28] S. Mahalik, A. K. Sharma, and K. J. Mukherjee, 'Genome engineering for improved recombinant protein expression in escherichia coli', *Microb. Cell Fact.*, vol. 13, no. 1, pp. 1–13, 2014.
- [29] R. Krishnaraj, G. Ho, and J. Christodoulou, 'RettBASE: Rett syndrome database update', *Hum. Mutat.*, vol. 38, no. 8, pp. 922–931, 2017.
- [30] L. S. Weaving *et al.*, 'Mutations of', *Mouse Genome*, pp. 1079–1093, 2004.
- [31] G. Della Sala *et al.*, 'Dendritic Spine Instability in a Mouse Model of CDKL5 Disorder Is Rescued by Insulin-like Growth Factor 1', *Biol. Psychiatry*, vol. 80, no. 4, pp. 302–311, 2016.
- [32] M. Tramarin *et al.*, 'The antidepressant tianeptine reverts synaptic AMPA receptor defects caused by deficiency of CDKL5', *Hum. Mol. Genet.*, vol. 27, no. 12, pp. 2052–2063, 2018.
- [33] C. Fuchs, N. Fustini, S. Trazzi, L. Gennaccaro, R. Rimondini, and E. Ciani, 'Treatment with the GSK3-beta inhibitor Tideglusib improves hippocampal development and memory performance in juvenile, but not adult, Cdkl5 knockout mice', *Eur. J. Neurosci.*, vol. 47, no. 9, pp. 1054–1066, 2018.
- [34] Y. Gao *et al.*, 'Gene replacement ameliorates deficits in mouse and human models of cyclin-dependent kinase-like 5 disorder', *Brain*, vol. 143, no. 3, pp. 811–832, 2020.
- [35] D. Balestra *et al.*, 'Splicing mutations impairing CDKL5 expression and activity can be efficiently rescued by U1snRNA-based therapy', *Int. J. Mol. Sci.*, vol. 20, no. 17, 2019.
- [36] S. Trazzi *et al.*, 'CDKL5 protein substitution therapy rescues neurological phenotypes of a mouse model of CDKL5 disorder', *Hum. Mol. Genet.*, vol. 27, no. 9, pp. 1572–1592, 2018.
- [37] A. Colarusso, C. Lauro, M. Calvanese, E. Parrilli, and M. L. Tutino, 'Improvement of pseudoalteromonas haloplanktis tac125 as a cell factory: Iptg-inducible plasmid construction and strain engineering', *Microorganisms*, vol. 8, no. 10, pp. 1–24, 2020.
- [38] H. Xia, Q. Mao, and B. L. Davidson, 'The HIV Tat protein transduction domain improves the biodistribution of β -glucuronidase expressed from recombinant viral vectors', *Nat.*

- Biotechnol.*, vol. 19, no. 7, pp. 640–644, 2001.
- [39] Michael W. Pfaffl, 'A new mathematical model for relative quantification in real-time RT-PCR', *Nucleic Acids Res.* 2001, Vol. 29, No. 9 00, 2001.
- [40] S. H. Jang, J. W. Cha, N. S. Han, and K. J. Jeong, 'Development of bicistronic expression system for the enhanced and reliable production of recombinant proteins in *Leuconostoc citreum*', *Sci. Rep.*, vol. 8, no. 1, pp. 1–11, 2018.
- [41] S. Edri and T. Tuller, 'Quantifying the effect of ribosomal density on mRNA stability', *PLoS One*, vol. 9, no. 7, 2014.
- [42] V. K. Mutalik *et al.*, 'Precise and reliable gene expression via standard transcription and translation initiation elements', *Nat. Methods*, vol. 10, no. 4, pp. 354–360, 2013.
- [43] W. Qi *et al.*, 'New insights on *Pseudomonas haloplanktis* TAC125 genome organization and benchmarks of genome assembly applications using next and third generation sequencing technologies', *Sci. Rep.*, vol. 9, no. 1, pp. 1–14, 2019.
- [44] M. L. Tutino, A. Duilio, E. Parrilli, E. Remaut, G. Sannia, and G. Marino, 'A novel replication element from an Antarctic plasmid as a tool for the expression of proteins at low temperature', *Extremophiles*, vol. 5, no. 4, pp. 257–264, 2001.
- [45] A. Duilio, S. Madonna, M. L. Tutino, M. Pirozzi, G. Sannia, and G. Marino, 'Promoters from a cold-adapted bacterium: Definition of a consensus motif and molecular characterization of UP regulative elements', *Extremophiles*, vol. 8, no. 2, pp. 125–132, 2004.
- [46] 2 Jeffrey G. Marblestone, 1 Suzanne C. Edavettal, 2 Yiting Lim, 2 Peter Lim, 1 Xun Zuo And A. T. R. Butt, 'Comparison of SUMO fusion technology with traditional gene fusion systems: Enhanced expression and solubility with SUMO', *182 Protein Sci. (2006)*, 15182–189. *Publ. by Cold Spring Harb. Lab. Press.*, 2006.
- [47] M. R. Bell, M. J. Engleka, A. Malik, and J. E. Strickler, 'To fuse or not to fuse: What is your purpose?', *Protein Sci.*, vol. 22, no. 11, pp. 1466–1477, 2013.
- [48] M. P. Malakhov, M. R. Mattem, O. A. Malakhova, M. Drinker, S. D. Weeks, and T. R. Butt, 'SUMO fusions and SUMO-specific protease for efficient expression and purification of proteins', *J. Struct. Funct. Genomics*, vol. 5, no. 1–2, pp. 75–86, 2004.
- [49] N. W. and A. S. Daniel Roth, Benjamin P. Fitton, Nikola P. Chmel, 'Spatial positioning of EB family proteins at microtubule tips involves distinct nucleotide- dependent binding properties', *Stem Cells*, no. February, 2012.
- [50] L. L. Baltussen *et al.*, 'Chemical genetic identification of CDKL 5 substrates reveals its role in neuronal microtubule dynamics', *EMBO J.*, vol. 37, no. 24, pp. 1–18, 2018.
- [51] R. D. Hector *et al.*, 'CDKL5 variants', *Neurol. Genet.*, vol. 3, no. 6, p. e200, 2017.
- [52] S. Fehr *et al.*, 'The CDKL5 disorder is an independent clinical entity associated with early-onset encephalopathy', *Eur. J. Hum. Genet.*, vol. 21, no. 3, pp. 266–273, 2013.
- [53] S. Katayama, N. Sueyoshi, and I. Kameshita, 'Critical determinants of substrate recognition by cyclin-dependent kinase-like 5 (CDKL5)', *Biochemistry*, vol. 54, no. 19, pp. 2975–2987, 2015.
- [54] I. Kameshita *et al.*, 'Cyclin-dependent kinase-like 5 binds and phosphorylates DNA methyltransferase 1', *Biochem. Biophys. Res. Commun.*, vol. 377, no. 4, pp. 1162–1167, 2008.
- [55] S. Katayama and T. Inazu, 'Straightforward and rapid method for detection of cyclin-dependent kinase-like 5 activity', *Anal. Biochem.*, vol. 566, no. November 2018, pp. 58–61, 2019.
- [56] T. A. Carrier and J. D. Keasling, 'Controlling messenger RNA stability in bacteria: Strategies for engineering gene expression', *Biotechnol. Prog.*, vol. 13, no. 6, pp. 699–708, 1997.
- [57] G. Boël *et al.*, 'Codon influence on protein expression in *E. coli*', vol. 529, no. 7586, pp. 358–363, 2016.
- [58] A. Deana and J. G. Belasco, 'Lost in translation: The influence of ribosomes on bacterial mRNA decay', *Genes Dev.*, vol. 19, no. 21, pp. 2526–2533, 2005.
- [59] A. V. Kochetov, A. Palyanov, I. I. Titov, D. Grigorovich, A. Sarai, and N. A. Kolchanov, 'AUG↔irpin: Prediction of a downstream secondary structure influencing the recognition of a translation start site', *BMC Bioinformatics*, vol. 8, pp. 3–9, 2007.

- [60] A. V. Kochetov, 'Alternative translation start sites and hidden coding potential of eukaryotic mRNAs', *BioEssays*, vol. 30, no. 7, pp. 683–691, 2008.
- [61] S. Lee, B. Liu, S. Lee, S. X. Huang, B. Shen, and S. B. Qian, 'Global mapping of translation initiation sites in mammalian cells at single-nucleotide resolution', *Proc. Natl. Acad. Sci. U. S. A.*, vol. 109, no. 37, 2012.
- [62] T. Tasaki, S. M. Sriram, K. S. Park, and Y. T. Kwon, 'The N-End rule pathway', *Annu. Rev. Biochem.*, vol. 81, no. 1, pp. 261–289, 2012.
- [63] D. K. Gonda, A. Bachmair, I. Wunning, J. W. Tobias, W. S. Lane, and A. Varshavsky, 'Universality and structure of the N-end rule', *J. Biol. Chem.*, vol. 264, no. 28, pp. 16700–16712, 1989.
- [64] M. Fahmi *et al.*, 'In silico study of rett syndrome treatment-related genes, MECP2, CDKL5, and FOXP1, by evolutionary classification and disordered region assessment', *Int. J. Mol. Sci.*, vol. 20, no. 22, pp. 1–19, 2019.
- [65] I. Arechaga, B. Miroux, M. J. Runswick, and J. E. Walker, 'Over-expression of Escherichia coli F1Fo-ATPase subunit a is inhibited by instability of the uncB gene transcript', *FEBS Lett.*, vol. 547, no. 1–3, pp. 97–100, 2003.
- [66] F. Sannino *et al.*, 'A novel synthetic medium and expression system for subzero growth and recombinant protein production in *Pseudoalteromonas haloplanktis* TAC125', *Appl. Microbiol. Biotechnol.*, vol. 101, no. 2, pp. 725–734, 2017.
- [67] Puigbo, P.; Guzmán, E.; Romeu, A.; Garcia-Vallve, S. OPTIMIZER: A web server for optimizing the codon usage of DNA sequences. *Nucleic Acids Res.* 2007, 35, W126–W131, doi:10.1093/nar/gkm219.

Supplementary materials

Cloning, expression and purification of EB2

The sequence encoding EB2 fused to an N-terminal 6xHis tag was cloned into pET40b bacterial vector using *NdeI/BamHI* double digestion. The expression levels were assessed in commercial *E. coli* BL21 DE3 strain by varying the temperature after the induction (37°C, 25°C and 15°C) and the inducer concentration (0.1 and 1 mM IPTG). The expression levels were evaluated on total cellular extracts through SDS-Page and Western blot analysis carried out with the anti-His antibody (Figure S1A). The recombinant protein (38 kDa) was successfully produced in all explored conditions. The different concentrations of inducer did not significantly influence the overall quantity and quality of recombinant protein. On the other hand, the temperature downshift after the induction seemed to be the main contributing factor in increasing the production yield and reducing the degradation forms. Indeed, the expression performed with 0.1 mM IPTG at 15°C was selected since it allowed to partially avoid the proteolytic process and obtain the recombinant protein mainly in a soluble form (Figure S1B).

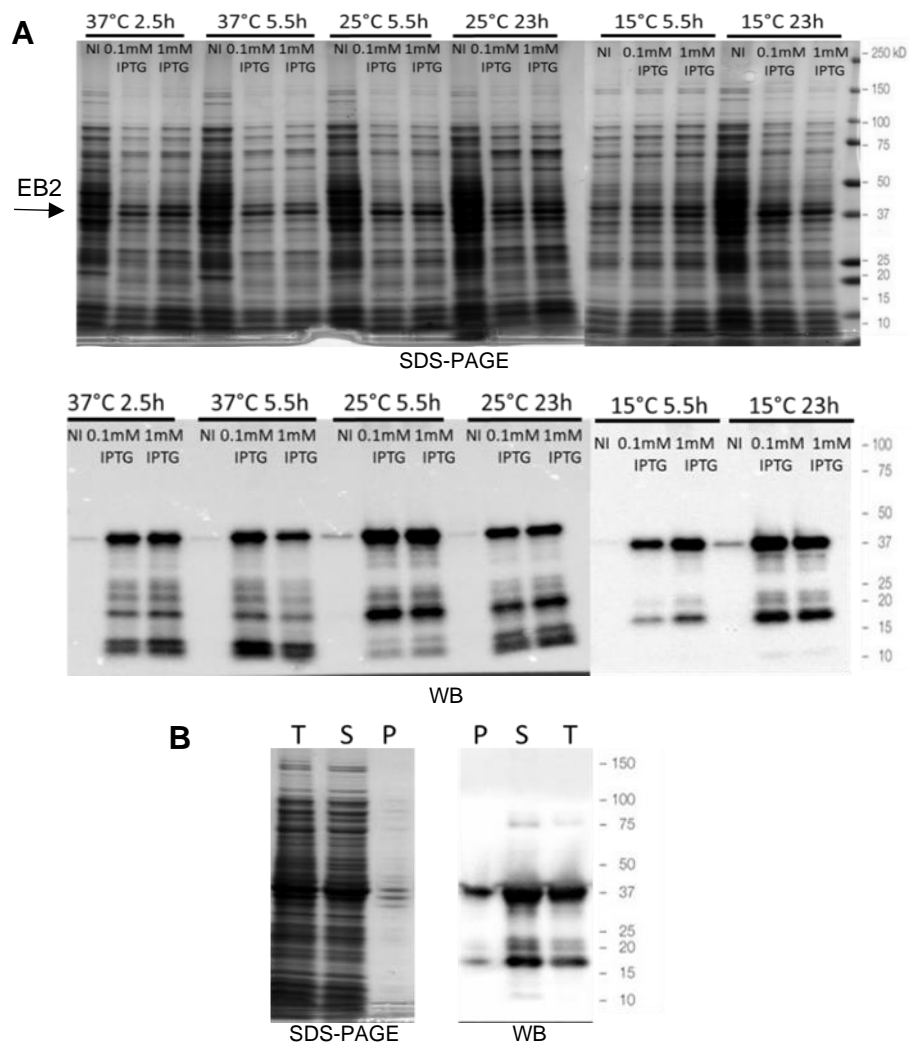


Figure S1. Recombinant EB2 expression levels in *E. coli* BL21(DE3). (A) Total cellular extracts obtained at 37°C, 25°C and 15 °C after 2.5, 5.5 and 23 hours from the induction with 1 and 0.1 mM IPTG were separated by SDS-PAGE and analysed by coomassie staining (upper panel) and Western blot (lower panel) using the anti-his antibody. NI: not induced. Full-length EB2 is indicated with an arrow. (B) Evaluation of EB2 solubility in *E. coli* extracts. After cellular lysis, insoluble (P) and soluble (S) fractions were analysed in comparison to the total extract (T) as described in point A.

Recombinant EB2 was then purified through affinity chromatography followed by size exclusion chromatography to increase the overall quality of the collected fractions (Figure S2). In detail, the clarified lysate harvested after cells disruption was applied to immobilized metal affinity chromatography (IMAC) using a 1 mL HisTrap HP column. The bound proteins were washed and eluted with IMAC Wash buffers and IMAC Elution buffer, respectively. The eluted fractions (peak I in panel A) were

pooled and analyzed by both SDS-PAGE and Western blot (panel B), which showed that the obtained samples contain contaminants and proteolyzed forms of the protein. A size exclusion chromatography (Superdex 75 prep grade) was carried out on partially purified EB2 to eliminate the remaining contaminants. The chromatogram presented a narrow peak (peak II) in the elution volume (V_e) range of 42-47 mL (panel C) compatible with the dimension of the dimers formed by EB2 proteins through their C-terminal domain [49]. The SDS-PAGE and Western blot analysis (panel D) revealed that most contaminants were lost but also the co-presence of few degradation products of EB2.

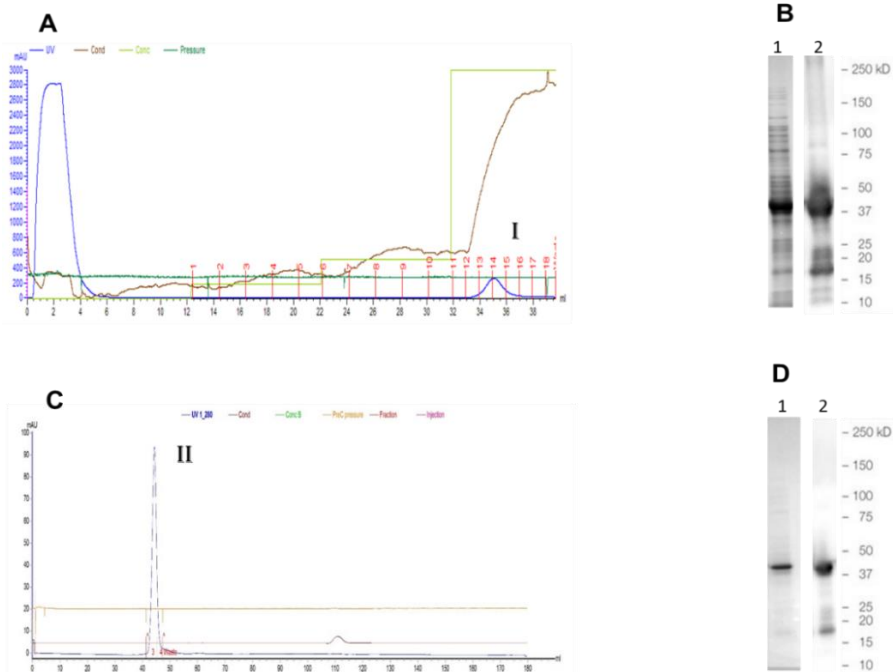


Figure S2. Two-step purification of EB2. (A) The chromatogram of IMAC separation (HisTrap HP) of *E. coli* BL21(DE3) soluble cellular extracts after EB2 production. After flow-through discard, two washing steps with 50 mM and 100 mM imidazole were followed by elution with 500 mM imidazole which led to the release of the target protein (Peak I). (B) Analysis of the eluted and pooled fractions after IMAC (Peak I). 1, SDS-PAGE; 2, Western blot. (C) The chromatogram of the second step purification of EB2 by size exclusion chromatography (Superdex 75 prep grade) displays a peak (peak II) representative of EB2 dimer released in the V_e 42-47 mL range. (D) Analysis of the eluted and pooled fractions corresponding to Peaks II of the size exclusion chromatography. 1, SDS-PAGE; 2, Western blot.

Chapter 3: Development of a novel genetic down-regulation system based on antisense RNAs in *Pseudoalteromonas haloplanktis* TAC125

The availability of precise and predictable genetic manipulation methodologies is a prerequisite for most strain engineering strategies, especially during gene screening and mutant strains development phases. As an unconventional host, the application of consolidated techniques in the psychrophilic bacterium *PhTAC125* still represents a troublesome challenge. The manuscript in preparation below reported a novel system for genetic down-regulation based on antisense RNAs successfully developed in *PhTAC125*. Two different and consolidated approaches were applied: the RNA chaperon Hfq-dependent one showed limited effectiveness in the psychrophilic bacterium, while the gene silencing system based on hairpin structured PTasRNAs successfully down-regulated the highly transcribed *Phlon* gene. Using this kind of asRNAs, efficient and durable gene silencing was observed, managing also the almost total repression of the less transcribed *hbO* gene.

Furthermore, the identification of critical parameters directly related to the repression efficiency allowed outlining valuable indications for designing systems for the control of gene expression in psychrophilic bacteria, thus laying the foundations for subsequent studies in synthetic biology and metabolic engineering.

A manuscript in preparation for these results

Conditional gene silencing in the Antarctic marine bacterium *Pseudoalteromonas haloplanktis* TAC125

Concetta Lauro, Andrea Colarusso, Marzia Calvanese, Ermenegilda Parrilli and Maria Luisa Tutino *

Dipartimento di Scienze Chimiche, Complesso Universitario Monte Sant'Angelo, Via Cintia, 80126 Napoli, Italy; concetta.lauro@unina.it (C.L.); andrea.colarusso@unina.it (A.C.); marzia.calvanese@unina.it (M.C.); erparril@unina.it (E.P.) * Correspondence: tutino@unina.it; Tel.: +39-081-674317

Abstract

The psychrophilic bacterium *Pseudoalteromonas haloplanktis* TAC125 (*PhTAC125*) has attracted significant attention as a platform for the production of “difficult” proteins and bioactive compounds as well as a model for environmental studies due to its capability to adapt at low temperatures. To broaden the application fields of this bacterium, we focused on establishing an asRNA regulatory system in *PhTAC125*, testing the feasibility of Hfq-dependent and PTasRNA strategies previously developed in *E. coli*. Stable and efficient silencing of two chromosomal genes was obtained by using PTasRNAs, reaching very high levels of downregulation. Furthermore, the obtained results laid the foundation for rational design and construction of synthetic asRNAs able to work in psychrophilic bacteria.

1. Introduction

Small RNAs (sRNAs) are regulatory RNAs involved in controlling gene expression at the post-transcriptional and/or translational level by base-pairing with their target mRNA [1]. Given the typical complementarity of their sequence with the targets, they are often denoted as antisense RNAs (asRNAs). Most bacterial asRNAs act by binding to the translation initiation region (TIR) of the transcripts altering the accessibility of the ribosomes. As a result, the translation is hindered, and the target mRNA is destabilized and susceptible to degradation [2]. Extensive analyses investigated the complex interplay and cross-regulation between asRNAs and transcriptional factors. Although a clear framework has not emerged yet, the multiple targeting of asRNAs explains why they are involved in various processes such as stress responses, metabolic switches, virulence, biofilm formation, and much more [1].

In recent years, the repurposing of natural sRNAs to develop gene regulation tools has widely spread. The plethora of the sRNAs engineered in bacteria counts quite a lot of technologies, such as CRISPR interference (CRISPRi) [3], CRISPR activation (CRISPRa) [4], riboswitch [5], small transcription activating RNA (STAR) [6] and synthetic asRNA [7]. Relying on the Watson-Crick base pairing principle, such strategies hold many advantages compared to DNA or protein-based methods. They allow easy, predictable, scalable, and finely tunable control of multiple and essential genes [8] for very diverse applications spanning from metabolic engineering to cellular RNA editing and therapeutics [9].

Na and coworkers reported an ingenious strategy to designing synthetic asRNAs in *E. coli* [7]. They developed an Hfq-dependent asRNA by the functional modularization of its sequence into a target binding region and a scaffold that recruits the RNA chaperone protein Hfq. Even if the gene silencing is strictly exerted by the target binding sequence and is strongly dependent on the efficiency of TIR masking, the interaction of asRNA with Hfq allows for a more efficient outcome.

E. coli Hfq is a homo-hexameric protein arranged in a doughnut-shaped ring [10]. Structural analyses revealed that the proximal face of this assembly binds the asRNA, while the opposite distal face binds the target mRNAs and a minor class of asRNAs (Class II) [11]. Instead, the arginine-rich patches exposed in the rim catalyse the base pairing between the two RNA molecules [12]. The formation of the asRNA-mRNA complex along the surface of the Hfq hexamer is a dynamic process that requires suitable cycling and turnover of substrates, ensured by the protruding intrinsically disordered region of the C-terminal domain. In particular, the acidic residues of such a domain interact with the rim arginine stretches, facilitating the displacement of the RNA duplex and the binding of a new couple of RNAs [13].

The reason for the particular interest that this protein arouses lies in the numerous functions it performs. Indeed, it is known: 1) to promote the binding of asRNA with their target mRNA; 2) to prolong the asRNAs half-life by protecting them from degradation; and 3) in some cases, to recruit RNase E aiding the degradation of asRNA-mRNA complex [14]. In their work, Na and coworkers screened numerous Hfq-binding scaffolds derived from natural asRNA characterized in *E. coli*. They identified MicC as the molecule able to better interact with such RNA chaperon, succeeding in constructing a synthetic asRNA with high repression capability (>90%). Furthermore, particular attention was paid to the design of the target sequence, demonstrating that the TIR is the most effective binding region in the mRNA since the docking of

ribosomes occurs in this region [7]. The optimal length of the antisense sequence resulted in being 24 nt as it is long enough to bind the target mRNA efficiently without off-target repression. Finally, a direct correlation between the silencing efficiency and the energy of hybridization of the asRNA with the target mRNA was also demonstrated, defining the optimal binding energy ranging from -30 to -40 kcal mol⁻¹ [7].

Nakashima and collaborators designed another exciting RNA-based regulatory tool in *E. coli*, known as Paired Termini antisense RNAs (or PTasRNAs). It is characterized by a hairpin structure whose loop holds the antisense sequence able to bind the RBS of the target mRNA [15]. The complementarity of terminal regions positively affects PTasRNAs stability, consequently on their cellular concentration and silencing efficacy compared to canonical asRNA. The optimal length of PTasRNAs paired termini proved to be 38 bp with a high GC content, yielding a high silencing efficiency in *E. coli* without triggering any interference on plasmid stability [15]. PTasRNAs turned out to be quite successful in regulating multiple essential genes in *E. coli* [16].

Notably, the versatility of such approaches paved the way for genetic engineering not only in conventional model systems like *E. coli* but also in less characterized microorganisms, often tricky to handle in routine genetic manipulations [17,18,19].

Pseudoalteromonas haloplanktis TAC125 (*PhTAC125*), also named *Pseudoalteromonas translucida*, is a psychrophilic marine bacterium [20] widely exploited as a cell factory for the production of “difficult” proteins [21, 22, 23] and bioactive compounds [24, 25, 26] as well as a model for studying microbial adaptations to cold environments [27, 28]. Although a genome mutagenesis technique was established by our group [29], it relies on homologous recombination and counterselection events, often occurring at a frequency only slightly higher than spontaneous mutations. Therefore, the construction of a simple, more efficient and multiple-gene knockdown system represents a milestone for implementing this promising host both in applied and fundamental research. Furthermore, the abundance of RNA helicase encoding genes in the genome of *PhTAC125* suggests a considerable capacity in controlling the RNA folding and degradation at low temperatures [20], encouraging the exploitation of RNA-based technology.

In this work, Hfq-dependent and PTasRNA strategies were applied to gene silencing in *PhTAC125* by exploiting a recent powerful psychrophilic inducible expression system [30]. The expression of two *PhTAC125* genes (characterized by quite a different transcription intensity) was efficiently triggered by an asRNA strategy, proposing

design principles of synthetic asRNAs able to function in psychrophilic unconventional bacteria.

2. Results

2.1 Construction of Hfq-dependent asRNA-*lon* and expression in *PhTAC125*

The first design, named asRNA-*lon*, was constructed according to the criteria defined by Na et al. [7, 31]. The Hfq-binding scaffold derived from *E. coli* MicC was fused to a sequence complementary to the first 24 bp of the coding region in the TIR of the Lon protease encoding *PSHA_RS10175* mRNA, able to bind its target with the predicted hybridization energy of $-42 \text{ kcal mol}^{-1}$. A strong transcription terminator T1/TE was also added to guarantee the release of the nascent asRNA transcript (Figure 1A, B). The gene coding for the Lon protease was chosen as the silencing target for several reasons: i) Lon is the main protease involved in the degradation of intracellular proteins and is a known target for the improvement of any strain as a host for recombinant protein production; ii) a *PhTAC125* strain bearing a knockout mutation in the Lon encoding gene has been already characterized and did not show any dramatic phenotypic change in comparison to the wild-type strain [30]. Furthermore, owing to the high sequence similarity between *E. coli* and *PhTAC125* Lon proteins, the specific anti-*EcLon* antibodies efficiently recognise also the psychrophilic protease, allowing the evaluation of the silencing effects at the protein level by Western blotting.

Once designed, asRNA-*lon* was cloned into pB40_79C, a high copy number variant of p79C [30] (unpublished data). Then, the recombinant vector was transferred into KrPL, a kanamycin resistant *PhTAC125* strain devoid of the endogenous plasmid pMtBL [30]. Recombinant KrPL was grown at 15 °C in GG medium [32] till the early exponential growth phase when the recombinant expression of Hfq-dependent asRNA-*lon* was induced by adding 10 mM IPTG to the culture. The comparison of the growth behaviour of asRNA expressing cells with the control strain carrying the empty vector pB40_79C did not highlight differences in specific growth rate and final biomass, suggesting no toxic off-target silencing and competition with endogenous asRNAs for Hfq binding took place [33] (Figure S1).

The occurrence of gene silencing was evaluated by Western Blotting through the measurement of Lon levels detected on total protein extracts of cells carrying the empty vector (NC) in comparison to cells

expressing the asRNA. In particular, to detect slight differences in Lon production between the two strains, a quantitative analysis of Western Blotting data was performed on samples collected 2, 4, 8, 24 and 32 hours after the induction (Figure 1C). The densitometric analysis was performed by normalizing the chemiluminescence intensity of the Lon-related bands to the total proteins loaded in each lane. A statistically relevant reduction in Lon production was recorded only 2 hours post-induction in cells expressing asRNA-*lon* compared to the control cells. Over the observed growth period, the protease was consistently detected in almost comparable quantities in the two strains.

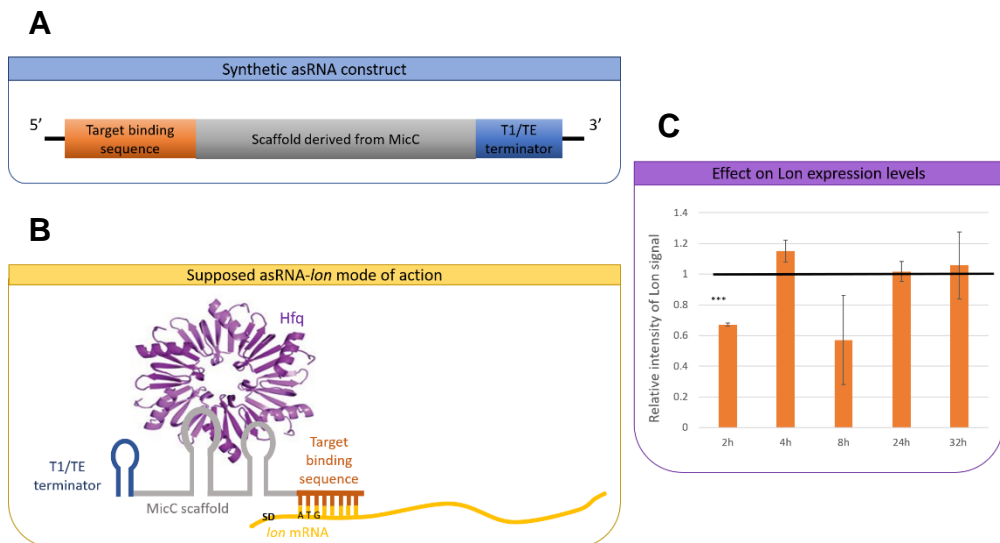


Figure 1. (A) Schematic representation of Hfq-dependent asRNA-*lon* construct. A sequence complementary to the TIR of *lon* mRNA (in orange) was fused to the sequence of *E. coli* MicC (in grey) recruiting Hfq proteins. To ensure the termination of the transcription, a synthetic T1/TE terminator was added (in blue). (B) Supposed mode of action of Hfq-dependent asRNA-*lon*. The antisense sequence (in orange) binds the TIR of *lon* mRNA (in yellow), sequestering the transcript from the ribosomes. In this way, it acts by repressing the translation. The Hfq protein (in violet), recruited from the scaffold derived from MicC (in grey), aids the formation of the asRNA-mRNA complex resulting in a more efficient silencing. (C) Evaluation of relative expression levels of Lon protease in cells expressing Hfq-dependent asRNA-*lon* compared to control cells, carrying the empty vector. The quantitative analysis of Lon signals detected via Western blotting was performed on total protein extracts of cells recovered 2, 4, 8, 24 and 32 hours after the recombinant induction. The black bar represents the baseline production of Lon detected in the control samples. The measurements are reported as the mean of two independent experiments whose standard deviation is indicated by the error bars. The data were considered significant when $p < 0.05$ (* $p < 0.05$, ** $p < 0.01$, *** $p < 0.001$) according to t-Student test.

2.2 PTasRNA as an alternative tool for *Phlon* gene silencing

A second approach was performed by using Paired Termini antisense RNAs containing terminal inverted repeats of 38 nt. A secondary structure prediction tool was used to arrange the antisense sequence (110 nt), harbouring the *Phlon* RBS and start codon, within a loop region easily accessible for the hybridization with the target mRNA (Figure 2A, B).

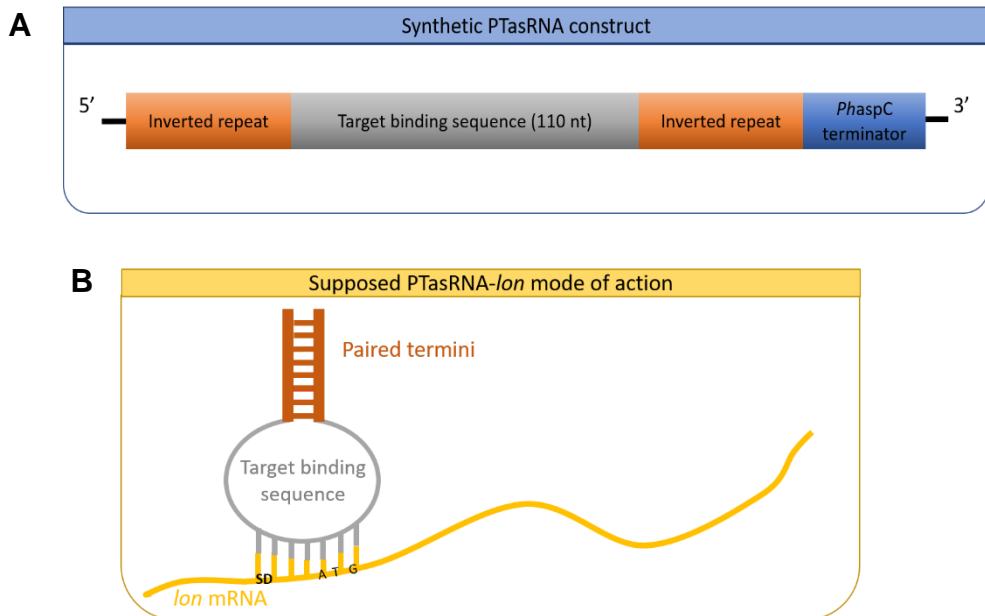


Figure 2. (A) Schematic representation of PTasRNA construct. The antisense sequence (in grey), complementary to the TIR of *lon* mRNA, was included between two inverted repeats (in orange). (B) The inverted repeats at the ends of the sequence (in orange) form a hairpin structure containing the antisense sequence into the loop (in grey).

Starting from the better target binding sequence predicted by the *in silico* analysis (PTasRNA1-*lon*), other variants were designed to explore the effect of the binding region on TIR sequestering and consequently repression efficiency (Figure 3A). These two variants were designed with a shift of 5 nt of the antisense sequence towards either *Phlon* 3'-end (PTasRNA2-*lon*) or 5'-end (PTasRNA3-*lon*). Furthermore, we were confident that the accessibility of the PTasRNAs to the target mRNA might be informative. RNApredator software was thus used to predict the interaction between the synthetic asRNAs and *lon* mRNA. The binding energies calculated for the interaction occurring in the stretch spanning the TIR and coding sequence of *lon* mRNA are reported in Figure 3B.

The constructs were cloned into the psychrophilic expression vector pB40-79C and expressed in KrPL without any noticeable effect on the growth behaviour of the recombinant cells (Figure S2).

As already described, changes in Lon protease synthesis levels in cells expressing the different PTasRNAs were evaluated through quantitative Western blot analysis (Figure 3C). PTasRNA1-*lon* markedly reduced the production of Lon by about 70% after 8 hours of induction, and the effect lasted up to 32 hours. Both the variants PTasRNA2-*lon* and PTasRNA3-*lon* resulted in less performance than the first version, with a maximum activity of about 54% and 47%, respectively. Furthermore, they showed a less durable effect since the repression began to wane after 24 hours post-induction. Interestingly, a direct correlation between repression efficiency and binding energy was consistently found, suggesting that a strong interaction is required for satisfying target suppression.

For the reasons stated above, the PTasRNA1-*lon* was selected for further experiments.

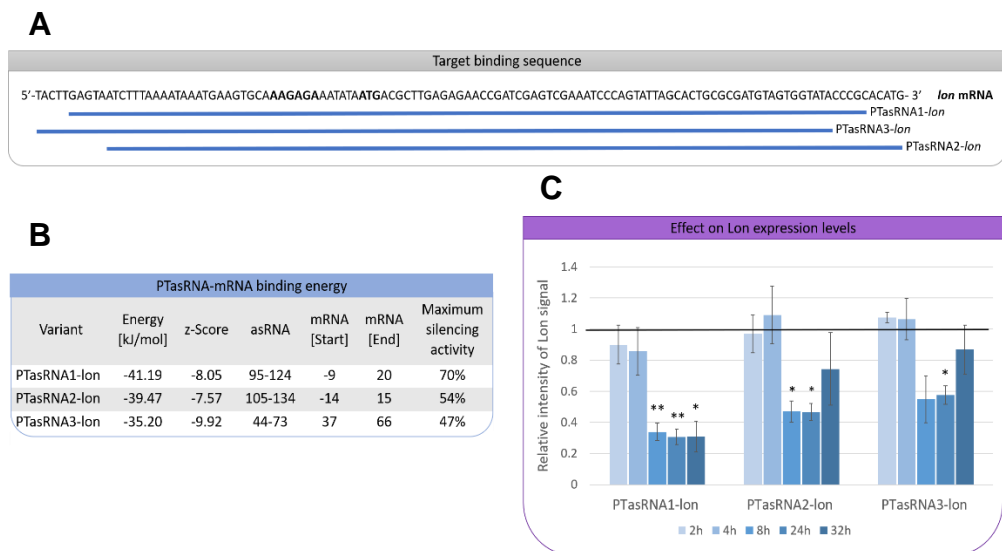


Figure 3. (A) Schematic illustration of the antisense fragment positions of PTasRNA-*lon* variants. The fragment position is shown referring to the *Phlon* mRNA. PTasRNA2-*lon* and PTasRNA3-*lon* were designed with a shift of 5 nt of the PTasRNA1-*lon* antisense sequence towards either *Phlon* mRNA 3'-end or 5'-end, respectively. **(B)** Prediction of the interactions occurring between PTasRNAs and their target *lon* mRNA in *PhTAC125*. RNAPredator tool was used to predict the total binding energy, the corresponding Z-score, the coordinates on asRNA and mRNA. Each prediction was supplemented with the experimental results achieved in *PhTAC125* expressed as maximum silencing activity. **(C)** Evaluation of relative expression levels of Lon protease in cells expressing three variants of PTasRNA-*lon* in comparison to control cells, carrying the empty vector. The quantitative analysis of Lon signals detected via

Western blotting was performed on protein total extracts of cells recovered after 2, 4, 8, 24 and 32 hours from the recombinant induction. The black bar represents the baseline production of Lon detected in the control samples. The measurements are reported as the mean of two independent experiments whose standard deviation is indicated by the error bars. The data were considered significant when $p < 0.05$ (* $p < 0.05$, ** $p < 0.01$, *** $p < 0.001$) according to t-Student test.

The effect of a 5' leader sequence upstream to the hairpin structure was then evaluated to improve the performance of PTasRNA1-*lon*, presumably acting as a stabilizer of the hairpin molecule.

Hence, 5'-PTasRNA1-*lon*, differing from PTasRNA1-*lon* just for the presence of the extremely stable 5'-UTR from *PhlacZ* [30], was constructed and cloned into pB40_79C (Figure 4A). The recombinant production in KrPI cells was then performed as described above.

Even then, the overexpression of asRNAs did not induce detrimental effects on bacterial growth (Figure S3). This result ruled out the occurrence of either plasmid instability or non-specific silencing of other essential genes. After the first hours of growth post-induction, where no silencing effect was evident (data not shown), the densitometric analysis confirmed about 70% reduction of Lon levels in the presence of PTasRNA1-*lon* starting from 8 hours of induction in comparison to the control cells (Figure 4B). The silencing mediated by 5'-PTasRNA1-*lon* appeared to be less effective during the first 8 hours of expression, then it became comparable to that induced by the other construct, suggesting that the 5'-UTR sequence did not contribute to the enhancement of the repression capability.

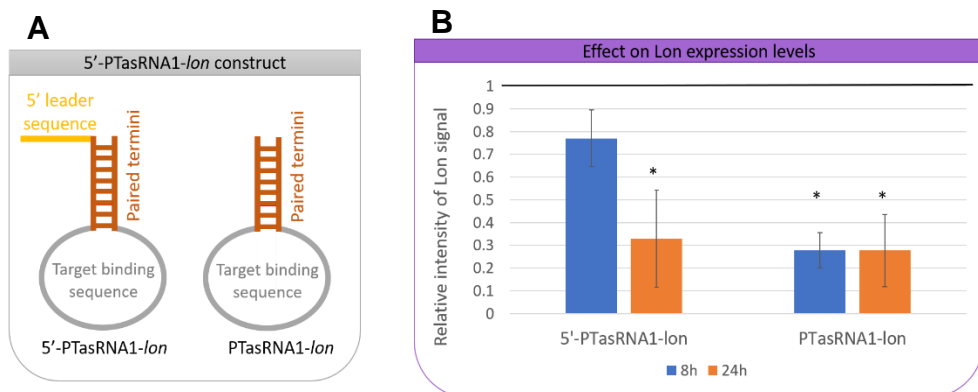


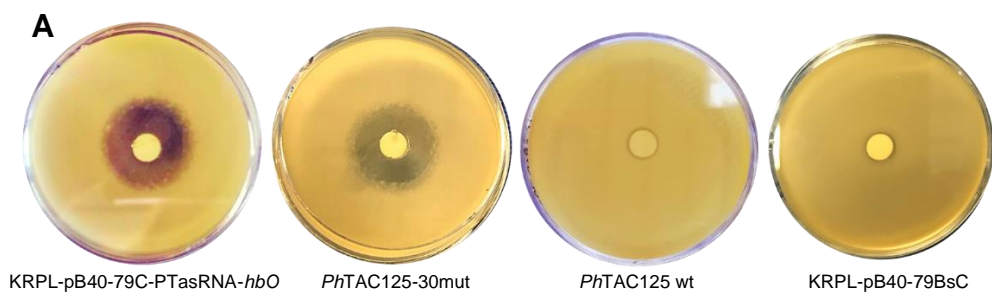
Figure 4. (A) Schematic representation of 5'-PTasRNA1-*lon* construct. The 5' leader sequence derived from *PhlacZ* (in yellow) was placed upstream to the inverted repeat (in orange) involved in the formation of the hairpin structure, whose loop holds the antisense sequence (in grey). **(B)** Evaluation of relative expression levels of Lon protease in cells expressing 5'-PTasRNA1-*lon* and PTasRNA1-*lon* in comparison to control cells, carrying the empty vector. The quantitative analysis of Lon signals

detected via Western blotting was performed on protein total extracts of cells recovered 8 and 24 hours after the recombinant induction. The black bar represents the baseline production of Lon detected in the control samples. The measurements are reported as the mean of two independent experiments whose standard deviation is indicated by the error bars. The data were considered significant when $p < 0.05$ (* $p < 0.05$, ** $p < 0.01$, *** $p < 0.001$) according to t-Student test.

2.3 Validation of PTasRNA technology in *PhTAC125* by targeting *PhHbO* encoding gene

The gene silencing of another *PhTAC125* chromosomal gene was attempted to confirm the robustness of the PTasRNA technology. *PSHA_RS00150* encodes truncated haemoglobin (trHbO) involved in the cellular protection against oxidative stress, as demonstrated by the study of a *PhTAC125* strain bearing the deletion of its encoding gene [34]. The design of the PTasRNA-*hbO* was performed considering the results obtained for the *lon* target. In detail, the synthetic asRNA was made up by the already used 38 bp long terminal inverted repeats, while the 110 bp long antisense sequence was selected, taking into account the predicted interaction with its target. Indeed, the RNAPredator tool was used to determine the antisense sequence to be used for the experiment, as its predictions helped rule out any non-specific off-target binding of the PTasRNA. Furthermore, this bioinformatic tool suggested the sequence potentially binding to the TIR elements of *hbO* mRNA with the highest estimated efficiency (binding energy of -36.81 kJ/mol).

The PTasRNA-*hbO* was cloned into the psychrophilic expression vector pB40_79C and recombinantly expressed in *PhTAC125* KrPL. Since the biochemical characterization of the *PhTAC125* trHbO demonstrated its peroxidase activity [34], a disk-diffusion assay in the presence of 256 mM H₂O₂ was used to quantify the conditional control of its encoding gene expression. Furthermore, as the knockout *PhTAC125*-30 mutant was already established and its enhanced H₂O₂ sensitivity described [34], this mutant was used as a reference phenotype stemming from the complete gene repression. As previously reported, the treatment of *PhTAC125* wild-type and mutant strains with H₂O₂ resulted in clearly distinguishable phenotypes (Figure 5). The effect of PTasRNA-*hbO* expression on KrPL H₂O₂ sensitivity was also evaluated by the disk diffusion assay, using recombinant KrPL cells harbouring the empty vector as the positive control. Interestingly, the PTasRNA-*hbO* expression was coupled to an H₂O₂ growth inhibition similar to that observed when the *PhTAC125* knockout mutant was tested in the same conditions, suggesting that the *PSHA_RS00150* gene silencing reached a level so high to be considered as total repression.



B

Strain	Diameter of the disk-inhibition zone (cm)
<i>PhTAC125</i> wt	0.16 ± 0.04
<i>PhTAC125</i> -30mut	1.24 ± 0.09
KRPL-pB40-79BsC	0.28 ± 0.06
KRPL-pB40-79C-PTasRNA- <i>hbO</i>	1.32 ± 0.08

Figure 5. Effect of PTasRNA-*hbO* on hydrogen peroxide sensibility. **(A)** Disk diffusion assay of *PhTAC125*, *PhTAC125*-30mut, KrPL-pB40-79BsC and KrPL-pB40-79C-PTasRNA-*hbO* grown in the presence of H₂O₂. **(B)** Diameter of the disk-inhibition zone. The reported values represented the mean of five independent experiments and were considered significant when p < 0.001 according to the t-Student test.

3. Discussion

The availability of consolidated techniques for common bacterial host genome-wide genetic manipulations paved the way for targeted strain engineering for fundamental and applied studies. However, the application of such methods in environmental strains still represents a challenging task.

Despite the psychrophilic bacterium *Pseudoalteromonas haloplanktis* TAC125 has been successfully used as a non-conventional platform for the recombinant production of difficult-to-produce proteins [21, 22, 23], the only genome mutagenesis technology set up in *PhTAC125* is based on a suicide vector and a two-steps integration-segregation procedure relying on homology recombination [29]. Nevertheless, the frequency of the second recombination event is often very low, and the “clean” gene deletion due to the proper excision of the suicide vector is a rare event. Furthermore, this disruption method is not suitable for essential genes. The present study intended to develop effective methods for conditional gene silencing and the control of gene expression in *PhTAC125* using synthetic antisense RNAs. Based on their mode of action, two kinds of asRNAs were evaluated: Hfq-dependent asRNA and Paired Termini asRNA. These synthetic asRNAs were challenged for their ability to

suppress potentially the translation of the protease Lon encoding mRNA.

Although no endogenous regulatory asRNAs of *PhTAC125* have been identified so far, the Hfq-dependent asRNA strategy was pursued relying on the observed high identity degree (85%) between the *PhTAC125* and *E. coli* Hfq amino acid sequences (Fig.S4). However, our results demonstrated a failure in silencing the *lon* gene by using MicC scaffold-based constructs in *PhTAC125*.

Cho et al. [18] described a quite similar outcome in *Clostridium acetobutylicum*, demonstrating that the scaffold derived from *E. coli* MicC did not competently interact with the Hfq of the host. Since the main difference in the psychrophilic and mesophilic Hfq was found in the C-terminal domain, we hypothesized that the same issue might also have occurred in the psychrophilic bacterium. The C-terminus of *PhTAC125* Hfq presents a shorter sequence than *E. coli* (Fig. S4) while conserving the acidic residues. Furthermore, the analysis of the *PhTAC125* Hfq amino acidic sequence does not suggest an intrinsically disordered region, as supported by the prediction of the secondary structure (Fig. S5). These findings led us to postulate that the different and stringent autoregulation mediated by the C-terminal domain is responsible for the weak interaction between *E. coli* MicC and *PhTAC125* Hfq, resulting in the silencing of the *lon* gene just in the first 2 hours of asRNA expression.

In the case of *C. acetobutylicum*, the authors remedied the problem by co-expressing *E. coli* Hfq with MicC-based asRNA in the Gram-positive bacterium [18]. However, this strategy did not seem suitable for our purpose since it could limit the applicability of the silencing system.

In this scenario, we decided to follow an alternative method for designing effective asRNA in *PhTAC125*. To overcome the main limiting determinants of canonical asRNA efficacy, we benefited from the structural features of PTasRNAs to obtain successful and efficient gene silencing. The different efficiency of *lon* repression obtained through the expression of the variants of PTasRNA-*lon*, depending on the accessibility and binding energy between the antisense molecules and the target mRNA, allowed us to define a critical parameter to consider for the establishment of an efficient gene control system in *PhTAC125*. Our finding is reflected in what described by Nakashima and coworkers [15]. Indeed, they reported that slightly different targeting sequences could influence the efficiency of down-regulation of *lacZ* mRNA but without delineating a designing rule.

However, despite our promising results, a complete silencing of *lon* was never observed. As already reported in *E. coli* [15], also in *PhTAC125*,

the presence of a 5' leader sequence upstream to the PTasRNA did not improve the repression, suggesting that the hairpin is sufficiently stable to induce the desired effect also in the psychrophilic bacterium.

The fundamental aspect considered for achieving a real improvement was the relative abundance of the target mRNA and PTasRNA. Indeed, a molar excess of asRNA is essential for efficient gene silencing because it should be able to out-compete ribosomes for binding with the target transcript. Since a transcriptomic analysis of *PhTAC125* grown at 15°C highlights that the *lon* gene is transcribed at a very high level, listing it among the 140 most transcribed genes (unpublished data), we hypothesized that total silencing could be obtained by targeting a less expressed gene. A good candidate for this new trial was the *hbO* gene, which is transcribed about 40 times less than *lon* (data not shown). Interestingly, the obtained results demonstrated a compelling reduction of HbO protein in cells expressing PTasRNA, showing an identical phenotype to the knockout mutant and claiming the total *hbO* repression.

In this work, we defined the guidelines for designing a conditional gene control system based on asRNA in *PhTAC125*. Through such a system, the down-regulation of different genes was reached at very high levels. These are relevant results if contextualized within processive mechanisms such as translation and RNA turnover, whose efficiency is a typical feature of *PhTAC125* [20]. Moreover, this developed asRNA regulatory tool acquires even more exceptional value if considering its promising applicability in synthetic biology and metabolic engineering.

4. Materials and Methods

4.1 Bacterial strains and growth conditions

E. coli DH5 α [*supE44*, Δ *lacU169* (ϕ 80 *lacZ* Δ M15) *hsdR17*, *recA1*, *endA1*, *gyrA96*, *thi-1*, *relA1*] was used for cloning procedures. *E. coli* S17-1(λ *pir*) [*thi*, *pro*, *hsd* (*r- m+*) *recA::RP4-2-TCr::Mu Kmr::Tn7*, *Tpr*, *Smr*, *lambda pir*] [35] constituted the donor strain in intergeneric conjugations for KrPL transformations [36]. KrPL was used as the host for expressing antisense RNAs throughout the study. Both *E. coli* strains were grown in LB broth (10 g/L bacto-tryptone, 5 g/L yeast extract, 10 g/L NaCl) supplemented with 34 μ g/mL chloramphenicol at 37 °C. KrPL was grown in TYP (16 g/L bacto-tryptone, 16 g/L yeast extract, 10 g/L NaCl) during conjugation experiments and in GG (10 g/L L-glutamic acid monosodium salt monohydrate, 10 g/L D-gluconic acid sodium salt, 10 g/L NaCl, 1 g/L NH₄NO₃, 1 g/L K₂HPO₄, 200 mg/L MgSO₄·7H₂O, 5 mg/L FeSO₄·7H₂O, 5 mg/L CaCl₂) [32] in recombinant production

transferred to an Immun-Blot low-fluorescence polyvinylidene fluoride (PVDF) membrane (BioRad) in 7 min using the TransBlot Turbo Transfer System (BioRad) with mixed molecular weight setting. After the transfer, the membrane was again imaged and blocked with PBS, 0.05% Triton X-100, 5% (w/v) milk for one hour. Then, an anti-Lon antibody (ab103809) was diluted 1:5,000 in the same buffer. After one hour of incubation at RT with the primary antibody, the membrane was washed with PBS, 0.05% Triton X-100 three times (5 min each) and incubated with an anti-rabbit antibody diluted 1:3,000 in PBS, 0.05% Triton X-100, 5% (w/v) milk for one hour at RT. Then, the membrane was washed again with PBS, 0.05% Triton X-100 three times (5 min each) and the secondary antibody was detected using the ECL method.

4.5 Western blotting data analysis

The signal intensities of Lon in each lane were determined by using the “Lane and Bands” tool of ImageLab software (version 6.0, BioRad). The densitometric analysis was performed by normalizing bands to total proteins in each lane detected on the blot membrane as described by Taylor et al., 2014 [37].

4.6 Bioinformatics analysis

The prediction of the secondary structure was performed using mFold website with default settings [38]. RNAPredator [39] was used for the prediction of PTasRNA-mRNA interaction setting NC_007481 for the selection of the genome of *PhTAC125* and submitting the PTasRNAs sequences.

4.7 Disk diffusion assay

Cultures of non-recombinant cells and cells harbouring PTasRNA and the empty vector were diluted in 7.5 mL warm Typ soft agar (4 g/L agar) at a final concentration of 0.2 OD/mL. When required, 12.5 µg/mL chloramphenicol and 10 mM IPTG were added to the media. Then, disks of Whatman filter paper were treated with 256 mM H₂O₂ and placed in the centre of each plate. After 24h of incubation at 15°C, the diameter of the killing zone was measured.

4.8 Statistics and reproducibility of results

Data were statistically validated using the t-Student test comparing the mean absorbance of treated and untreated samples. The significance of differences between mean absorbance values was calculated using a two-tailed Student’s t-test. A P value of <0.05 was considered significant.

5. References

- [1] E. G. H. Wagner and P. Romby, *Small RNAs in Bacteria and Archaea: Who They Are, What They Do, and How They Do It*, vol. 90. Elsevier Ltd, 2015.
- [2] G. Storz, J. Vogel, and K. M. Wassarman, "Regulation by Small RNAs in Bacteria: Expanding Frontiers," *Mol. Cell*, vol. 43, no. 6, pp. 880–891, 2011.
- [3] L. S. Qi *et al.*, "Repurposing CRISPR as an RNA-guided platform for sequence-specific control of gene expression," *Cell*, vol. 152, no. 5, pp. 1173–1183, 2013.
- [4] D. Bikard, W. Jiang, P. Samai, A. Hochschild, F. Zhang, and L. A. Marraffini, "Programmable repression and activation of bacterial gene expression using an engineered CRISPR-Cas system," *Nucleic Acids Res.*, vol. 41, no. 15, pp. 7429–7437, 2013.
- [5] S. H. Jang, J. W. Cha, N. S. Han, and K. J. Jeong, "Development of bicistronic expression system for the enhanced and reliable production of recombinant proteins in *Leuconostoc citreum*," *Sci. Rep.*, vol. 8, no. 1, pp. 1–11, 2018.
- [6] J. Chappell, M. K. Takahashi, and J. B. Lucks, "Creating small transcription activating RNAs," *Nat. Chem. Biol.*, vol. 11, no. 3, pp. 214–220, 2015.
- [7] D. Na, S. M. Yoo, H. Chung, H. Park, J. H. Park, and S. Y. Lee, "Metabolic engineering of *Escherichia coli* using synthetic small regulatory RNAs" *Nat. Biotechnol.*, vol. 31, no. 2, pp. 170–174, 2013.
- [8] L. S. Qi and A. P. Arkin, "A versatile framework for microbial engineering using synthetic non-coding RNAs," *Nat. Rev. Microbiol.*, vol. 12, no. 5, pp. 341–354, 2014.
- [9] W. Ahmed, M. A. Hafeez, and R. Ahmed, "Advances in engineered trans-acting regulatory RNAs and their application in bacterial genome engineering," *J. Ind. Microbiol. Biotechnol.*, vol. 46, no. 6, pp. 819–830, 2019.
- [10] S. A. Woodson, S. Panja, and A. Santiago-Frangos, "Proteins That Chaperone RNA Regulation," *Regul. with RNA Bact. Archaea*, vol. 6, no. 4, pp. 383–397, 2018.
- [11] D. J. Schu, A. Zhang, S. Gottesman, and G. Storz, "Alternative Hfq- sRNA interaction modes dictate alternative mRNA recognition ," *EMBO J.*, vol. 34, no. 20, pp. 2557–2573, 2015.
- [12] S. Panja, D. J. Schu, and S. A. Woodson, "Conserved arginines on the rim of Hfq catalyze base pair formation and exchange," *Nucleic Acids Res.*, vol. 41, no. 15, pp. 7536–7546, 2013.
- [13] A. Santiago-Frangos, J. R. Jeliaskov, J. J. Gray, and S. A. Woodson, "Acidic C-terminal domains autoregulate the RNA chaperone Hfq," *Elife*, vol. 6, pp. 1–25, 2017.
- [14] H. Aiba, "Mechanism of RNA silencing by Hfq-binding small RNAs," *Curr. Opin. Microbiol.*, vol. 10, no. 2, pp. 134–139, 2007.
- [15] N. Nakashima, T. Tamura, and L. Good, "Paired termini stabilize antisense RNAs and enhance conditional gene silencing in *Escherichia coli*," *Nucleic Acids Res.*, vol. 34, no. 20, pp. 1–10, 2006.
- [16] N. Nakashima and T. Tamura, "Conditional gene silencing of multiple genes with antisense RNAs and generation of a mutator strain of *Escherichia coli*," *Nucleic Acids Res.*, vol. 37, no. 15, 2009.
- [17] E. K. Zess, M. B. Begemann, and B. F. Pflieger, "Construction of new synthetic biology tools for the control of gene expression in the cyanobacterium *Synechococcus* sp. strain PCC 7002," *Biotechnol. Bioeng.*, vol. 113, no. 2, pp. 424–432, 2016.
- [18] C. Cho, S.Y. Lee, "Efficient gene knockdown in *Clostridium acetobutylicum* by synthetic small regulatory RNAs," *Biotechnol. Bioeng.*, vol. 114, no. 2, pp. 374–383, 2017.
- [19] T. Sun *et al.*, "Re-direction of carbon flux to key precursor malonyl-CoA via artificial small RNAs in photosynthetic *Synechocystis* sp. PCC 6803," *Biotechnol. Biofuels*, vol. 11, no. 1, pp. 1–17, 2018.
- [20] E. C. Medigue *et al.*, "Coping with cold : The genome of the versatile marine Antarctica bacterium *Pseudoalteromonas haloplanktis* TAC125," *Genome Res.*, pp. 1–12, 2005.
- [21] I. Vigentini, A. Merico, M. L. Tutino, C. Compagno, and G. Marino, "Optimization of recombinant human nerve growth factor production in the psychrophilic *Pseudoalteromonas haloplanktis*," *J. Biotechnol.*, vol. 127, no. 1, pp. 141–150, 2006.

- [22] M. Giuliani, E. Parrilli, F. Sannino, G. A. Apuzzo, G. Marino, and M. L. Tutino, "Recombinant production of a single-chain antibody fragment in *Pseudoalteromonas haloplanktis* TAC125," *Appl. Microbiol. Biotechnol.*, vol. 98, no. 11, pp. 4887–4895, 2014.
- [23] U. Unzueta *et al.*, "Strategies for the production of difficult-to-express full-length eukaryotic proteins using microbial cell factories: production of human alpha-galactosidase A," *Appl. Microbiol. Biotechnol.*, vol. 99, no. 14, pp. 5863–5874, 2015.
- [24] F. Sannino *et al.*, "Pseudoalteromonas haloplanktis produces methylamine, a volatile compound active against Burkholderia cepacia complex strains," *N. Biotechnol.*, vol. 35, pp. 13–18, 2017.
- [25] F. Sannino *et al.*, "Pseudoalteromonas haloplanktis TAC125 produces 4-hydroxybenzoic acid that induces pyroptosis in human A459 lung adenocarcinoma cells," *Sci. Rep.*, vol. 8, no. 1, pp. 1–10, 2018.
- [26] A. Casillo *et al.*, "Anti-biofilm activity of a long-chain fatty aldehyde from antarctic *Pseudoalteromonas haloplanktis* TAC125 against *Staphylococcus epidermidis* biofilm," *Front. Cell. Infect. Microbiol.*, vol. 7, no. FEB, pp. 1–13, 2017.
- [27] F. Piette, S. D'Amico, G. Mazzucchelli, A. Danchin, P. Leprince, and G. Feller, "Life in the cold: A proteomic study of cold-repressed proteins in the antarctic bacterium *Pseudoalteromonas haloplanktis* TAC125," *Appl. Environ. Microbiol.*, vol. 77, no. 11, pp. 3881–3883, 2011.
- [28] S. Mocali *et al.*, "Ecology of cold environments: New insights of bacterial metabolic adaptation through an integrated genomic-phenomic approach," *Sci. Rep.*, vol. 7, no. 1, pp. 1–13, 2017.
- [29] M. Giuliani *et al.*, "A novel strategy for the construction of genomic mutants of the antarctic bacterium *Pseudoalteromonas haloplanktis* TAC125," *Methods Mol. Biol.*, vol. 824, 2012.
- [30] A. Colarusso, C. Lauro, M. Calvanese, E. Parrilli, and M. L. Tutino, "Improvement of pseudoalteromonas haloplanktis tac125 as a cell factory: Iptg-inducible plasmid construction and strain engineering," *Microorganisms*, vol. 8, no. 10, pp. 1–24, 2020.
- [31] S. M. Yoo, D. Na, and S. Y. Lee, "Design and use of synthetic regulatory small RNAs to control gene expression in *Escherichia coli*," *Nat. Protoc.*, vol. 8, no. 9, pp. 1694–1707, 2013.
- [32] F. Sannino *et al.*, "A novel synthetic medium and expression system for subzero growth and recombinant protein production in *Pseudoalteromonas haloplanktis* TAC125," *Appl. Microbiol. Biotechnol.*, vol. 101, no. 2, pp. 725–734, 2017.
- [33] K. Moon and S. Gottesman, "Competition among Hfq-binding small RNAs in *Escherichia coli*," *Mol. Microbiol.*, vol. 82, no. 6, pp. 1545–1562, 2011.
- [34] E. Parrilli *et al.*, "The role of a 2-on-2 haemoglobin in oxidative and nitrosative stress resistance of Antarctic *Pseudoalteromonas haloplanktis* TAC125," *Biochimie*, vol. 92, no. 8, 2010.
- [35] R. I. Tascon, E. F. Rodriguez-Ferri, C. B. Gutierrez-Martin, I. Rodriguez-Barbosa, P. Berche, and J. A. Vazquez-Boland, "Transposon mutagenesis in *Actinobacillus pleuropneumoniae* with a Tn10 derivative," *J. Bacteriol.*, vol. 175, no. 17, 1993.
- [36] M. L. Tutino, A. Duilio, E. Parrilli, E. Remaut, G. Sannia, and G. Marino, "A novel replication element from an Antarctic plasmid as a tool for the expression of proteins at low temperature," *Extremophiles*, vol. 5, no. 4, pp. 257–264, 2001.
- [37] S. C. Taylor and A. Posch, "The design of a quantitative western blot experiment," *Biomed Res. Int.*, vol. 2014, no. March, 2014.
- [38] M. Zuker, "Mfold web server for nucleic acid folding and hybridization prediction," *Nucleic Acids Res.*, vol. 31, no. 13, pp. 3406–3415, 2003.
- [39] F. Eggenhofer, H. Tafer, P. F. Stadler, and I. L. Hofacker, "RNAPredator: Fast accessibility-based prediction of sRNA targets," *Nucleic Acids Res.*, vol. 39, no. 2, pp. 149–154, 2011.
- [40] T. A. Kumar, "CFSSP: Chou and Fasman Secondary Structure Prediction server," *Wide Spectr.*, vol. 1, no. 9, pp. 15–19, 2013.

Supplementary materials

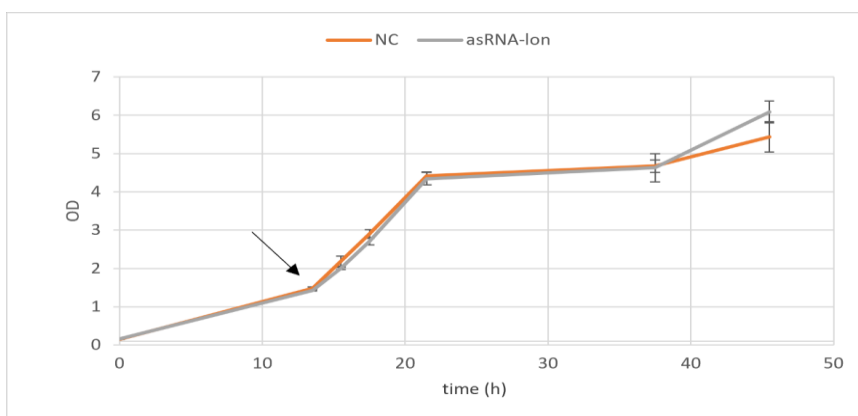


Figure S1. Growth curves of KrPL carrying pB40_79C-asRNA-lon (in grey) and the empty vector pB40_79C (in orange). The growth was performed at 15° C in GG medium. The induction was performed with 10 mM IPTG at the exponential growth phase as marked by the black arrow. The measurements are reported as the mean of two independent experiments whose standard deviation is indicated by the error bars.

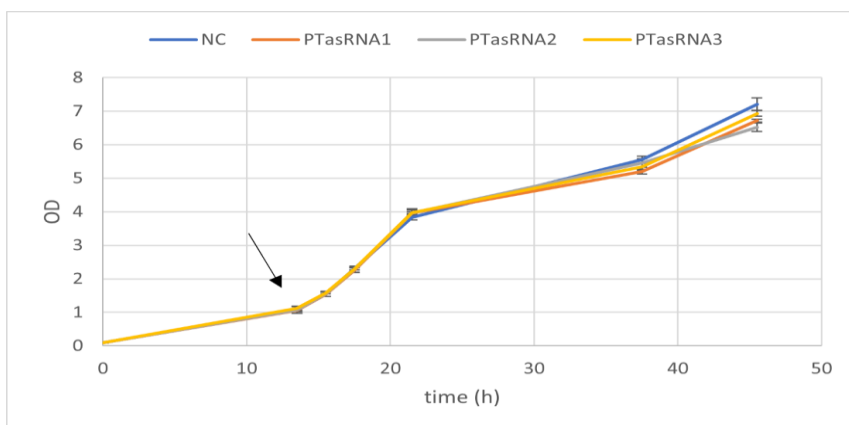


Figure S2. Growth curves of KrPL carrying pB40_79C-PTasRNA1-lon, pB40_79C-PTasRNA2-lon, pB40_79C-PTasRNA3-lon and the empty vector pB40_79C. The growth was performed at 15° C in GG medium. The induction was performed with 10mM IPTG at the exponential growth phase as marked by the black arrow. The measurements are reported as the mean of two independent experiments whose standard deviation is indicated by the error bars.

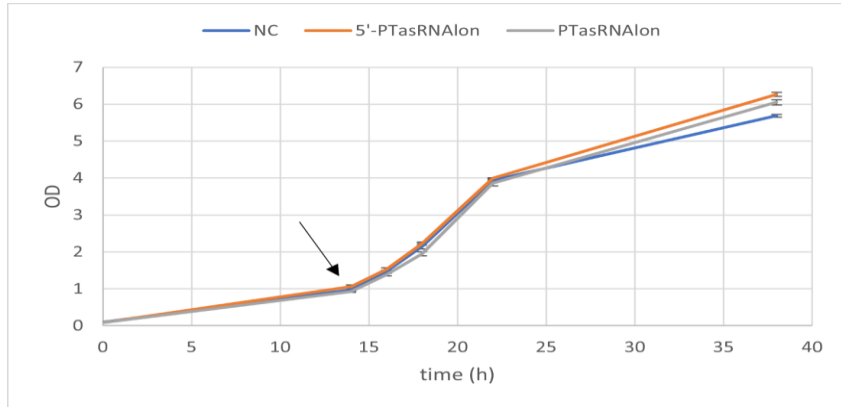


Figure S3. Growth curves of KrPL carrying pB40_79C-5'-PTasRNA-Ion, pB40_79C-PTasRNA-Ion and the empty vector pB40_79C. The growth was performed at 15° C in GG medium. The induction was performed with 10mM IPTG at the exponential growth phase as marked by the black arrow. The measurements are reported as the mean of two independent experiments whose standard deviation is indicated by the error bars.

```

PSHA_RS01345_PhTAC125  MAKGQSLQDPFLNALRRERIPVSI F L V N G I K L Q G K I Q S F D Q F V I L L E N T V N Q M V Y K H A I S
POA6X3_E.coli          MAKGQSLQDPFLNALRRERVPVSI Y L V N G I K L Q G Q I E S F D Q F V I L L K N T V S Q M V Y K H A I S
*****:*****:*****:*:*****:***:*****

PSHA_RS01345_PhTAC125  TVVPARAVNFQGVQENDDTEEPE-AGNI----- 87
POA6X3_E.coli          TVVPSRPVSHHSNNAGGGTSSNYHHGSSAQNTSAQQDSEETE 102
****:* *...: :...*... *

```

Figure S4. Alignment of *E. coli* and *PhTAC125* Hfq protein sequences. The residues involved in the binding with asRNAs and mRNAs are highlighted in yellow [36]. The perfect alignments are indicated with the asterisks, the residues with substantial similarity are indicated with colons, the residues with weak similarity are indicated with dots.

Appendix

Poster communications

1. 12th edition of the International Congress on Extremophiles – “Extremophiles 2018”. Ischia (Napoli), Italia. 16 -20 September 2018. “Living in the cold: a proteo-transcriptomic analysis of *Pseudoalteromonas haloplanktis* TAC125”. C. Lauro, A. Colarusso, A. Landolfi, M. Calvanese, C. D’Errico, M. Monti, E. Parrilli, and ML Tutino.
2. “2018 CDKL5 Forum”. London, UK. 22-23 October 2018. “Use of sulforaphane to relieve both BDNF production and Nrf2-dependent antioxidant potential in CDKL5 Deficiency Disease: a case study”. A. Colarusso, M. Calvanese, C. Lauro, E. Parrilli and ML Tutino.
3. CDKL5 Alliance Edinburgh Royal College of Surgeons, Edinburgh, Jun 21, 2019 - Jun 23, 2019. “Why the recombinant production of human TAT-CDKL5 in bacteria is so complex?”. A. Colarusso, M. Calvanese, C. Lauro, E. Parrilli, S. Clark and M.L. Tutino.
4. CDKL5 Alliance Edinburgh Royal College of Surgeons, Edinburgh, Jun 21, 2019 - Jun 23, 2019. “Exploiting the use of sulforaphane to relieve both BDNF production and NRF2-dependent antioxidant potential in CDKL5 deficiency disease: a case study”. M. Calvanese, A. Colarusso, C. Lauro, Apuzzo G.A., D’Alessio P., Del Vecchio G., Parrilli E and M.L. Tutino.
5. Escmid Study Group For Biofilms (Esgb) Eurobiofilms 2019, Glasgow, 3 - 6th September 2019. “A new weapon against biofilm: a lipopeptide from Antarctica”. A. Ricciardelli, A. Casillo, R. Papa, M. Artini, G. Vrenna, L. Selan, C. Lauro, M. M. Corsaro, M. L. Tutino, E. Parrilli.
6. 2019 CDKL5 Forum Boston. Boston, USA. 4-5 November 2019. “The recombinant production of full-length human TAT-CDKL5 in an Antarctic marine bacterium”. A. Colarusso, M. Calvanese, C. Lauro, E. Parrilli, S. Clark and M.L. Tutino.
7. IX meeting of Neapolitan Brain Group NBG. Telethon Institute of Genetics And Medicine (Tigem), Pozzuoli, IT. 12 December 2019. “The recombinant production of full-length human

CDKL5_1 in an Antarctic marine bacterium". A. Colarusso, M. Calvanese, Totò, C. Lauro, E. Parrilli and M.L. Tutino.

8. 14th International Symposium on the Genetics of Industrial Microorganisms GIM 2019. Pisa, IT. 8 - 11 September 2019. "Strain improvement of *Pseudoalteromonas haloplanktis* TAC125 towards its industrial exploitation as cell factory". C. Lauro, A. Colarusso, M. Calvanese, E. Parrilli, M.L. Tutino.


Publications

1. M. Artini, R. Papa, G. Vrenna, C. Lauro, A. Ricciardelli, A. Casillo, M. M. Corsaro, M. L. Tutino, E. Parrilli, L. Selan. "Cold-adapted bacterial extracts as source of anti-infective and antimicrobial compounds against *Staphylococcus aureus*". Future Microbiology. 2019 Oct 9. doi: 10.2217/fmb-2019-0147 C _ 2019
2. Andrea Colarusso †, Concetta Lauro †, Marzia Calvanese, Ermenegilda Parrilli and Maria Luisa Tutino. "Improvement of *Pseudoalteromonas haloplanktis* TAC125 as a Cell Factory: IPTG-Inducible Plasmid Construction and Strain Engineering". Microorganisms. 2020 Sept 24. doi:10.3390/microorganisms8101466

Book chapters

Marzia Calvanese[#], Andrea Colarusso[#], Concetta Lauro[#], Ermenegilda Parrilli and Maria Luisa Tutino^{*}. Soluble recombinant protein production in *Pseudoalteromonas haloplanktis* TAC125: the case study of the full-length human CDKL5 protein. in Insoluble Proteins: Methods and Protocols, Second Edition, Garcia-Fruitos E and Aris Giralt A Editors, Springer, 2021 in press.

Cold-adapted bacterial extracts as source of anti-infective and antimicrobial compounds against *Staphylococcus aureus*

Marco Artini^{‡,1}, Rosanna Papa^{‡,1}, Gianluca Vrenna¹, Concetta Lauro², Annarita Ricciardelli², Angela Casillo², Maria M Corsaro², Maria L Tutino², Ermenegilda Parrilli² & Laura Selan^{*.1} 

¹Department of Public Health & Infectious Diseases, Sapienza University, 00185 Rome, Italy

²Department of Chemical Sciences, Federico II University, 80126 Naples, Italy

*Author for correspondence: Tel.: +39 0649 694 261; Fax: +39 0649 694 298; laura.selan@uniroma1.it

‡ Authors contributed equally

Aim: The dramatic emergence of antibiotic resistance has directed the interest of research toward the discovery of novel antimicrobial molecules. In this context, cold-adapted marine bacteria living in polar regions represent an untapped reservoir of biodiversity endowed with an interesting chemical repertoire. The aim of this work was to identify new antimicrobials and/or antibiofilm molecules produced by cold-adapted bacteria. **Materials & methods:** Organic extracts obtained from polar marine bacteria were tested against *Staphylococcus aureus*. Most promising samples were subjected to suitable purification strategies. **Results:** Results obtained led to the identification of a novel lipopeptide able to effectively inhibit the biofilm formation of *S. aureus*. **Conclusion:** New lipopeptide may be potentially useful in a wide variety of biotechnological and medical applications.

First draft submitted: 17 May 2019; Accepted for publication: 22 August 2019; Published online: 9 October 2019

Keywords: antibacterial • antibiofilm • antimicrobial • lipopeptide • organic extract • polar bacteria • *Pseudomonas* • *Staphylococcus aureus*

In recent years, bacterial infections represent a serious challenge for human health due to the widespread diffusion of resistance to antibiotics, since more than 70% of pathogenic bacteria display resistance to at least one antibiotic commonly used in therapy [1]. This feature is often related to the ability to form biofilm [2], a phenotypic lifestyle that renders bacteria highly tolerant to exogenous stressors, including antibiotics or other biocides.

Staphylococci represent a prevalent cause of chronic infections associated to biofilm phenotype [3]; *Staphylococcus aureus* in particular, deploying a wide array of virulence factors, can acquire resistance to the majority of antibacterial compounds. This feature makes *S. aureus* a ‘superbug’ further reinforced by continuous emergence of new clones [4].

S. aureus can be frequently isolated as a commensal of the human body, colonizing districts of healthy individuals such as skin and mucous membranes, including nares and guts. *S. aureus* can be persistently isolated from the nasal cavity of 20% of healthy individuals, while 30% are intermittent carriers. This colonization represents an important reservoir of this pathogen, and significantly increases the chances of infections [4].

Within the past two decades, the continuous and rapid emergence of antibiotic resistance has directed the interest of research toward the discovery of novel antibiofilm compounds and antimicrobial molecules [5]. In the literature, there are several reports about the novel synthesis of biomaterials effective against *S. aureus* and able to combat drug resistance phenomenon [6].

Recently, many scientists are analyzing natural compounds extracted from plants and marine microorganisms, in order to identify new and effective antibiofilm molecules [7–10]. Indeed, the bioprospecting of natural environments has allowed to discover, produce and commercialize many new antibiotics [11] and offers novel key scaffolds for drug development [12].

Table 1. Strains used in this study.

Strain	Origin	Ref.
<i>P. haloplanktis</i> TAE79	Antarctic seawater† (algae necrosized suspended in seawater)	Liège collection
<i>P. haloplanktis</i> TAE80	Antarctic seawater† (algae necrosized suspended in seawater)	Liège collection
<i>Pseudomonas</i> sp. TAD15	Antarctic seawater†	Liège collection
<i>Pseudomonas</i> sp. TAD18	Antarctic seawater† (frozen algae)	Liège collection
<i>Pseudomonas</i> sp. TAA207	Antarctic seawater† (marine sediment)	Liège collection
<i>Psychromonas arctica</i>	Arctic seawater (Svalbard islands, Arctic)	[53]
<i>P. haloplanktis</i> TAB23	Antarctic seawater†	[54]
<i>P. haloplanktis</i> TAE56	Antarctic seawater† (algae necrosized suspended in seawater)	Liège collection
<i>P. haloplanktis</i> TAE57	Antarctic seawater† (algae necrosized suspended in seawater)	Liège collection
<i>S. aureus</i> 6538P	Clinical isolate, reference strain for antimicrobial tests	ATCC collection
<i>S. aureus</i> 20372	Clinical isolate	ATCC collection
<i>S. aureus</i> 25923	Clinical isolate, reference strain for antimicrobial tests	ATCC collection

†Isolated from Antarctic coastal seawater sample collected in the vicinity of the French Antarctic station Dumont d'Urville, Terre Adélie (66°40' S; 140° 01' E).

Marine microorganisms are considered an inexhaustible source for the discovery of new antimicrobial compounds, since they must survive in an environment characterized by climatic variations and compete with others for space and nutrition. Several biologically active compounds (such as antifouling, anticancer, antimicrobial) have been obtained from marine sources [13]. Some of them are already investigated for the treatment of various diseases [14–16].

In this context, cold-adapted marine bacteria deriving from polar regions represent an unexploited reservoir of biodiversity provided with an attracting chemical repertoire. Unusual survival strategies have been developed by bacteria living in prohibitive environmental conditions, according to an antagonistic behavior mandatory offering competitive advantages due to the limitation of the growth of other microorganisms [17]. When procurement of nutrients is limited or difficult, this behavior offers a growth advantage; in this view, Antarctic microorganisms could have developed peculiar characteristics, such as chemically complex metabolites, that guarantee survival in extreme habitats [18]. Some molecules obtained from these bacteria display antifouling, antimicrobial and other activities interesting for possible pharmaceutical applications [19]. We recently reported that *Pseudoalteromonas haloplanktis* TAC125, an Antarctic marine bacterium, produce and secrete many different compounds of biotechnological interest. These compounds include molecules that inhibit biofilm growth by *Staphylococcus epidermidis*, a saprophyte of the human skin acting as a pathogen after colonization of artificial medical devices [20–23], and antimicrobial compounds that inhibit the growth of *Burkholderia cepacia complex* (Bcc), organisms that pose a significant health risk to cystic fibrosis patients [24,25]. Furthermore, cell-free supernatants obtained from different bacterial cultures of polar marine bacteria showed interesting antibiofilm activities on *S. epidermidis*, *Pseudomonas aeruginosa* and *S. aureus* [26].

The aim of this paper was the identification of new antimicrobials and/or antibiofilm molecules produced by bacteria adapted to cold habitats. Intracellular and extracellular organic extracts obtained from polar marine bacteria, such as *Psychromonas*, *Pseudomonas* and *Pseudoalteromonas* genera, have been tested against *S. aureus*. Most promising samples were subjected to suitable purification strategies in order to identify molecules responsible for the sought biological activity.

Materials & methods

Bacterial strains & culture conditions

Bacterial strains used in this work are reported in Table 1. Polar bacteria were grown in flasks in synthetic medium GG (D-gluconic acid sodium 10 g/l, L-glutamic acid 10 g/l, NaCl 10 g/l; NH₄NO₃ 1 g/l; KH₂PO₄·7H₂O 1 g/l; MgSO₄·7H₂O 200 mg/l; FeSO₄·7H₂O 5 mg/l; CaCl₂·2H₂O 5 mg/l) at 15°C under vigorous agitation (180 r.p.m) until stationary phase (72–90 h).

S. aureus was grown in Brain Heart Infusion (BHI) broth (Oxoid, Basingstoke, UK) at 37°C. Culture broths were performed under vigorous agitation (180 rpm), while biofilm formation was assessed in static conditions.

Bacterial strains grown in BHI broth were kept at -80°C with glycerol at a final concentration of 15%.

Organic extract preparation

Polar bacterial cultures previously described were collected and subjected to a liquid–liquid extraction as an initial separation technique to process the cell-free supernatants and the cellular pellets, to obtain ‘extracellular extracts’ and ‘intracellular extracts’, respectively.

Cell-free supernatants and cell pellets were recovered by centrifugation at 6000 r.p.m at 4°C for 50 min. After centrifugation, the supernatants were separated from the cells and were sterilized by filtration through membranes with a pore diameter of $0.22\ \mu\text{m}$. Cell pellets and cell-free supernatants were frozen at -80°C until use.

Liquid–liquid extraction was performed on cell pellets and cell-free supernatants separately, without adding cryoprotectants. In detail, cell pellets and supernatants were thawed, then cell pellets were resuspended in an opportune volume of sterile distilled water. Obtained samples were stirred with ethyl acetate in a volume ratio of 2:1 (assay percent range $\geq 99.5\%$) (Sigma-Aldrich, St. Louis, MO, US) and mixed at 1% with acid formic (assay percent range = 90%; JT Baker, Munich, Germany). Each solution was stirred at least for 30 min and then centrifuged at 3000 r.p.m for 30 min. The resulting two phases were separated, and the organic phase was recovered and dried using a rotary evaporator Rotavapor (Buchi R-210) at a temperature lower than 40°C . The resulting organic extracts were aliquoted in 4 mg dry-weight samples and stored at -20°C .

Fractionation of the intracellular extract of TAA207 & TAD1S

The intracellular extracts (named IN_) from *Pseudomonas* sp. TAA 207 (IN_TAA207, 100 mg) and from *Pseudomonas* sp. TAD1S (IN_TAD1S, 113 mg) were both fractionated on silica gel columns. The columns (30 ml, 50×0.7 cm for IN_TAA207 and 49 ml, 32×0.7 cm for IN_TAD1S, respectively) were initially eluted with $\text{CHCl}_3:\text{CH}_3\text{OH}$ ranging from 100 to 70% of CHCl_3 , and then with $\text{CHCl}_3:\text{CH}_3\text{OH}:\text{H}_2\text{O}$ 9/3/0.5 v/v/v. Only for IN_TAD1S, a further elution with $\text{CHCl}_3:\text{CH}_3\text{OH}:\text{H}_2\text{O}$ 6/4/0.5 v/v/v was performed.

The fractions resulted to be active against *S. aureus* (IN_TAA207: fraction 3; and IN_TAD1S: fractions 5-8-11-20, respectively) were acetylated and analyzed by GC–MS technique. In detail, fraction 3 from IN_TAA207 was analyzed on an Agilent Technologies gas chromatograph 6850A equipped with a mass selective detector 5973N and a Zebron ZB-5 capillary column (Phenomenex, 30 m \times 0.25 mm i.d., flow rate 1 ml/min, He as carrier gas); fractions 5-8-11-20 from IN_TAD1S were analyzed on a Agilent Technologies gas chromatograph 7820A equipped with a mass selective detector 5977Band a HP-5 capillary column (Agilent, 30 m \times 0.25 mm i.d., flow rate 1 ml/min, He as carrier gas). All derivatives were analyzed by using the following temperature program: 150°C for 3 min, from 150 to 300°C at $15^{\circ}\text{C}/\text{min}$, at 300°C for 5 min.

The same purification procedure was used for EX_TAD1S (70 mg). The silica gel column (46 ml, 30×0.7 cm) was eluted with the same solvent mixtures used for IN_TAD1S. Fraction 15, active against *S. aureus* USA300, was analyzed by ^1H NMR spectrum performed by using a Bruker Avance-DRX 600 MHz spectrometer equipped with a cryoprobe. The spectrum was acquired at 298 K in $\text{CDCl}_3:\text{CD}_3\text{OD}$ 3:1.

Minimal inhibitory concentration

The antimicrobial activity of each extract was evaluated. The minimal inhibitory concentration (MIC) was defined as the lowest concentration of antimicrobial that yields at least 99.9% reduction (i.e., three log-units) of bacterial growth compared with the untreated bacteria as reported by Clinical & Laboratory Standards Institute (CLSI) and National Committee for Clinical Laboratory Standards (NCCLS) methods. MIC was determined in duplicate by twofold serial dilution (CLSI, 2017), as reported [27].

The wells of a sterile 48-well flat-bottomed polystyrene plate were filled with 400 μl of 1/100 diluted overnight bacterial cultures grown in BHI. Each extract was tested starting from a concentration of 4 mg/ml, as reported in the literature [28]. After overnight incubation at 37°C , the antimicrobial activity was optically evaluated comparing treated and untreated samples.

Biofilm formation by *S. aureus*

Biofilm formation by *S. aureus* was evaluated in the presence of organic extracts. Quantification of *in vitro* biofilm production was based on a method previously reported [29]. Briefly, the wells of a sterile 96-well flat-bottomed polystyrene plate were filled with 100 μl of BHI broth. 1/100 dilution of overnight bacterial cultures was added

into each well. Dried extracts were first dissolved in DMSO at an opportune concentration, then diluted in BHI before use.

The first row of the multiwell contained the untreated bacteria, while each of the remaining rows contained serial dilutions of the organic extract, starting from the second row.

After the inoculation, the plates were incubated aerobically for 20 h at 37°C in static condition. Biofilm formation was measured by crystal violet staining. After treatment, culture broths were gently removed; each well was washed three-times with water and patted dry on a piece of paper towel in an inverted position. Each well was stained with 0.1% crystal violet (incubation at room temperature for 15 min). To remove the excess of dye, each well was washed three-times with water, and thoroughly dried. The remaining dye, bound to biofilm, was solubilized with 80% (v/v) ethanol and 20% (v/v) glacial acetic acid. After 30 min of incubation at room temperature, (optical density) OD at 590 nm was measured to quantify the total biomass of biofilm formed in each well. Each data point is composed of three independent experiments each performed at least in six replicates.

Statistics & reproducibility of results

Data reported were statistically validated using Student's *t*-test comparing the mean absorbance of treated and untreated samples. The significance of differences between mean absorbance values was calculated using a two-tailed Student's *t*-test. A *p*-value of less than 0.05 was considered significant.

Results

Setup of two libraries from polar bacterial cultures

A selection of nine polar marine bacteria (Table 1) were grown, as described in the Materials & methods section. The synthetic minimal medium named D-gluconic and L-glutamic acid medium (GG) [25] was chosen to minimize the potential interference of culture medium on the organic extraction step due to reduction of the sample complexity, and to exploit the biosynthetic potential of bacterial metabolism. Furthermore, the choice of a minimum medium should promote in the bacterial cell the activation of alternative metabolic pathway that could maximize the production of secondary metabolites. The whole bacterial cultures were then recovered and separately extracted (cell pellet and supernatant) by using ethyl acetate. It is often adopted for the downstream recovery of fermentation products such as antibiotics or secondary metabolite.

In this way, for each bacterial strain, we obtained an intracellular extract (IN_ *StrainName*) and an extracellular one (EX_ *StrainName*).

Screening of antimicrobial activities of extracts against *S. aureus*

Intracellular and extracellular extracts were analyzed for their antimicrobial activity against *S. aureus* 6538P. The MIC of extracts is reported in Table 2. A discrete number of selected extracts showed antimicrobial activity against *S. aureus* 6538P. In detail, IN_TAB23, EX_TAE56 and EX_TAE57 showed antimicrobial activity at a concentration higher than 1 mg/ml.

Screening of antibiofilm activity of intracellular extracts against *S. aureus*

Intracellular extracts were also screened for their ability to inhibit biofilm formation of *S. aureus* 6538P. Several extracts were able to inhibit biofilm formation (Figure 1). Considering that IN_TAB23 displayed an antimicrobial activity at a concentration of 1 mg/ml (Table 2), it was tested for antibiofilm activity at a concentration of 0.5 mg/ml (1/2 MIC value). Results obtained showed that this extract also possessed an antibiofilm activity at sub-MIC concentration. Best results were obtained with IN_TAA207 and IN_TAD1S extracts and, for this reason, they were selected for further analyses.

Experiments were performed on three different *S. aureus* strains, characterized by qualitative and quantitative differences in biofilm composition [29], using serial dilutions of each extract, starting from a concentration of 4 mg/ml (Figure 2). Figure 2A describes the activity of IN_TAA207 on biofilm formation of *S. aureus* 6538P, 20372 and 25923 strains. A strong inhibitory effect was confirmed for all tested strains, despite their differences in biofilm composition. Furthermore, inhibition of biofilm formation is clearly dose-dependent, starting from a reduction of about 40% at a concentration of 0.5 mg/ml.

As shown in Figure 2B, IN_TAD1S extract reduced biofilm production of all three tested *S. aureus* strains, with different extent. However, in these experiments, a clear dose-dependent effect was not observed.

Table 2. Minimal inhibitory concentration of organic extracts from bacterial supernatants and whole cells on *S. aureus* 6538P.

Extract	<i>S. aureus</i> 6538P
Intracellular extracts	
IN.TAE79	>4 mg/ml
IN.TAE80	>4 mg/ml
IN.TAD15	>4 mg/ml
IN.TAD18	>4 mg/ml
IN.TAA207	>4 mg/ml
IN.ARTICA	>4 mg/ml
IN.TAB23	1 mg/ml
IN.TAE56	>4 mg/ml
IN.TAE57	>4 mg/ml
Supernatant extracts	
EX.TAE79	>4 mg/ml
EX.TAE80	>4 mg/ml
EX.TAD15	>4 mg/ml
EX.TAD18	>4 mg/ml
EX.TAA207	>4 mg/ml
EX.ARTICA	>4 mg/ml
EX.TAB23	>4 mg/ml
EX.TAE56	1 mg/ml
EX.TAE57	1 mg/ml

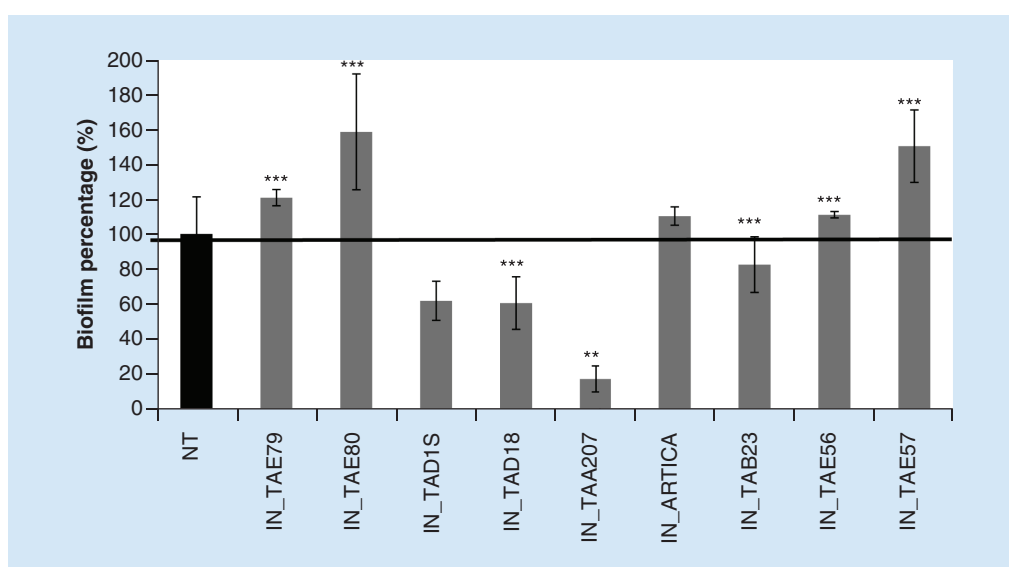


Figure 1. Intracellular extracts from cold-adapted bacteria on *S. aureus* 6538P biofilm formation. Data are reported as the percentage of residual biofilm after the treatment. Each data point represents the mean \pm SD of five independent samples. Differences in mean absorbance were compared with the untreated control (NT, black bar) and considered significant when $p < 0.05$ according to Student's *t*-test.

* $p < 0.05$; ** $p < 0.01$; *** $p < 0.001$.

NT: Not treated; SD: Standard deviation.

Fractionation of intracellular extracts from *Pseudomonas* sp. TAA207 & from *Pseudomonas* sp. TAD15

IN_TAA207 and IN_TAD15 were fractionated on a silica gel column as reported in the Methods section (Figure 3). The fractions obtained from IN_TAA207 were tested, at a concentration of 200 μ g/ml, to evaluate the antibiofilm

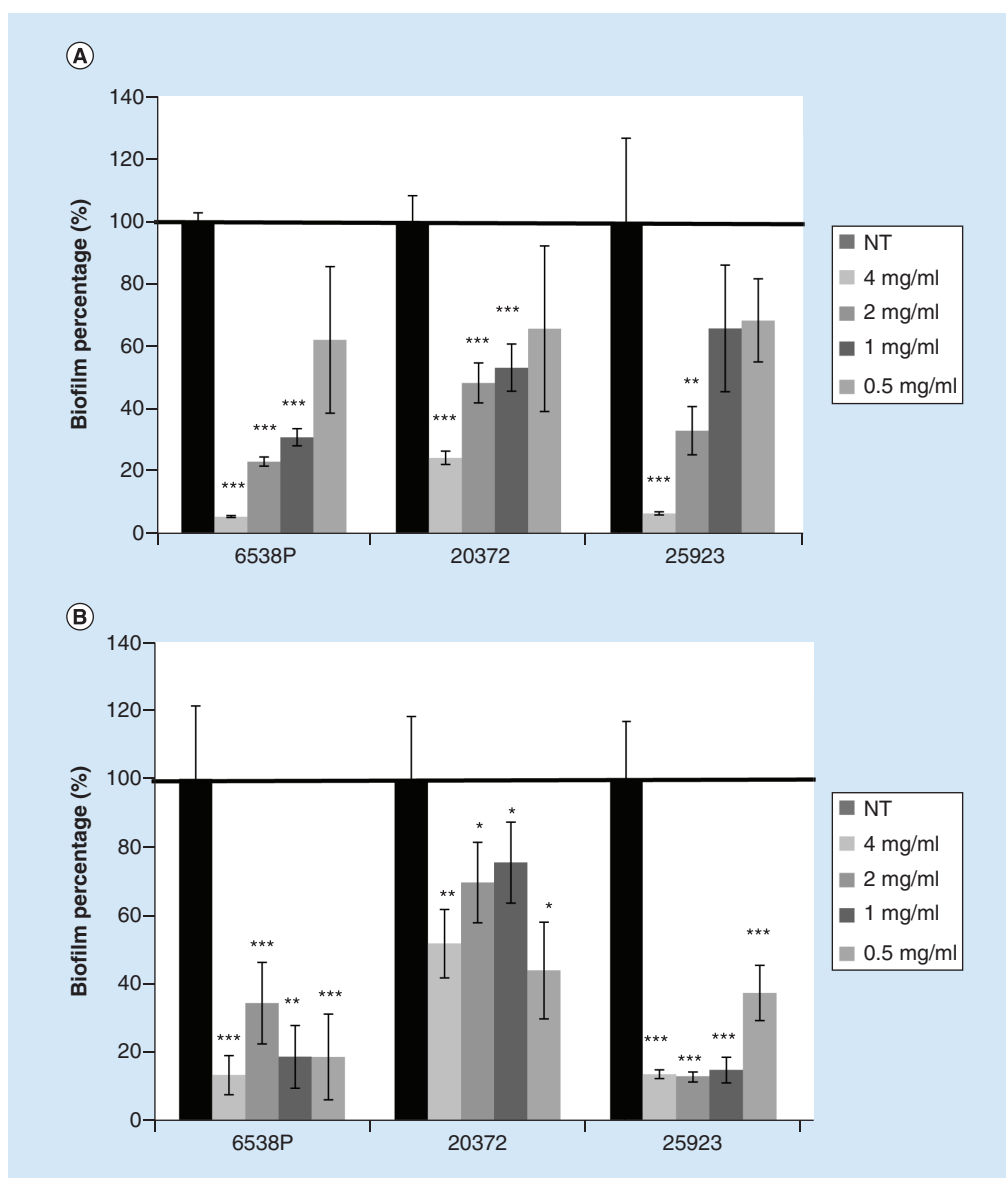


Figure 2. IN_TAA207 (A) and IN_TAD15 (B) extracts on biofilm formation of different *S. aureus* strains. Serial dilutions of each extract starting from 4 mg/ml were evaluated. Data are reported as the percentage of residual biofilm. Each data point represents the mean \pm SD of three independent samples. Differences in mean absorbance were compared with the untreated control (NT, black bar) and considered significant when $p < 0.05$ according to Student's *t*-test. * $p < 0.05$; ** $p < 0.01$; *** $p < 0.001$. NT: Not-treated; SD: Standard deviation.

activity on *S. aureus* strain 6538P (Figure 3A). Results showed strong antibiofilm activity in fraction 3, eluted with only chloroform. This sample was analyzed by GC–MS revealing the presence of saturated and unsaturated long-chain fatty acids as follows: C14:0, C14:1, C16:0, C16:1, C18:1, and a very low amount of C18:0 (Figure 3B).

Antibiofilm activity of fractions derived from chromatographic separation of IN_TAD15 was also evaluated, as reported in Figure 3C. In this case, different fractions were able to inhibit biofilm formation of *S. aureus* 6538P. The strongest effect was observed for fractions 5, 8, 11 (eluted with chloroform) and 20 (eluted with the chloroform/methanol 99:1). Moreover, for these fractions, an antibacterial activity has been observed.

To obtain more information about the chemical composition, each fraction was analyzed by GC–MS. Also, in this case, chromatograms revealed the presence of saturated and unsaturated long-chain fatty acids, with slight differences in the relative amount of each chemical species (Supplementary Figure 1). A comparison between

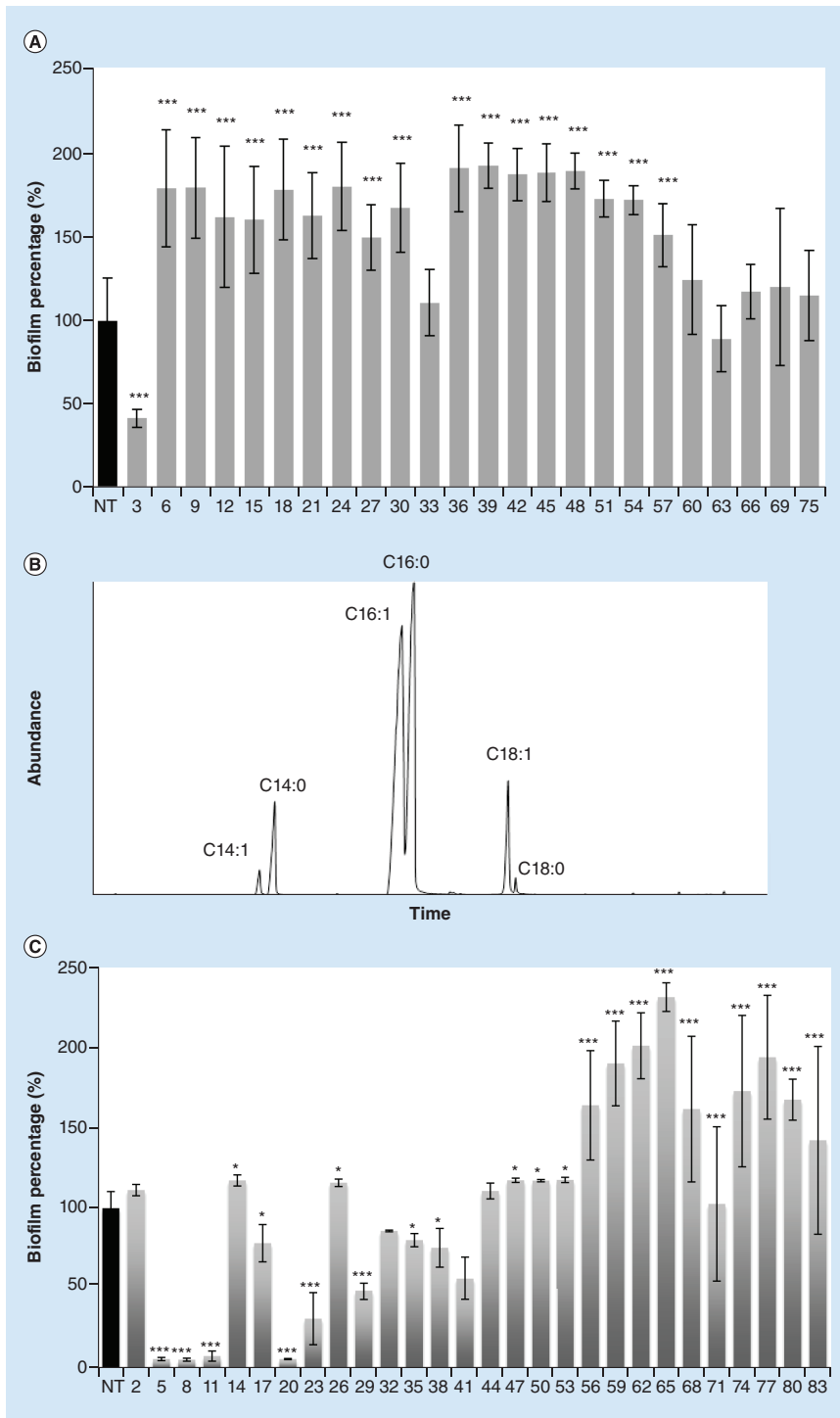


Figure 3. Chromatographic fractions from IN.TAA207 (A) and IN.TAD15 (C) on biofilm formation of *S. aureus* 6538P. Chromatographic profile of fraction 3 from IN.TAA207 (B). Each fraction was used at a concentration of 250 $\mu\text{g/ml}$. Data are reported as the percentage of residual biofilm. Each data point represents the mean \pm SD of three different samples. Biofilm formation was considered unaffected in the range of 90–100%. Differences in mean absorbance were compared with the untreated control and considered significant when $p < 0.05$ according to Student's *t*-test. * $p < 0.05$; ** $p < 0.01$; *** $p < 0.001$.
SD: Standard deviation.

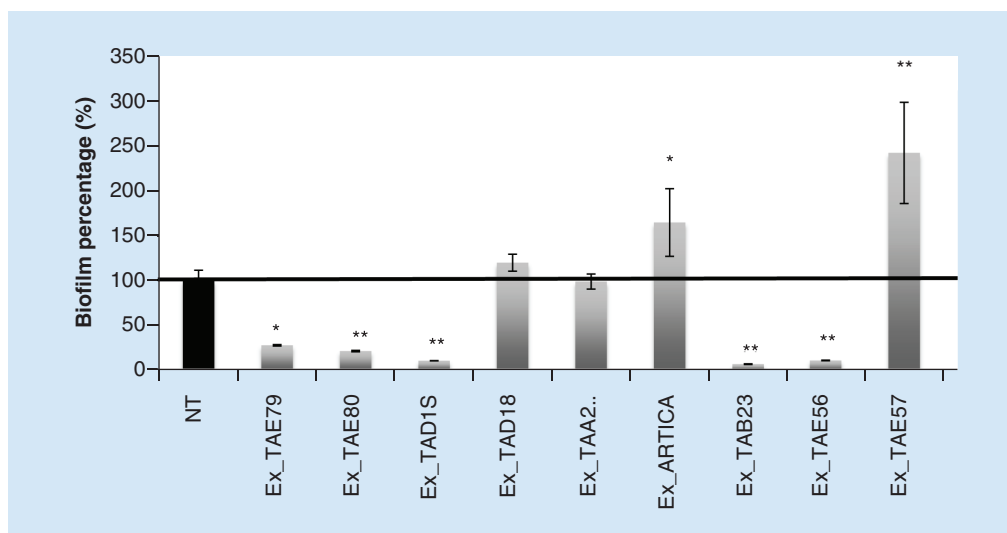


Figure 4. Extracellular extracts from cold-adapted bacteria on *S. aureus* 6538P biofilm formation. Data are reported as the percentage of residual biofilm after the treatment. Each data point represents the mean \pm SD of five independent samples. Differences in mean absorbance were compared with the untreated control (NT, black bar) and considered significant when $p < 0.05$ according to Student's *t*-test.

* $p < 0.05$; ** $p < 0.01$; *** $p < 0.001$.

NT: Not-treated; SD: Standard deviation.

IN_TAA207 and IN_TAD1S composition profiles revealed the presence in IN_TAD1S extract of fatty acids with an odd number of carbon atoms (i.e., C17:1; Supplementary Figure 1).

Screening of antibiofilm activity of extracellular organic extracts against *S. aureus*

Figure 4 shows the results obtained on *S. aureus* 6538P biofilm formation in the presence of different extracellular extracts from polar bacteria. Several extracts induced a strong reduction in biofilm formation by *S. aureus* 6538P. EX_TAE56 and EX_TAE57 were tested at a concentration of 0.5 mg/ml (1/2 MIC value), considering their antimicrobial activity reported in Table 2. Active extracts were selected for further analysis and tested on biofilm formation of three different *S. aureus* strains (65385P, 20372 and 25923). Furthermore, an assessment of the activity at different concentrations suggested a dose-dependent effect (Figure 5). Best inhibition in biofilm formation was obtained using EX_TAD1S on all tested strains (Figure 5C), indeed the percentage of residual biofilm was lower than 40%, even at a lower concentration of the extract (0.5 mg/ml). For this reason, EX_TAD1S was chosen for further analysis.

Fractionation of extracellular extract from *Pseudomonas* sp. TAD1S

EX_TAD1S was analyzed by ^1H NMR. This latter suggests the presence of a complex mixture of compounds (data not shown). To isolate the active molecule/s from EX_TAD1S, a preliminary purification step on a silica gel column was carried out, as reported in the Materials & methods section. The obtained fractions were tested to evaluate the antibiofilm activity on *S. aureus* (Figure 6A). The results clearly indicated the presence of the active molecule/s in fractions 15 and 17 (eluted with chloroform/methanol 8:2). The ^1H NMR spectra showed a profile almost identical for these two fractions. The analysis of the spectrum of fraction 15, reported in Figure 6B, suggested the presence of hydrocarbon chains, as indicated by the signals in the range of δ 0.5–1.5 ppm. In addition, signals appearing between δ 6.4 and 8.8 ppm strongly supported N–H protons (Figure 6B) that together with signals around δ 4 ppm, indicated a peptide backbone. All together, these signals indicated the lipopeptide nature of the active compound [30–32]. The GC–MS analysis of products obtained after the sample methanolysis followed by acetylation revealed the presence of the following amino acids: serine, valine, leucine and glutamic acid. This aminoacidic composition suggests a structure like those usually found for lipopeptides isolated from *Bacillus* and *Pseudomonas* species [33]. In addition, GC–MS analysis suggested that the lipopeptide was constituted by various isoforms, due to the difference in the length of the fatty acids, since it revealed a mixture of C15:0, C16:0, C16:1, C17:0, C18:0 and C18:1. Finally, the absence in the GC–MS chromatogram of peaks attributable to β -hydroxylated fatty acids

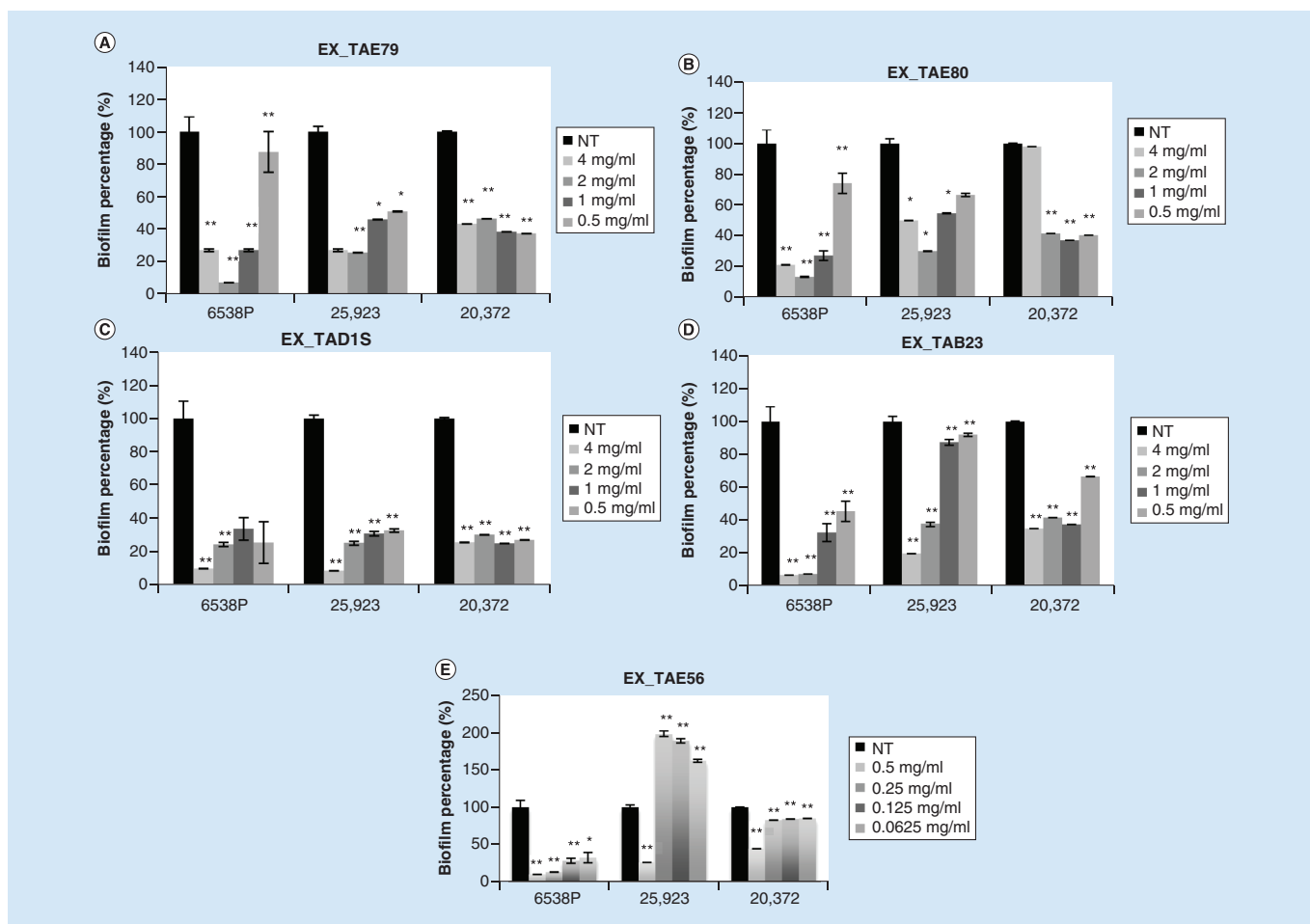


Figure 5. Selected extracellular extracts on biofilm formation of different *S. aureus* strains. Biofilm formation was evaluated after incubation of serial dilutions of extracts starting from 4 mg/ml (EX_TAE56 was tested starting from $\frac{1}{2}$ MIC value corresponding to 1 mg/ml). Data are reported as the percentage of residual biofilm. Each data point represents the mean \pm SD of three independent samples. Differences in mean absorbance were compared with the untreated control (NT, black bar) and considered significant when $p < 0.05$ according to Student *t*-test.

* $p < 0.05$; ** $p < 0.01$; *** $p < 0.001$.

NT: Not-treated; SD: Standard deviation.

suggested a cyclic structure with a terminal amide-linked fatty acid [34]. We also evaluated the antimicrobial activity of this fraction on *S. aureus* 6538P that was found at a concentration of 400 $\mu\text{g/ml}$.

Discussion

The investigation of new unexplored habitats and uncommon environments has become an important source for the discovery of novel bacterial metabolites with antimicrobial activity [35]. Since the antimicrobial activity of microorganisms living in extreme environments has not been explored as widely as for mesophilic microorganisms, the traditional approach of isolating and cultivating new microorganisms from underexplored habitats can be productive.

In this paper, polar marine bacteria belonging to *Pseudoalteromonas*, *Pseudomonas* and *Psychromonas* genera were grown in a synthetic medium and organic extracts of intracellular and from extracellular contents were analyzed to identify novel antibiofilm/antimicrobial molecules. The MIC evaluation against *S. aureus* 6538P revealed that the samples did not possess a relevant antimicrobial activity, while some of them strongly prevented biofilm formation by *S. aureus* 6538P.

IN_TAA207 and IN_TAD1S revealed a similar antibiofilm activity but were both selected because a preliminary analysis indicated that their chemical composition was different (data not shown). The samples were tested against

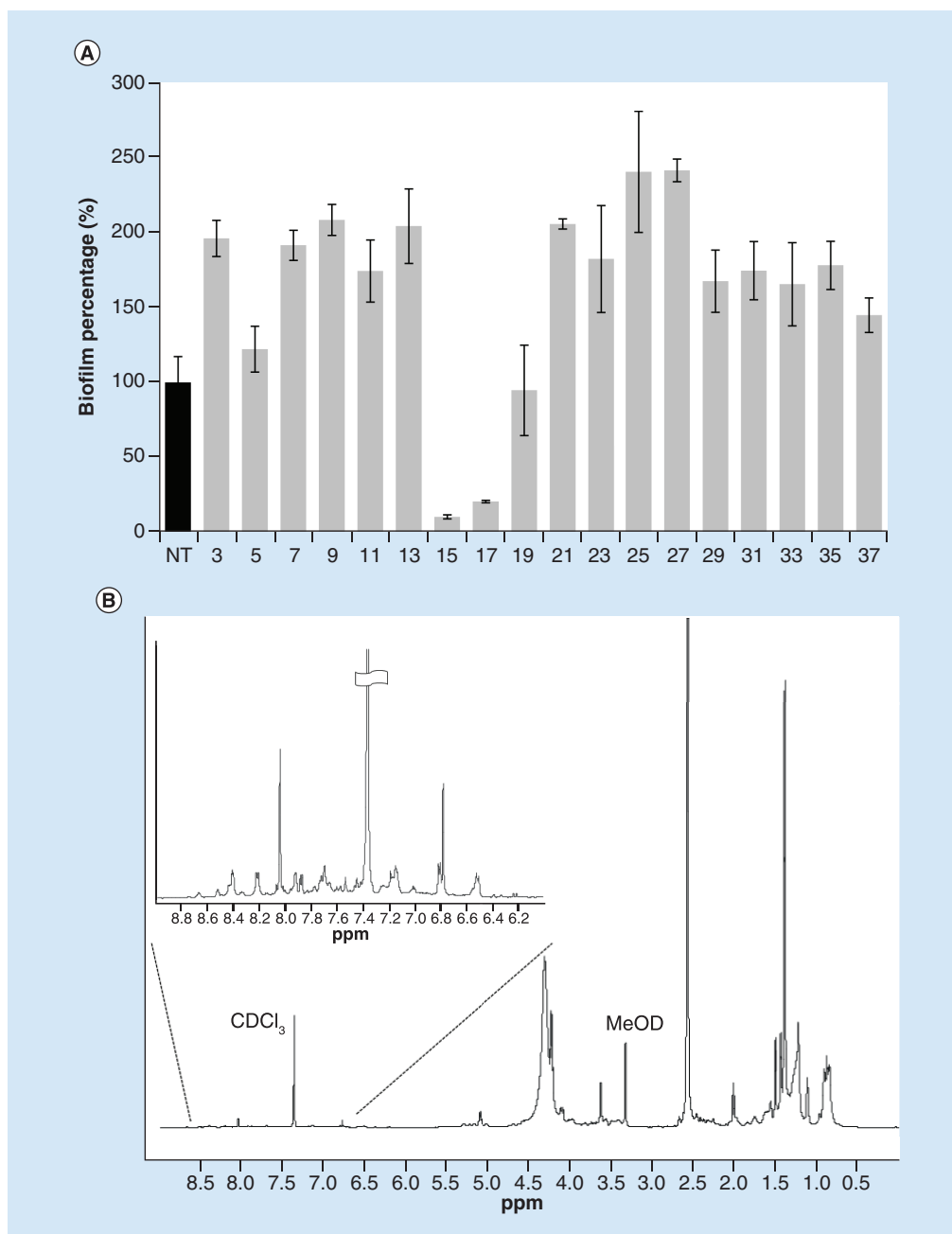


Figure 6. Chromatographic fractions from EX_TAD1S against *S. aureus* 6538P (A) and ¹H NMR spectrum of the active fraction (B). Each fraction was used at a concentration of 250 μg/ml. Data are reported as the percentage of residual biofilm. Each data point represents the mean ± SD of three different samples. Biofilm formation was considered unaffected in the range of 90–100%. Differences in mean absorbance were compared with the untreated control and considered significant when $p < 0.05$ according to Student's *t*-test. (B) ¹H NMR spectrum of the active fraction 15 from EX_TAD1S. Spectrum was recorded in CDCl₃:CD₃OD at 600 MHz and 298 K.

* $p < 0.05$; ** $p < 0.01$; *** $p < 0.001$.

SD: Standard deviation.

three different *S. aureus* strains: ATCC 6538P and ATCC 25923 are both reference strains for antimicrobial testing, while ATCC 20372 is a clinical isolate. These strains show a different ability to form biofilm: ATCC 25923 is classified as a strong biofilm producer, ATCC 6538P is a medium/strong biofilm producer and ATCC 20372 is considered a medium/weak biofilm producer [36]. IN_TAA207 and IN_TAD1S were both able to inhibit biofilm formation of all tested *S. aureus* strains, and the effect of IN_TAA207 was clearly dose dependent, whereas

the activity of IN_TAD1S was independent of the extract concentration. The different chemical composition of IN_TAA207 and IN_TAD1S extracts and the different features of the three tested *S. aureus* strains could explain the reported results. Both extracts were fractionated, and the resulting fractions were tested to assess their antibiofilm activity. The chromatographic fraction 3, obtained from IN_TAA207 extract, and chromatographic fractions 5, 8, 11 and 20 from IN_TAD1S extract showed the best antibiofilm activity. Moreover, all fractions from IN_TAD1S with antibiofilm action showed antimicrobial activity. All these fractions contained saturated and unsaturated long-chain fatty acids. Free fatty acids are ubiquitous on the surface of human skin and represent the predominant components in human sebum [37]. Particularly, medium- to long-chain fatty acids (C8 to C18) display antibacterial activity against a broad range of Gram-positive bacteria and are considered responsible for at least part of the direct antimicrobial activity of the skin surface against pathogen colonization and infection [38]. The antibacterial efficacy of fatty acids stems from their membrane-destabilizing activity that causes increased cell permeability and cell lysis.

Some of the identified fatty acids were common to different active fractions; in detail, either fraction 3 from IN_TAA207 and fractions 5, 8, 11 from IN_TAD1S contained C16:1 (palmitoleic), C16:0 and C18:1 (oleic acid). For these fatty acids, the antibacterial activity against *S. aureus* was previously observed [39–41]. Two odd long fatty acids, C17:1 and C19:1, were identified in fractions 5, 8, 11 and 20 from IN_TAD1S. Although several bacteria produce odd-numbered fatty acid [42,43], to the best of our knowledge, no information about their possible antimicrobial activity against *S. aureus* was previously recorded. Future studies will be aimed to clarify if these molecules contribute to the antimicrobial activity of IN_TAD1S fractions and if they can be considered responsible for the differences in the activity of IN_TAD1S and IN_TAA207 extracts. Anyway, the reported antibiofilm activity of IN_TAD1S and IN_TAA207 was found at sub-MIC concentrations.

The screening of polar extracellular extracts revealed that EX_TAE79, EX_TAE80 EX_TAB23, EX_TAD1S and EX_TAE56 were able to affect *S. aureus* biofilm formation. The attention was focused on EX_TAD1S since this sample efficiently impairs biofilm formation in all three tested strains, with a percentage of residual biofilm lower than 40% as compared with the untreated sample. Also, in this case, the extract was fractionated, and the corresponding fractions were analyzed. Fractions 15 and 17 displayed a high level of activity against *S. aureus* biofilm (Figure 6A). The ¹H NMR spectrum of fraction 15 (Figure 6B) indicated the presence of N-H (6.4–8.6 ppm) and C-H (4.5–5.5 ppm) signals that, together with signals of a long aliphatic chain (0.5–1.5 ppm) suggested the lipopeptide nature of the active compound [30–32]. The GC–MS analysis revealed the presence of serine, leucine, valine and glutamic acid, an amino acid composition agreed with the compositions obtained for other lipopeptides [30,31], moreover this analysis suggests a cyclic structure of this lipopeptide.

Lipopeptides are produced by several bacterial species; they are amphiphilic molecules consisting of short linear chains or cyclic structures of amino acids, linked to a fatty acid via ester or amide bonds or both. They are proved to act as antibiotics, antiadhesives, antitumor compounds and foaming agents [44–48]. Very few examples of lipopeptides isolated from cold-adapted bacteria were reported. *Pseudomonas fluorescens* BD5, a bacterium isolated from Archipelago of Svalbard, produces a cyclic lipopeptide named pseudofactin [49] endowed with a very good emulsification activity and with antiadhesive activity against several pathogenic microorganisms (*Escherichia coli*, *Enterococcus faecalis*, *Enterococcus hirae*, *S. epidermidis*, *Proteus mirabilis* and *Candida albicans*) [49]. Another cold-adapted bacterium able to produce lipopeptides is *Bacillus amyloliquefaciens* Pc3 that was isolated from Antarctic seawater [50].

Although in the literature few publications describe lipopeptides from cold-adapted bacteria, many reports describe the ability of lipopeptides to kill pathogenic bacteria. Interestingly, several lipopeptides are active against *S. aureus*. Some examples are Daptomycin, a cyclic lipopeptide, that was approved as an antibiotic by the US FDA in 2003 for the treatment of complicated skin [51]; brevivacillin, a lipopeptide produced by a strain of *Brevibacillus laterosporus* showing antimicrobial activity against *S. aureus* [52].

Conclusion

The cyclic lipopeptide isolated from *Pseudomonas* sp. TAD1S does not display antimicrobial activity on *S. aureus* (MIC resulted to be 400 µg/ml) but it resulted to be an effective antibiofilm molecule able to strongly reduce the *S. aureus* biofilm formation. Furthermore, preliminary results indicate that it also works as a biosurfactant (Supplementary Figure 2).

Future perspective

The new cyclic lipopeptide isolated from Antarctic bacterium *Pseudomonas* sp. TAD1S may be potentially useful in a wide variety of biotechnological and medical applications. Further studies are needed to better define its chemical structure and to explore its biological activity and applicability as an anti-infective agent.

Summary points

Among bacteria, staphylococci are recognized as the most frequent causes of biofilm-associated infections

- *Staphylococcus aureus* is often present asymptotically on districts of the human body.
- *S. aureus* possesses a collection of virulence factors and displays the ability to acquire resistance to most antibiotics.
- The antibiotic resistance of *S. aureus* is related, in most cases, to its ability to develop a protective architecture called biofilm.

Unexplored habitats & uncommon environments can be considered an important source for the discovery of novel bacterial metabolites with antimicrobial activity

- Marine microorganisms are considered potential sources for the discovery of new metabolically active molecules.
- Some of these bioactive molecules have already been selected for the treatment of various diseases and many of them are under clinical investigations.
- Cold-adapted marine bacteria deriving from polar regions represent an untapped reservoir of biodiversity endowed with an interesting chemical repertoire.
- Intracellular and extracellular organic extracts obtained from cultures of polar marine bacteria were tested against *S. aureus*.

Conclusion

- Identification of a lipopeptide able to strongly reduce the *S. aureus* biofilm formation with antimicrobial activity at high concentration.
- The new cyclic lipopeptide isolated from Antarctic bacterium *Pseudomonas* sp. TAD1S may be potentially useful in a wide variety of biotechnological and medical applications.
- Our findings indicate that the lipopeptide also works as a biosurfactant.

Supplementary data

To view the supplementary data that accompany this paper please visit the journal website at: www.futuremedicine.com/doi/full/10.2217/fmb-2019-0147

Author contributions

Design of the work, acquisition of data, analysis and interpretation, drafting and critical revision, approval of the final version and agreement to be accountable for the work were performed by all the authors.

Financial & competing interests disclosure

The authors have no relevant affiliations or financial involvement with any organization or entity with a financial interest in or financial conflict with the subject matter or materials discussed in the manuscript. This includes employment, consultancies, honoraria, stock ownership or options, expert testimony, grants or patents received or pending, or royalties.

No writing assistance was utilized in the production of this manuscript.

References

Papers of special note have been highlighted as: • of interest; •• of considerable interest

1. Katz ML, Mueller LV, Polyakov M, Weinstock SF. Where have all the antibiotic patents gone? *Nat. Biotechnol.* 24, 1529–1531 (2006).
2. Hall CW, Mah TF. Molecular mechanisms of biofilm-based antibiotic resistance and tolerance in pathogenic bacteria. *FEMS Microbiol. Rev.* 41, 276–301 (2017).
- **Description of mechanisms of biofilm-based antibiotic resistance in pathogenic bacteria.**
3. Otto M. Staphylococcal biofilms. *Curr. Top. Microbiol. Immunol.* 322, 207–228 (2008).
4. Lakhundi S, Zhang K. Methicillin-resistant *Staphylococcus aureus*: molecular characterization, evolution, and epidemiology. *Clin. Microbiol. Rev.* 31, pii:e00020-18 (2018).
- **Shows the evolution of methicillin-resistant *Staphylococcus aureus*.**
5. Hall-Stoodley L, Stoodley P. Evolving concepts in biofilm infections. *Cell. Microbiol.* 11, 1034–1043 (2009).

6. Liu W, Li J, Cheng M *et al.* A surface-engineered polyetheretherketone biomaterial implant with direct and immunoregulatory antibacterial activity against methicillin-resistant *Staphylococcus aureus*. *Biomaterials* 208, 8–20 (2019).
7. Talbot GH, Bradley J, Edwards JE Jr, Gilbert D, Scheld M, Bartlett JG. Antimicrobial Availability Task Force of the Infectious Diseases Society of America. Bad bugs need drugs: an update on the development pipeline from the Antimicrobial Availability Task Force of the Infectious Diseases Society of America. *Clin. Infect. Dis.* 42, 657–668 (2006).
8. Artini M, Papa R, Barbato G *et al.* Bacterial biofilm formation inhibitory activity revealed for plant derived natural compounds. *Bioorg. Med. Chem.* 20, 920–926 (2012).
9. Manivasagan P, Kang KH, Sivakumar K, Li-Chan EC, Oh HM, Kim SK. Marine actinobacteria: an important source of bioactive natural products. *Environ. Toxicol. Pharmacol.* 38, 172–188 (2014).
10. Mehbub MF, Lei J, Franco C, Zhang W. Marine sponge derived natural products between 2001 and 2010: trends and opportunities for discovery of bioactives. *Mar. Drugs* 12, 4539–4577 (2014).
11. Artini M, Patsilina A, Papa R *et al.* Antimicrobial and antibiofilm activity and machine learning classification analysis of essential oils from different Mediterranean plants against *Pseudomonas aeruginosa*. *Molecules* 23, pii:E482 (2018).
12. Newman DJ, Cragg GM, Snader KM. Natural products as sources of new drugs over the period 1981–2002. *J. Nat. Prod.* 66, 1022–1037 (2003).
13. Katz L, Baltz RH. Natural product discovery: past, present, and future. *J. Ind. Microbiol. Biotechnol.* 43, 155–176 (2016).
14. Bhatnagar I, Kim SK. Immense essence of excellence: marine microbial bioactive compounds. *Mar. Drugs* 8, 2673–2701 (2010).
15. Ng TB, Cheung RC, Wong JH, Bekhit AA, Bekhit Ael-D. Antibacterial products of marine organisms. *Appl. Microbiol. Biotechnol.* 99, 4145–4173 (2015).
- **An overview of new antimicrobials isolated from marine organisms.**
16. Molinski TF, Dalisay DS, Lievens SL, Saludes JP. Drug development from marine natural products. *Nat. Rev. Drug. Discov.* 8, 69–85 (2009).
17. Liu Y. Renaissance of marine natural product drug discovery and development. *J. Mari. Sci. Res. Dev.* 2, e106 (2012).
18. Lo Giudice A, Bruni V, Michaud L. Characterization of Antarctic psychrotrophic bacteria with antibacterial activities against terrestrial microorganisms. *J. Basic Microbiol.* 47, 496–505 (2007).
19. Núñez-Montero K, Barrientos L. Advances in Antarctic research for antimicrobial discovery: a comprehensive narrative review of bacteria from Antarctic environments as potential sources of novel antibiotic compounds against human pathogens and microorganisms of industrial importance. *Antibiotics (Basel)* 7, pii:E90 (2018).
- **An overview of new antimicrobials isolated from Antarctic bacteria.**
20. Neifar M, Maktouf S, Ghorbel RE, Jaouani A, Cherif A. Extremophiles as a source of novel bioactive compounds with industrial potential. In: *Biotechnology of Bioactive Compounds: Sources and Applications*. John Wiley & Sons, Chichester, West Sussex, UK (2015).
21. Papa R, Parrilli E, Sannino F *et al.* Anti-biofilm activity of the Antarctic marine bacterium *Pseudoalteromonas haloplanktis* TAC125. *Res. Microbiol.* 164, 450–456 (2013).
22. Parrilli E, Papa R, Carillo S *et al.* Anti-biofilm activity of *Pseudoalteromonas haloplanktis* TAC125 against *Staphylococcus epidermidis* biofilm: evidence of a signal molecule involvement? *Int. J. Immunopathol. Pharmacol.* 28, 104–113 (2015).
23. Casillo A, Papa R, Ricciardelli A *et al.* Anti-biofilm activity of a long-chain fatty aldehyde from Antarctic *Pseudoalteromonas haloplanktis* TAC125 against *Staphylococcus epidermidis* biofilm. *Front. Cell. Infect. Microbiol.* 7, 46 (2017).
- **Describes a new small antibiofilm molecule isolated from an Antarctic bacterium.**
24. Papaleo MC, Romoli R, Bartolucci G *et al.* Bioactive volatile organic compounds from Antarctic (sponges) bacteria. *N. Biotechnol.* 30, 824–838 (2013).
25. Sannino F, Parrilli E, Apuzzo GA *et al.* *Pseudoalteromonas haloplanktis* produces methylamine, a volatile compound active against *Burkholderia cepacia* complex strains. *N. Biotechnol.* 35, 13–18 (2017).
26. Papa R, Selan L, Parrilli E *et al.* Anti-biofilm activities from marine cold adapted bacteria against Staphylococci and *Pseudomonas aeruginosa*. *Front. Microbiol.* 6, 1333 (2015).
- **Shows the antibiofilm activities of several polar bacteria against different pathogens.**
27. CLSI Supplement M100. *Performance Standards for Antimicrobial Susceptibility Testing (27th Edition)*. Clinical and Laboratory Standards Institute, Wayne, PA, USA (2017).
28. Busetti A, Shaw G, Megaw J, Gorman SP, Maggs CA, Gilmore BF. Marine-derived quorum-sensing inhibitory activities enhance the antibacterial efficacy of tobramycin against *Pseudomonas aeruginosa*. *Mar. Drugs* 13, 1–28 (2014).
29. Artini M, Papa R, Scoarughi GL *et al.* Comparison of the action of different proteases on virulence properties related to the staphylococcal surface. *J. Appl. Microbiol.* 114, 266–277 (2013).
30. Liu XY, Yang SZ, Mu BZ. Production and characterization of a C15-surfactin-O-methyl ester by a lipopeptide producing strain *Bacillus subtilis* HSO121. *Process Biochem.* 44, 1144–1151 (2009).

31. Naruse N, Tenmyo O, Kobaru S et al. Pumilacidin, a complex of new antiviral antibiotics production, isolation, chemical properties, structure and biological activity. *J. Antibiot.* 43, 267–280 (1990).
32. Saggese A, Culurciello R, Casillo A, Corsaro MM, Ricca E, Baccigalupi L. A marine isolate of *Bacillus pumilus* secretes a pumilacidin active against *Staphylococcus aureus*. *Mar. Drugs* 16, 180 (2018).
33. Inès M, Dhouha G. Lipopeptide surfactants: production, recovery and pore forming capacity. *Peptides* 71, 100–112 (2015).
34. Janek T, Łukaszewicz M, Rezanka T, Krasowska A. Isolation and characterization of two new lipopeptide biosurfactants produced by *Pseudomonas fluorescens* BD5 isolated from water from the Arctic Archipelago of Svalbard. *Bioresour. Technol.* 101, 6118–6123 (2010).
35. Donadio S, Maffioli S, Monciardini P, Sosio M, Jabes D. Antibiotic discovery in the twenty-first century: current trends and future perspectives. *J. Antibiot.* 63, 423–430 (2010).
36. Cafiso V, Bertuccio T, Santagati M et al. agr-Genotyping and transcriptional analysis of biofilm-producing *Staphylococcus aureus*. *FEMS Immunol. Med. Microbiol.* 51, 220–227 (2007).
37. Wille JJ, Kydonieus A. Palmitoleic acid isomer (C16:1delta6) in human skin sebum is effective against Gram-positive bacteria. *Skin Pharmacol. Appl. Skin Physiol.* 16, 176–187 (2003).
38. Drake DR, Brogden KA, Dawson DV, Wertz PW. Thematic review series: skin lipids. Antimicrobial lipids at the skin surface. *J. Lipid Res.* 49, 4–11 (2008).
39. Kabara JJ, Swieczkowski DM, Conley AJ, Truant JP. Fatty acids and derivatives as antimicrobial agents. *Antimicrob. Agents Chemother.* 2, 23–28 (1972).
40. Kitahara T, Koyama N, Matsuda J et al. Antimicrobial activity of saturated fatty acids and fatty amines against methicillin-resistant *Staphylococcus aureus*. *Biol. Pharm. Bull.* 27, 1321–1326 (2004).
41. Kelsey JA, Bayles KW, Shafii B, McGuire MA. Fatty acids and monoacylglycerols inhibit growth of *Staphylococcus aureus*. *Lipids* 41, 951–961 (2006).
42. Kamimura K, Fuse H, Takimura O, Yamaoka Y, Ohwada K, Hashimoto J. Pressure-induced alteration in fatty acid composition of barotolerant deep-sea bacterium. *J. Oceanogr.* 48, 104 (1992).
43. Ponder MA, Gilmour SJ, Bergholz PW et al. Characterization of potential stress responses in ancient Siberian permafrost psychrotolerant bacteria. *FEMS Microbiol. Ecol.* 53, 103–115 (2005).
44. Das P, Mukherjee S, Sivapathasekaran C, Sen R. Microbial surfactants of marine origin: potentials and prospects. *Adv. Exp. Med. Biol.* 672, 88–101 (2010).
45. Banat IM, Franzetti A, Gandolfi I et al. Microbial biosurfactants production, applications and future potential. *Appl. Microbiol. Biotechnol.* 87, 427–444 (2010).
46. Biniarz P, Łukaszewicz M, Janek T. Screening concepts, characterization and structural analysis of microbial-derived bioactive lipopeptides: a review. *Crit. Rev. Biotechnol.* 8551, 1–18 (2016).
- **An overview of microbial-derived bioactive lipopeptides.**
47. Nielsen TH, Nybroe O, Koch B, Hansen M, Sørensen J. Genes involved in cyclic lipopeptide production are important for seed and straw colonization by *Pseudomonas* sp. strain DSS73. *Appl. Environ. Microbiol.* 71, 4112–4116 (2005).
48. Raaijmakers JM, de Bruijn I, de Kock MJ. Cyclic lipopeptide production by plant-associated *Pseudomonas* spp.: diversity, activity, biosynthesis, and regulation. *Mol. Plant Microbe Interact.* 19, 699–710 (2006).
49. Janek T, Łukaszewicz M, Krasowska A. Antiadhesive activity of the biosurfactant pseudofactin II secreted by the Arctic bacterium *Pseudomonas fluorescens* BD5. *BMC Microbiol.* 12, 24 (2012).
50. Ding L, Zhang S, Guo W, Chen X. Exogenous indole regulates lipopeptide biosynthesis in Antarctic *Bacillus amyloliquefaciens* Pc3. *J. Microbiol. Biotechnol.* 28, 784–795 (2018).
51. Marty FM, Yeh WW, Wennersten CB et al. Emergence of a clinical daptomycin-resistant *Staphylococcus aureus* isolate during treatment of methicillin-resistant *Staphylococcus aureus* bacteremia and osteomyelitis. *J. Clin. Microbiol.* 44, 595–597 (2006).
52. Yang X, Huang E, Yuan C, Zhang L, Yousef AE. Isolation and structural elucidation of brevibacillin: an antimicrobial lipopeptide from *Brevibacillus laterosporus* that combats drug-resistant Gram-positive bacteria. *Appl. Environ. Microbiol.* 82, 2763–2772 (2016).
- **Describes the antimicrobial activity of a natural lipopeptide against drug-resistant Gram-positive bacteria.**
53. Groudieva T, Grote R, Antranikian G. *Psychromonas arctica* sp. nov., a novel psychrotolerant, biofilm-forming bacterium isolated from Spitzbergen. *Int. J. Syst. Evol. Microbiol.* 53, 539–545 (2003).
54. Feller G, D'Amico S, Benotmane AM, Joly F, Van Beeumen J, Gerday C. Characterization of the C-terminal propeptide involved in bacterial wall spanning of alpha-amylase from the psychrophile *Alteromonas haloplanktis*. *J. Biol. Chem.* 273, 12109–12115 (1998).